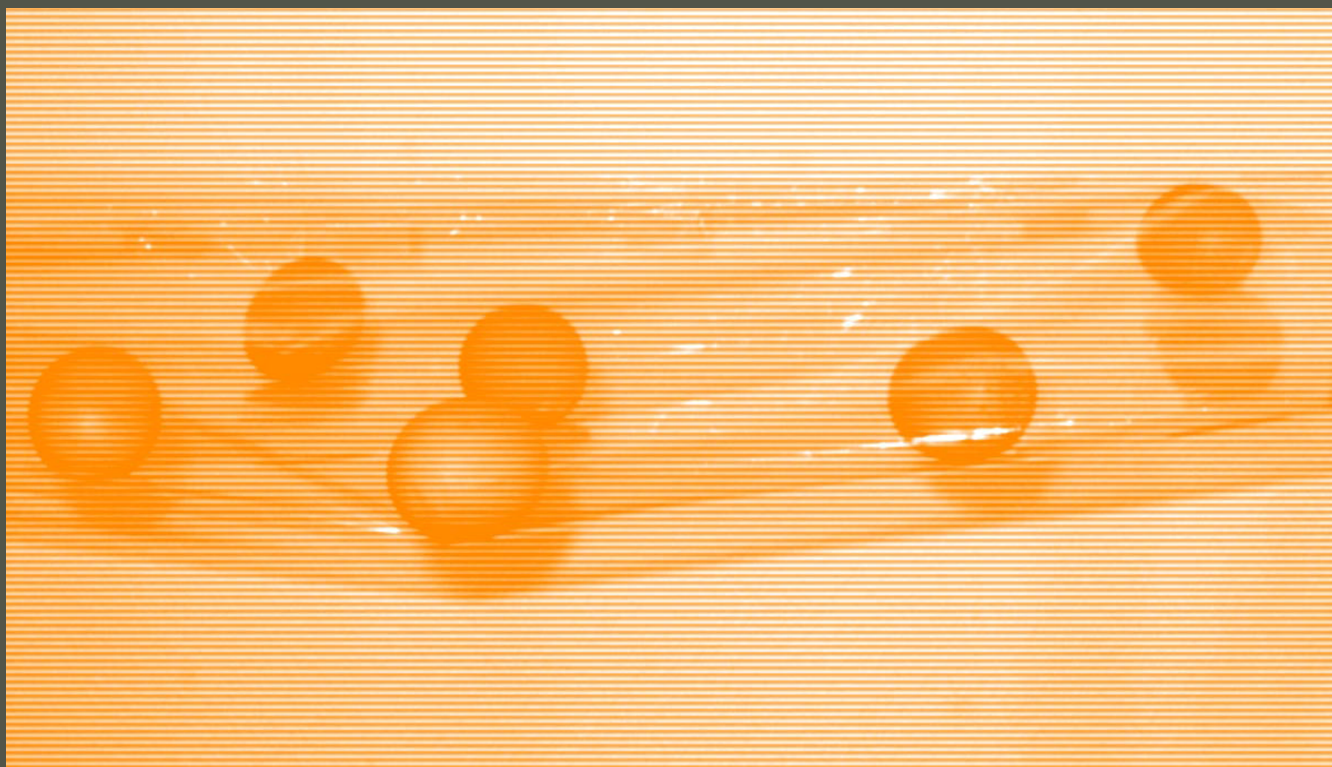


Thomas Haefele

*INTERACTIONS OF AN ANTIMICROBIAL PEPTAIBOL
WITH AMPHIPHILIC BLOCK COPOLYMERS*

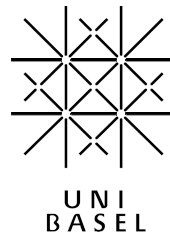


Cuvillier Verlag Göttingen

INTERACTIONS OF AN ANTIMICROBIAL PEPTAIBOL WITH AMPHIPHILIC BLOCK COPOLYMERS

Inauguraldissertation
zur
Erlangung der Würde eines Doktors der Philosophie

vorgelegt der
Philosophisch-Naturwissenschaftlichen Fakultät
der Universität Basel



von
Thomas Friedrich Haefele

aus
Oberbüren/SG, Gossau/SG und Basel/BS

Göttingen, 2006

Genehmigt von der Philosophisch-Naturwissenschaftlichen Fakultät

auf Antrag von

Prof. Dr. Wolfgang Meier (Universität Basel)

und

Prof. Dr. Ulrich Schwaneberg (International University Bremen)

Basel, den 22. Dezember 2005

Prof. Dr. Hans-Jakob Wirz
Dekan

To my parents

Abstract

In this thesis the behavior of binary membranes from amphiphilic PMOXA-PDMS-PMOXA triblock copolymers and the peptaibol alamethicin, an antimicrobial peptide, was investigated in the context of formation of novel biocomposite nanostructured materials. This task was achieved by employing monolayer and bilayer systems. Pure systems as well as mixtures of the individual materials were considered.

The properties of mixed monolayers were studied by surface pressure-area isotherms and Brewster angle microscopy. Both pure and binary systems exhibit a rich phase behavior. As reported previously, functionality of alamethicin relies on its aggregation properties in lipid membranes. This is also the case in polymer matrices; however, here the mixing properties differ from lipid-peptide systems due to the polymers' structural specificity. The peptide influence on the polymer films is provided in detail, and supported by the compressibility data to assess the elastic properties of such composite membranes. Surface topography of deposited Langmuir-Blodgett films was analyzed by scanning force microscopy to foster the conclusions drawn from results obtained for the air-water interface. Although natural membrane proteins are optimized for lipid bilayers, our results suggest that block copolymers membranes may provide a better environment for the peptide.

The pore forming behavior of alamethicin in vesicular systems built from amphiphilic block copolymers was further investigated by transmission electron microscopy and dynamic light scattering. A significant increase in cation permeability was assigned to the intrinsic ion transport activity of alamethicin and therefore a functional reconstitution of the peptide in self-assembled membranes built from synthetic block copolymers could be proven.

This thesis is structured into seven chapters. In the introductory chapter the basic idea and the goals of this work are elucidated. Chapter two provides the theoretical background explaining the molecular interactions at the air-water interface subsequently pursued by insights into the amphiphilic and self-assembly behavior of phospholipids and block copolymers as well as the functionalization of natural and synthetic membranes by integration of membrane proteins. In chapter three the experimental conditions are revealed followed by chapter four in which the obtained results are discussed in depth. The conclusions which were drawn as well as an outlook for prospective investigations are given in chapter five. The thesis is finalized by the list of literature references and an appendix.

Keywords: *alamethicin, amphiphilic block copolymers, antimicrobial peptides, bilayers, biomimetic mineralization, Brewster angle microscopy, compressional modulus, Langmuir monolayers, Langmuir-Blodgett films, lyotropic mesophases, mixed monolayers, peptaibols, phase behavior, phosphatidylcholine, polymersomes, self-assembly, transmission electron microscopy*

Deep in the human unconsciousness is a pervasive need for a logical universe that makes sense. But the real universe is always one step beyond logic.

-from 'The Sayings of Muad'Dib' by the Princess Irulan [Herbert 1968]



Der, die, das
Wer, wie, was?
Wieso, weshalb, warum?
Wer nicht fragt, bleibt dumm.



Tausend tolle Sachen
gibt es überall zu sehn.
Manchmal muss man fragen,
um sie zu versteh'n.



Der, die, das
Wer, wie, was?
Wieso, weshalb, warum?
Wer nicht fragt, bleibt dumm.

[Hoffmann, 1973]

Acknowledgement

This thesis was performed between January 2002 and November 2005 at the Department of Chemistry of the University of Basel. I wish to gratefully acknowledge the following persons who contributed considerably to the success of this work:

Prof. Dr. Wolfgang Meier, for supervising my thesis, for all his helpful advices and discussions during the development of this work, his support when it was needed as well as for his kind and cheerful way of motivating people.

Prof. Dr. Ulrich Schwaneberg, for corefering this thesis and in addition for his encouragements and cheer ups during my stay in Bremen.

Prof. Dr. Edwin Constable, for his precious time he sacrificed to preside my Ph.D. defense.

Dr. Katarzyna Kita-Tokarczik, for introducing me to the realms of air-water interface science, for the pressure and the motivation boosts she applied when it was necessary, for advice and revision of the manuscript of my thesis, but especially for her humor and friendship, her patience and loyalty and for perfectly hosting the team spirit.

Dr. Almut Mecke, for teaching, assistance and support concerning scanning force microscopy and substrate transfers.

Dr. Andreas Taubert, for training, help and fruitful discussions concerning transmission electron microscopy.

Dr. Roxana Timmermans-Stoenescu, for synthesis and provision of functionalized block copolymers, for her advice and support with practical problems, but in particular for her friendship and encouragement.

Dr. Corinne Vebert-Nardin, for aid and backing of issues with dynamic light scattering together with the pleasant collaboration in evaluating and acquiring microscopic equipment.

Dr. Daniel Streich, for his faithful friendship and loyalty and all the boosts of motivation gained during many wisely used and very valuable breaks and moments of distraction.

Dr. Jörg Widmer, for synthesis and provision of the PMOXA₁₃-PDMS₂₃-PMOXA₁₃ polymer used in this work as well as for his reliability as a ski mate.

Diana Seboek, for countless distracting discussions, for illuminating me the edge between sense and nonsense plus for her spontaneous and helpful nature.

Urs Buser, for all the exciting discussions on technical and IT problems, for his psychological assistance as well as for his reliability as a lunch partner.

All present and past members of the Meier-group for the enjoyable & cheerful atmosphere, for an excellent team spirit, and numerous fruitful and rewarding discussions.

I especially acknowledge my family and my friends for their endless support throughout my whole course of study and my doctoral thesis.

This work was financially supported by the Swiss National Science Foundation, the NCCR Nanoscale Science and the University of Basel.

Content

1. Introduction and objective	1
2. Theoretical background	5
2.1. Molecular interactions at the air-water interface	6
2.1.1. History of monolayer research.....	6
2.1.2. Forces at the air-water interface.....	9
2.1.3. Langmuir films.....	11
2.1.3.1. Surface pressure-area isotherms.....	12
2.1.3.2. Mixed monolayers.....	14
2.1.3.3. Surface elasticity.....	18
2.1.4. Brewster angle microscopy.....	20
2.1.5. Langmuir-Blodgett films.....	22
2.1.6. Biological relevance of monolayers.....	25
2.2. Biological surfactants	26
2.2.1. Phospholipids.....	27
2.2.2. Lyotropic phase behavior.....	28
2.2.2.1. Amphiphilic properties of lipids.....	28
2.2.2.2. Lyotropic mesophases.....	29
2.2.2.3. Morphology of self-assembled structures.....	32
2.2.3. Lamellar phases from phospholipids.....	35
2.3. Amphiphilic polymers	36
2.3.1. Macromolecules.....	36
2.3.1.1. Polymer constitution.....	37
2.3.1.2. Polymer architecture.....	38
2.3.2. Amphiphilic block copolymers.....	39
2.3.2.1. Lyotropic phase behavior of amphiphilic block copolymers.....	41
2.3.2.2. Isothermal phase behavior of amphiphilic block copolymers.....	45
2.4. Membrane active peptides	47
2.4.1. Membrane proteins.....	47
2.4.1.1. Integral membrane proteins.....	47
2.4.1.2. Peripheral membrane proteins.....	48
2.4.2. Antimicrobial peptaibols.....	49
2.4.2.1. Molecular structure of alamethicin.....	50
2.4.2.2. Structure of ion channels and mechanisms of pore formation.....	52

3. Materials and methods	55
3.1. Materials	56
3.1.1. Reagents.....	56
3.1.2. Triblock copolymer synthesis.....	57
3.1.2.1. PMOXA ₁₆ -PDMS ₇₄ -PMOXA ₁₆	58
3.1.2.1.1. Activated Poly(dimethylsiloxane).....	59
3.1.2.1.2. Hydroxy terminated triblock copolymer.....	59
3.1.2.2. PMOXA ₁₃ -PDMS ₂₃ -PMOXA ₁₃	59
3.1.2.3. Amino terminated triblock copolymers.....	60
3.1.2.4. Dye labeled triblock copolymers.....	60
3.1.2.4.1. DTAF labeled polymers.....	60
3.1.2.4.2. TAMRA labeled polymers.....	60
3.2. Methods	61
3.2.1. Langmuir monolayers.....	61
3.2.2. Brewster angle microscopy (BAM).....	61
3.2.3. Langmuir-Blodgett (LB) film transfers.....	62
3.2.4. Contact angle measurements.....	62
3.2.5. Preparation of polymersomes.....	62
3.2.5.1. Vesicles by film rehydration.....	63
3.2.5.2. Giant vesicles by electroformation.....	64
3.2.6. Transmission electron microscopy (TEM).....	65
3.2.7. Atomic force microscopy (AFM).....	66
3.2.8. Light microscopy.....	66
3.2.9. Confocal laser scanning microscopy (CLSM).....	66
3.2.10 Dynamic light scattering (DLS).....	67
3.2.11 ¹ H Nuclear magnetic resonance spectroscopy (NMR).....	67
3.2.12. Infrared spectroscopy (IR).....	67
4. Results and discussion	69
4.1. Langmuir monolayers from pure amphiphiles	70
4.1.1. Compressional modulus of pure amphiphiles.....	72
4.1.2. Film thickness of pure triblock copolymers.....	73
4.1.3. Isothermal phase behavior of triblock copolymers.....	74
4.1.4. Film thickness and BAM of pure alamethicin.....	75

4.2. Mixed films at the air-water interface	77
4.2.1. Monolayers from lipid-alamethicin mixtures.....	77
4.2.1.1. Langmuir isotherms of mixed monolayers PC-alm.....	77
4.2.1.2. Compressional modulus of mixed monolayers PC-alm.....	80
4.2.2. Monolayers from polymer-alamethicin mixtures.....	81
4.2.2.1. Langmuir isotherms of mixed monolayers ABA-alm.....	81
4.2.2.2. Compressional modulus of mixed monolayers ABA-alm.....	83
4.2.2.3. Isothermal phase behavior of mixed monolayers ABA-alm.....	86
4.2.2.4. Brewster angle microscopy of mixed monolayers ABA-alm.....	87
4.2.2.5. Excess mixing energies of mixed monolayers.....	88
4.3. Langmuir-Blodgett films of mixed monolayers	90
4.3.1. Contact angle measurements.....	93
4.4. Bilayer systems of mixed membranes from copolymers and alm	95
4.4.1. Biological relevance of mixed monolayers.....	95
4.4.2. Mixed vesicles from block copolymers and alamethicin.....	96
4.4.2.1. Dynamic light scattering of mixed polymersomes.....	99
4.4.3. Ion transport activity of alamethicin in block copolymer membranes	102
4.4.3.1. Biomimetic mineralization in giant polymersomes.....	102
4.4.3.2. Biomimetic mineralization in small unilamellar polymersomes...	106
5. Conclusions and outlook	109
5.1. Conclusions	110
5.2. Outlook	112
6. References	113
7. Appendix	123
A Abbreviations.....	124
B Historical timeline of natural and synthetic macromolecules.....	127
C Curriculum vitae.....	131
D List of publications.....	132

*Das Leben ist wert, gelebt zu werden,
sagt die Kunst, die schönste Verführerin;
das Leben ist wert, erkannt zu werden,
sagt die Wissenschaft.*

Friedrich Nietzsche

CHAPTER 1

INTRODUCTION AND OBJECTIVE

1. Introduction and objective

In living systems, communication and interaction between cells and their environment is provided through membrane proteins. Transmembrane proteins transport various species across the lipid bilayers, either ions and larger substances [Nikaido 1992, Eisenberg 1998, Sansom 1999, Nardin 2001b, Braun 2002, Klebba 2002] or genetic material [Graff 2002, Duckely 2003, Abu-Arish 2004]. Also, proton gradient can be controlled to regulate the cells' energetic machinery, ATP synthesis etc. [Friedrich 1998].

Motivated by Nature, material science has recently taken advantage of certain solutions to implement membrane proteins in creating new materials with novel functions. The key issue is to create submicron-scale devices to serve as an innovative interface for controlling processes either in artificial systems, or complicated environments like cells. They also offer a new perspective in controlling or introducing new types of interactions at the boundary between natural and synthetic species.

It is well known that proteins' application could not always be straightforward due to their intrinsic properties: poor stability, changes in functionality in certain conditions, folding processes, solubility problems, etc. In cells, membrane proteins are embedded in or attached to lipid membranes, which provide protection and ensure functional conformation of the protein. Therefore, the most straightforward approach to produce membrane protein-based nanostructures is the use of artificial lipid membranes. Indeed, multiple examples of successful protein incorporation in lipid membranes were presented, employing various morphologies of the self assembled lipid superstructures.

Scotto et al. reported that bacteriorhodopsin incorporated spontaneously into both large unilamellar and multilamellar vesicles of various lipid compositions (liposomes) (Fig. 1.1a), including dimyristoyl phosphatidylcholine (DMPC), DMPC and cholesterol, dioleoyl phosphatidylcholine (DOPC), and DOPC and cholesterol. The examinations were made under either fluid-phase or gel conditions. The lipid/protein ratio as well as the vesicle size in function of protein content was investigated [Scotto 1990]. The insertion of membrane proteins depending on the lipid bilayer composition was successfully determined employing liposomes pointing that the highest incorporation of multiple proteins was found with dipalmitoylphosphatidylcholine (DPPC) [Daghastanli 2004].

Van Gelder et al. successfully employed free standing lipid membranes (black lipid membranes) (Fig. 1.1b) to detect the single channel activity of *OmpF*, a bacterial outer membrane porin [van Gelder 2000].

The protein structure within a membranelike environment was

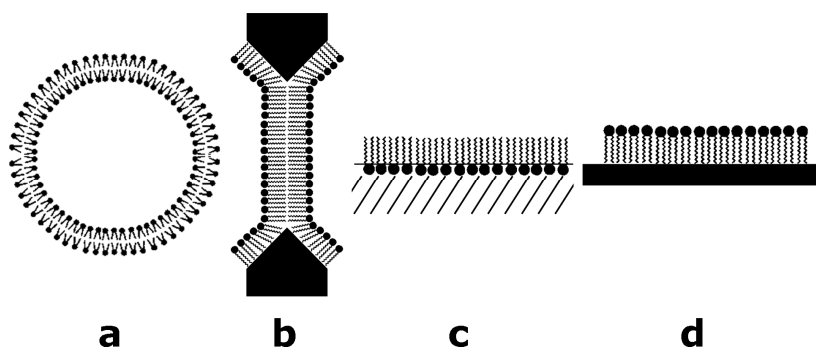


Figure 1.1. Artificial membrane systems to produce membrane protein-based nanostructures; a) vesicle, b) free standing membrane, c) Langmuir film, d) solid supported planar film.

investigated by Zheng et al. employing Langmuir films at the air-water interface (Fig. 1.1c). The transmembrane domains of Vpu, a HIV-1 accessory protein, were unidirectionally incorporated in lipid monolayers and probed by x-ray reflectivity and grazing incidence diffraction [Zheng 2004]. Specific membrane interactions of model cell membranes with blood-clotting proteins in Langmuir films at the air-water interface were reported by Brancato [Brancato 2001].

Rhodopsin has been reconstituted into supported planar lipid membranes (Fig. 1.1d) to measure coupling reactions with transducin to mimic receptor activation and interaction of a membrane receptor with its G protein [Heyse 1998].

In such materials, the membrane proteins were shown to remain functional and that some of them could serve for biomimetic transportation of different species.

Living cells, however, are highly dynamic systems, where every membrane defect will immediately be detected and repaired. In laboratory conditions and applied science any replacement of damaged or oxidized lipids is not achievable. Additionally, lipids themselves lack long-term stability and rigidity, which would render them applicable in biomaterials engineering. The most disadvantageous feature of (fluid) lipid bilayers is their rather high permeability, especially in what may seem the most obvious application of liposomes, i.e. drug delivery. Uncontrolled leakage through liposome membranes additionally poses storage problems.

For these reasons, it has been challenging to find other environments, in which the proteins would remain in their 'native' conformation, thus retaining functionality, and be protected from the hostile surrounding by a compatible matrix. A solution to this problem has been the use of other amphiphilic species, for example amphiphilic block copolymers. Shortly, they are built from at least two chemically incompatible parts (blocks) of different affinity to water. With a plethora of possibilities to create such polymers, in the context of block compositions, block lengths, and polymer architecture, polymer science offers the potential to engineer the most suitable polymers for specific applications. As macromolecules, such polymers may be very well suited to mimic biological amphiphiles and therefore are subject to studies as a complementary component in various bio-composite materials [Discher 2002].

There already exist a few literature reports proving experimentally successful incorporations of proteins into purely polymeric membranes, including evidence of protein functionality in such an artificial environment. Nardin et al. successfully reconstituted OmpF, a channel-forming protein from the outer cell wall of Gram-negative bacteria, into self-assembled membranes from amphiphilic PMOXA-PDMS-PMOXA triblock copolymers. Although two to three times thicker than biological membranes, the polymer membranes serve as a functional matrix for membrane-spanning proteins [Nardin 2000b, Nardin 2001b].

Employing vesicles made from the same PMOXA-PDMS-PMOXA block copolymer, Graff et al. proved that reconstituted LamB λ phage receptors effectively serve as binding site for phage transfection and DNA translocation over the artificial membrane barrier [Graff 2002].

PMOXA-PDMS-PMOXA triblock copolymer membranes were further reported to be successfully functionalized by bacteriorhodopsin and cytochrome c oxidase ion transport proteins [Ho 2004].

Pata and Dan [Pata 2003] proved theoretically that protein insertion into polymer membrane at least two-fold thicker than lipid bilayers is possible.

Even though the literature evidence proved successful incorporations of proteins into polymer matrices, nearly nothing is known on the physical chemistry of the insertion process, as well as the material properties of protein-reconstituted polymer membranes. Therefore, the motivation of this thesis is to investigate the behavior of a membrane active peptide, alamethicin, in the membranes from amphiphilic ABA triblock copolymers. As a model system, poly(2-methyloxazoline)-block-poly(dimethylsiloxane)-block-poly(2-methyloxazoline) (PMOXA-PDMS-PMOXA) copolymers were used, well characterized in previous studies concerning protein insertions [Nardin 2001b, Graff 2002].

The choice of alamethicin is justified by the fact that it is a relatively small amphiphilic peptide and could serve as a starting point for further work employing more complex proteins. Alamethicin is a peptide antibiotic naturally produced by *trichoderma viride*, which contains the non-proteinogenic amino acid, 1-amino isobutyric acid (Aib), inducing α -helical peptide structures. The peptide sequence is: Ac-Aib-Pro-Aib-Ala-Aib-Ala-Gln-Aib-Val-Aib-Gly-Leu-Aib-Pro-Val-Aib-Aib-Glu-Gln-Phe, where Phe is phenylalaninol. As a polyene ionophore, in cell membranes it is reported to form voltage-gated non-specific anion or cation transporting pores by aggregation of four to twelve molecules [Marsh 1996]. For further details and specifications on membrane materials and peptaibol employed I refer to chapter two of this thesis.

So far, organization of alamethicin in lipid membranes is still under discussion, even though data from various groups are available [Aguilella 2001, Taylor 1991]. The commonly accepted barrel stave model [Duclouhier 2001] has recently been confronted with a different explanation by Ionov et al. [Ionov 2000], who proposed a lipid-covered ring model. In the latter, alamethicin helices adopt stable planar orientation at the air-water interface, form aggregates with a ring-shaped hole and insert at one side of the lipid membrane. This model has been supported by AFM and X-ray diffraction experiments [Ionov 2004].

A recent report [Vijayan 2005] presents the influence of alamethicin on stability of membranes from amphiphilic diblock copolymers. Fluorescence dye leakage and micropipette manipulation studies showed that the membrane permeability strongly depends on its thickness and therefore on the size of the constituting blocks.

The purpose of this work is to characterize peptide-polymer composite materials in terms of miscibility (or phase separation), aggregation behavior and ion permeability, firstly to find the most favorable conditions for the insertion, and secondly, to get more insight into the process itself and the material properties further on. Investigations on planar membranes at the air-water interface were performed employing the Langmuir monolayer technique, supported by Brewster angle microscopy imaging, and further solid supported Langmuir-Blodgett films in combination with topography analysis by atomic force microscopy. The membrane interactions of alamethicin with block copolymer membranes, especially in the context of membrane permeability, were probed in addition employing fully hydrated bilayer systems. Experiments were carried out with giant and small polymersomes characterized by transmission electron microscopy and dynamic light scattering.

*Wer sich Steine zurechtlegen kann,
über die er stolpert, hat Erfolg
in den Naturwissenschaften.*

Erwin Chargaff

CHAPTER 2

THEORETICAL BACKGROUND

2. Theoretical Background

2.1. Molecular interactions at the air-water interface

2.1.1. History of monolayer research

The effects of oil on water surfaces have been known for many centuries [Gaines 1983, Tredgold 1987]. Babylonians in the eighteenth century BC already practiced divinity by observing effects of oils spread on water. From the shape and movement of olive oil stains poured on water surfaces, the future of both the country and individual citizens was predicted [Tabor 1980].

The first definite historical reference was made by Aristoteles (BC 384-322). He stated, that 'oil poured on to water makes it more transparent' [Hett 1937]. Gaius Plinius Secundus (Fig. 2.1) was rather more explicit when he noted in AD 77 in his famous encyclopedia *Naturalis Historia* 'again everybody is aware that ... all sea water is made smooth by oil, and so divers sprinkle oil from their mouth because it calms the rough element and carries light down with them...' [Rackham 1964]. Similar observations were made by Plutarch (AD 45-125) in Greece [Tabor 1980].



Figure 2.1. Gaius Plinius Secundus Maior (23-79) [Rackham 1964].

One of the first technical applications of floating monolayers reported was the Japanese printing art of *sumi-nagashi* of the 12th century, in which a suspension of colloidal carbon particles and proteins was spread on water, mixed to give diffuse patterns, fixated with gelatine and then transferred onto a sheet of paper [Albertova 1987].

In 1757, aboard one of 96 ships traveling together from America to Europe, Benjamin Franklin (Fig. 2.2) noticed, that ships in the back seemed to have smoother sailing than ships in the front. The captain explained that 'The cooks have been just emptying their greasy water through the scuppers, which has greased the sides of those ships a little.' [Bigelow 1966]. In 1762 Franklin was told by an old sailor, that Bermudians put oil on water to smooth the surface when they would strike fish which they could not see when the water was ruffled by the wind. The same gentleman told him that it was a practice with the fishermen in Lisbon when about to return into the river to empty a bottle or two of oil into the sea to suppress the breakers and allow them to pass safely. He further learned from a friend, Sir John Pringle, that those employed in herring fishery in Scotland could at a distance see where the shoals of herring were by the smoothness of the water over them, which might possibly be occasioned, he thought, by some oiliness proceeding from their bodies [Fulford 1968].

All those informations caught Franklin's scientific interest and he wondered to find no mention of them in the books of experimental philosophy of that time. Once in London he spread oil onto a pond and observed a calming influence on the water

surface. In 1774 he reported to the Royal Society of London that ‘At length at Clapham where there is, on the common, a large pond, which I observed to be one day very rough with the wind, I fetched out a cruet of oil, and dropped a little of it on the water. I saw it spread itself with surprising swiftness upon the surface... the oil, though not more than a teaspoonful, produced an instant calm over a space several yards square, which spread amazingly, and extended itself gradually, making the pond as smooth as a looking glass.’ He suggested that due to a mutual repulsion between the oil particles and no attraction between oil and water, the oil film expands on the surface to an extension until the repulsion between the oil particles is minimized. If wind is blowing over the water, the oil film prevents friction and the wind cannot catch the water to raise wrinkles. Further he described the ‘interesting effect of monolayer films on supposedly dead flies’ [Franklin 1774], inventing the first fruit fly trap [Ringhof 2004].

However neither Aristoteles, nor Plinius, nor Franklin recognized the monolayers for what they were, and they could scarcely have had a realistic idea of the true nature of what they were seeing, because they did not have the scientific concept of atoms and molecules.



Figure 2.3. Agnes Pockles 1862-1935 [Beisswanger 1991].

olive oil. This effect was noted to be accompanied by a change in molecular area values [Rayleigh 1890]. He additionally suspected that the maximum extension of an oil film on water represents a layer one molecule thick [Rayleigh 1899]. Further investigations by Devaux [Devaux 1913], Hardy [Hardy 1911] and Harkins [Harkins 1917] confirmed the mono-molecular nature of such films [Giles 1971].

However it was Irwing Langmuir (Fig. 2.5) who contributed the greatest advances. In his experiments, he used chemically pure substances, both solids and liquids, instead of oil or olive oil used previously. By investigating the pressure-



Figure 2.2. Benjamin Franklin (1706-1790) posing on the US one hundred dollar bill.

Modern investigations began with Agnes Pockles (Fig. 2.3) experimenting with a very rudimentary setup (an ordinary baking tray, waxed to make it hydrophobic, as trough and a button as duNoüy ring) in her kitchen. She was the first to measure the film behavior depending on the amount of olive oil spread. Her surface pressure versus area per molecule isotherms are in good agreement with those obtained presently using modern experimental techniques. Her findings on technical and practical aspects were published in Nature in 1891 [Pockles 1891].

Scientific activity in thin film studies increased after the reports of Lord Rayleigh (Fig 2.4). One of his most important conclusions was that the surface tension of an aqueous solution decreases as the surface is ‘contaminated’ with

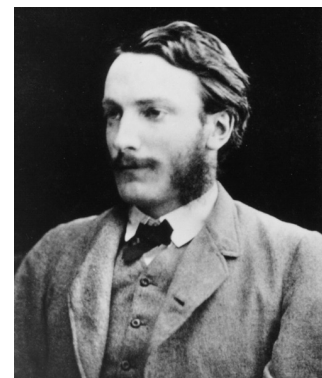


Figure 2.4. John William Strutt Lord Rayleigh (1842-1919) [AIP].

area relationship of molecules on aqueous surfaces he found, that the areas occupied by molecules such as acids, alcohols and esters are independent of the hydrocarbon chain length, thus showing that only the hydrophilic head groups are immersed in the subphase [Langmuir 1916, 1917a, 1917b]. For his discoveries and investigations in surface chemistry he was awarded the Nobel Prize in Chemistry in 1932.

Katherine Blodgett (Fig. 2.6), who worked with Langmuir, developed the technique of transferring the films on solid substrates and hence building up multilayer films in 1934 [Blodgett 1934, 1935] and published its first application as anti-reflection coatings on glass [Blodgett 1939]. Such built-up monolayer assemblies transferred to a solid substrate are therefore referred to as Langmuir-Blodgett (LB) films. The term Langmuir film is normally reserved for a floating monolayer.

Interest in Langmuir-Blodgett films subsided with the outbreak of the Second World War and remained low until the 1960's when Hans Kuhn showed how monolayer films with molecular-scale patterning could be fabricated industrially and further manipulated to build up more complex systems [Kuhn 1967, 1971, 1972]. His work and the publications of Gaines [Gaines 1966] initiated a revival of interest in the field.



Figure 2.6. Katherine Blodgett (1898-1979) working in her laboratory [GE 1992].

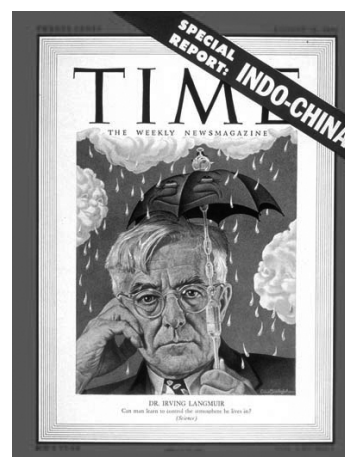


Figure 2.5. Irving Langmuir (1881-1957) posing on a Time Magazine cover (August 28, 1950).

The first international conference on LB-films was held in 1979 and since then many possible investigations using Langmuir and Langmuir-Blodgett films in the fields of chemistry, physics, biology and engineering for applications such as sensors, detectors, displays and electronic circuits are performed by researchers throughout the world.

2.1.2. Forces at the air-water interface

Molecules in a solution are subject to attractive forces. In the bulk, these forces are equal. However, at an interface the forces are dissimilar and the net effect is to pull the peripheral molecules into the bulk of the solution. At the interface there are fewer molecules on the vapor side than on the liquid side. This leads to a net attractive force towards the bulk and hence the density increases gradually from the surface to the bulk. Therefore liquids tend to decrease the surface energy by minimizing the surface (Fig. 2.7) [Adamson 1976, Wu 1982].

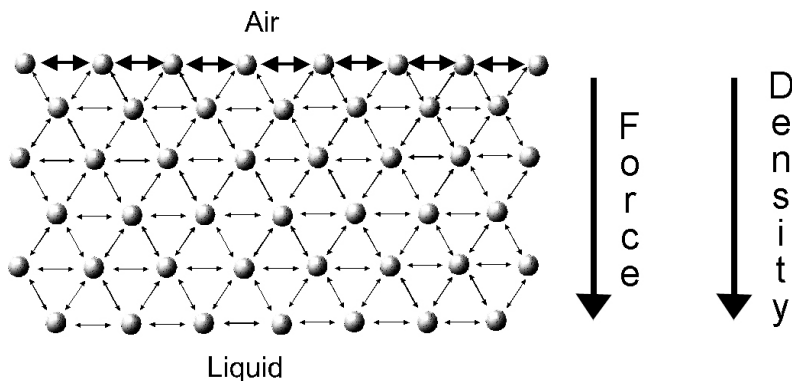


Figure 2.7. Schematic illustration of the interactions of molecules at an interface and in bulk [KSV].

The surface tension γ is a measure of the cohesive energy present at an interface and can be defined as the work dW required to expand the surface isothermally by unit area dA . The tendency of surface active molecules to accumulate at interfaces favors expansion of the interface and hence lowers the surface tension.

$$dW = \gamma dA$$

(Eq. 2.1)

Surface tension readings are made by means of Wilhelmy plates [Wilhelmy, 1863, Dettre 1966, Pallas 1983] or DuNoüy rings [Harkins 1930, Huh 1975] attached to a sensitive electrobalance (Figures 2.8 – 2.10). The force necessary to detach the Wilhelmy plate or the DuNoüy ring from the liquid surface is measured. The Wilhelmy plate is usually a strip of chromatography paper or a platinum plate whereas the DuNoüy ring is made of platinum. When such a probe is suspended at an air-water interface, it is pulled down into the bulk of the subphase by the surface tension of the water. The forces upon the probe are gravity and surface tension acting downwards and buoyancy due to displacement of water acting upwards.

Surface tension readings are made by means of Wilhelmy plates [Wilhelmy, 1863, Dettre 1966, Pallas 1983] or DuNoüy rings [Harkins 1930, Huh 1975] attached to a sensitive electrobalance

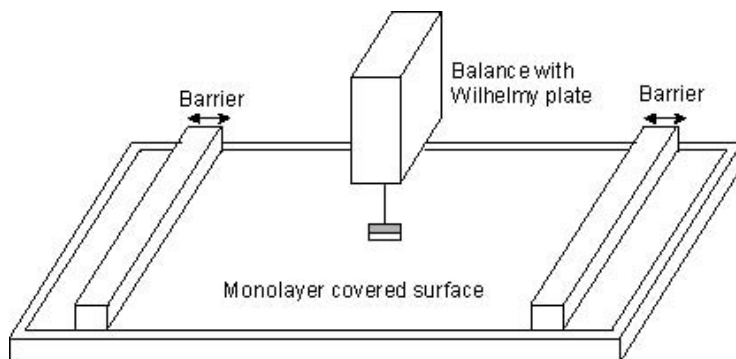


Figure 2.8. Schematic representation of a Langmuir film balance [KSV].

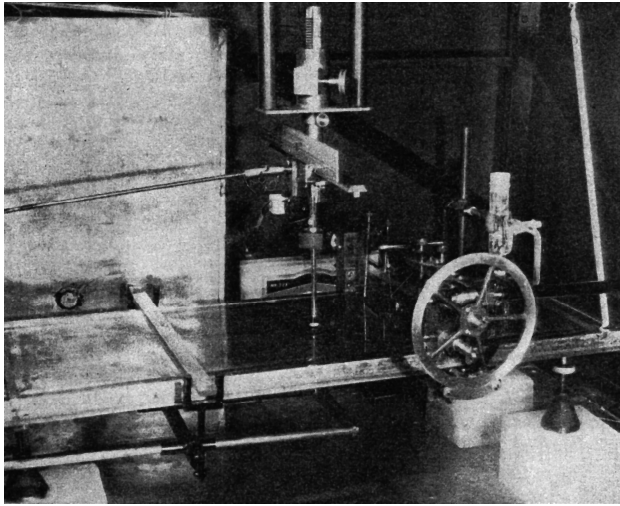


Figure 2.9. Langmuir film balance (1932 model) [Harkins 1952].

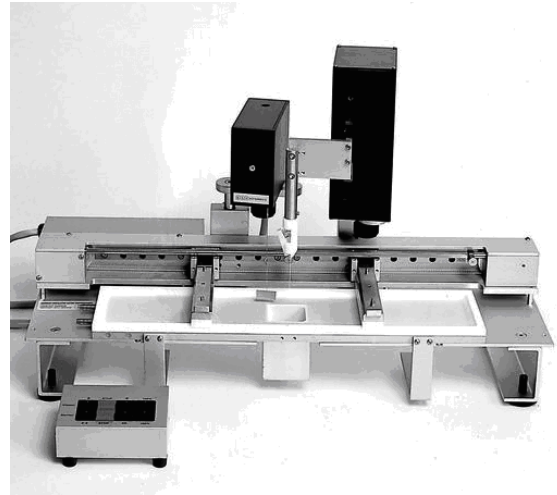


Figure 2.10. Langmuir film balance (2005 model) [KSV].

The net force downwards, F , is described as

$$F = m_p g - m_w g + P \gamma \cos \theta. \quad (\text{Eq. 2.2})$$

(force = gravity – up thrust + surface tension)

m_p = mass of probe

g = specific gravity

P = Perimeter of probe

θ = contact angle

m_w = mass of displaced water

By zeroing the initial pressure the weight term can be eliminated. The up thrust is eliminated as the probe is always kept at constant level. Finally the contact angle is constant yielding a reduced expression.

$$F = P \gamma \quad (\text{Eq. 2.3})$$

Hence the surface tension can be expressed in general as the fraction of the force divided by the perimeter. Thus the sensitivity of a surface tension measurement can be increased by utilizing a very thin probe.

$$\gamma = F / P \quad [\text{mN/m} = \text{dyne/cm} = \text{erg/cm}^2 = \text{mJ/m}^2] \quad (\text{Eq. 2.4})$$

Surface tension can also be expressed as energy needed to alter the surface area.

2.1.3. Langmuir films

A Langmuir film consists of surface active agents (surfactants) trapped at the interface between two dissimilar phases, either liquid-liquid or liquid-gas [Roberts 1990, Martin 1999]. Surfactants are molecules which are amphiphilic that is molecules which are composed of a hydrophilic part and a hydrophobic part. The hydrophilic groups are attracted to polar media predominantly driven by Coulomb-type forces (r^{-2}). Hydrophobic groups are much less (if at all) soluble in polar solvents and the forces acting upon them are mostly Van der Waal's type (r^{-12} and r^{-6}).

When surfactants, dissolved in a volatile solvent, are introduced onto a polar liquid surface, the solvent will evaporate leaving the surfactants oriented at the liquid-gas interface – the hydrophilic groups pulled into the bulk of the water and the hydrophobic parts pointing to the air. A monolayer will be achieved only for a certain amphiphatic balance of hydrophobic and hydrophilic parts of the molecules. The size and shape of the apolar moiety and the size, charge and hydration of the polar segment are the important physical and chemical properties. If the hydrophobic segment is too short or not hydrophobic enough, the molecules will be dragged into the water. If there is no hydrophilic part, the molecules may form thicker multilayer films or even evaporate.

As most solvents used are slightly soluble in water, depletion of the spreading solvent will not be due exclusively to evaporation but also to some dissolution of it into the subphase.

Spontaneous spreading of the surfactant will continue until the surface pressure of the monolayer is equal to the equilibrium spreading pressure. At this point, the entire available surface is homogeneously covered by single molecules distributed at equal distances.

Compressing a monolayer e.g. by sweeping a barrier over the water surface will force the surfactant molecules to come closer together and eventually form an ordered monolayer. The film produced by such a method is known as Langmuir film.

2.1.3.1. Surface pressure-area isotherms

The characteristics of a monolayer at the air-water interface can be studied by measuring the changes of surface tension upon compressing the monolayer. The reduction of surface tension is known as the surface pressure π which is proportional to the concentration c_i of surfactant [Traube 1891].

$$\pi = \gamma_0 - \gamma = kc_i \quad (\text{Eq. 2.5})$$

γ_0 = surface tension in absence of surfactants

γ = surface tension with the monolayer present

k = empirical constant

The plot of surface pressure π versus area occupied per molecule A is known as a surface pressure-area isotherm or π - A -isotherm because compression takes place at constant temperature. The distinct regions apparent on examining an isotherm are called phases, which are identified as discontinuities in the isotherm. The shape of the isotherm and the phase behavior of the monolayer are characteristic of the molecules making the film and hence provide a two-dimensional fingerprint (Figure 2.11).

A simple terminology used to classify different monolayer phases of fatty acids has been proposed by Harkins [Harkins 1952].

After initial deposition of surfactant at low concentration onto the sub phase, when no external pressure is applied to the monolayer, the molecules behave as a two-dimensional gas (G). The average area per molecule is large, although locally they can cluster into small islands or clumps.

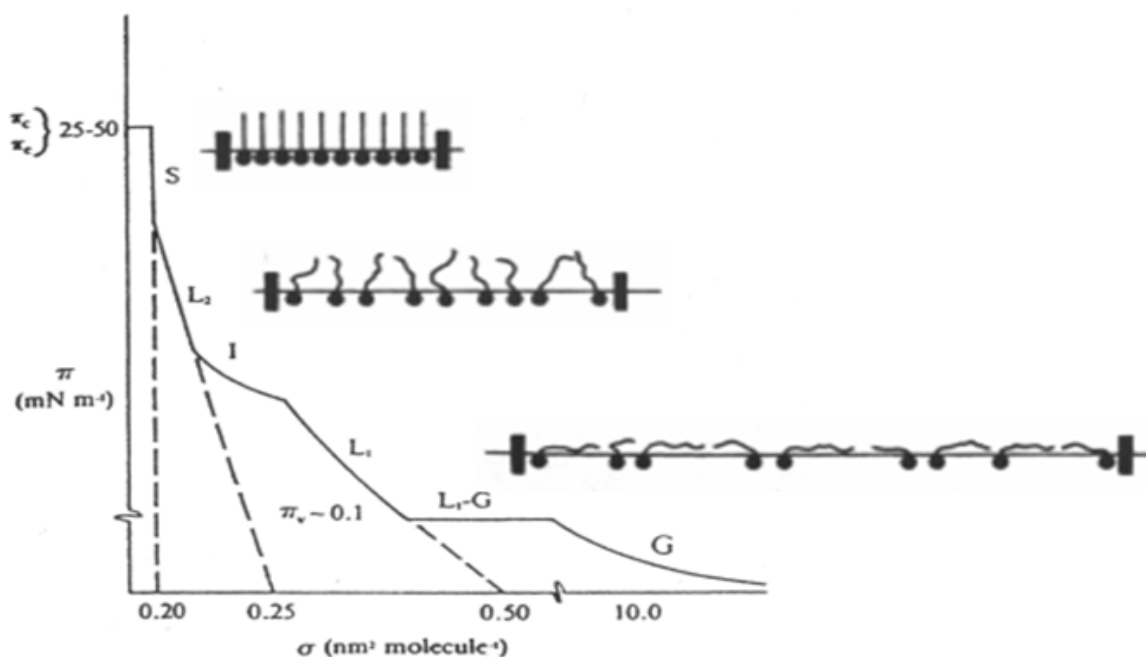


Figure 2.11. Schematic illustration of a π - A -isotherm and orientation of molecules in different phases [Gaines 1966, Roberts 1990].

On compression of the film, lateral interactions between the individual surfactant molecules develop and ordering of the films takes place. A phase transition to a two-dimensional liquid-expanded state (L_1) occurs. The area per molecule is smaller than in the G phase, but still significantly greater than that of close-packed molecules. This phase is often followed by a plateau [Hamley 2000]. Further ordering causes additional increase in pressure, yielding a monolayer in liquid-condensed state (L_2) and at even higher densities a quasi-solid or superliquid state (S). A steep rise of surface pressure indicates the formation of two-dimensional condensed phases.

If the forces exerted become too strong for confinement in two dimensions, molecules are ejected out of the monolayer into either the subphase (micellization; more hydrophilic molecules) or the superphase (multilayer formation; more hydrophobic molecules). This collapse is not uniform across the monolayer but is usually initiated near the leading edge of the barrier or at discontinuities in the trough. The collapse is generally seen as a rapid decrease in the surface pressure or as a horizontal break. The collapse pressure π_c can be defined as the maximum to which a monolayer can be compressed without detectable expulsion of molecules from the film.

Quantitative information can be achieved on the molecular dimensions of the surfactants. When the monolayer is in the two-dimensional solid or liquid condensed phase the molecules are well oriented and closely packed. The zero-pressure molecular area A_0 can then be obtained by extrapolating the slope of the condensed phase to zero pressure. Such an area corresponds to a hypothetical cross-sectional area occupied by one molecule in the condensed phase at zero pressure.

Although amphiphiles form lyotropic liquid crystalline phases in the bulk, these two-dimensional monolayer phases are in fact analogues of thermotropic liquid crystalline phases. This is because the symmetry of the structure is determined by the packing of molecules and not by the packing of molecular aggregates [Hamley 2000].

2.1.3.2. Mixed monolayers

Monolayers can not only be one- but also multi component [Dynałowicz-Łatka 1999]. A very interesting feature of two-dimensional monolayers, formed by two components each capable of independent monolayer formation, is the fact that they show different interfacial properties than those of individual components. It is well known that the particular components in the mixture can interact with each other to produce either favorable or unfavorable effects. Generally, four types of mixed systems behavior are known, i.e. synergy, antagonism, additivity or indifference. The first two effects are due to the existence of molecular interaction - in other words - ideality deviations.

The origin of the interactions existing in mixed monolayers comes from the chemical structure of individual components, possessing a hydrophilic 'head' and a hydrophobic 'tail'. Two different effects influence the strength of interactions. One of them is the attractive forces between hydrocarbon chains. The other effect is due to interacting 'heads' which can be of the same or different kind, e.g. non-ionic, cationic or anionic. The electric charge causes them to attract or repulse each other. These interactions are much stronger in comparison to the hydrocarbon chains association and therefore are mostly responsible for the deviations from ideality [Holland 1991]. Due to the fact that intermolecular forces occur in all monolayers, it has been suggested, that the term 'excess interaction' shall be used for mixed monolayers instead of 'molecular interaction' [Costin 1975].

Interactions can be interpreted based on miscibility of mixed monolayer components, analogically to the interpretation of binary volume mixtures which components can be completely miscible, partially miscible or immiscible (Fig. 2.12).

A mixed monolayer shows non-ideal behavior, caused by significant molecular interactions, when its properties do not depend linearly on the monolayer composition [Costin 1975]. For binary mixtures the Goodrich-Gaines thermodynamic model [Gaines 1966] can be applied and in favorable circumstances information obtained on the miscibility of the two components in the amphiphile mixture which forms the film [Jones 1999].

The area of mixed monolayer can be compared to that of the unmixed, pure component monolayers at the same surface pressure to give the excess area of mixing A^{exc} . The excess area of mixing is the difference between this ideal value A_{id} calculated from the surface pressure data of the two components and the value recorded for the mixture A_{12} .

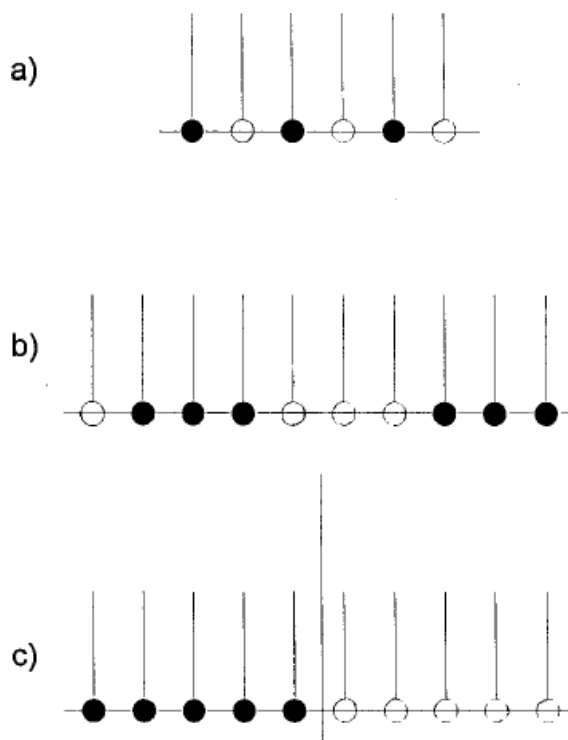


Figure 2.12. Possible distribution of molecules in mixed monolayers (a) miscible components, homogenous mixed film; (b) immiscible components, non-homogenous mixed film; (c) immiscible components, complete separation [Dynałowicz-Łatka 1999].

$$A_{id} = A_1X_1 + A_2X_2 \quad (\text{Eq. 2.6})$$

$$A^{exc} = A_{12} - A_{id} \quad (\text{Eq. 2.7})$$

A_{id} = calculated mean molecular area in an ideal mixed monolayer

A_1, A_2 = mean molecular area in single component monolayer

X_1, X_2 = mole fractions of components

A_{12} = effective mean molecular area in the mixed monolayer

If the mixture is ideal or if the components are immiscible A^{exc} is zero [Gaines 1966], condensation [Cadenhead 1980] or contraction [Costin 1975] lead to negative values contrary to expansion where A^{exc} is positive [Galvez Ruiz 1991].

Further, if the mixture is ideal or if the components are immiscible the plot $A^{exc} = f(X_i)$ is linear [Gaines 1966, Chatteraj 1984], partially miscible if there are linear segments [Bacon 1978] and deviations from these conditions indicate miscibility and non-ideality [Cadenhead 1968].

The excess Gibbs free energy of mixing ΔG^{exc} of the mixed film can be obtained from

$$\Delta G^{exc} = \int_0^\pi A^{exc} d\pi = A^{exc} \pi . \quad (\text{Eq. 2.8})$$

A stable monolayer is formed if the excess Gibbs free energy is negative. If ΔG^{exc} is positive the film is likely to phase separate.

The Gibbs free energy of ideal mixing ΔG^{id} is given as follows

$$\Delta G^{id} = RT(X_1 \ln X_1 + X_2 \ln X_2) \quad (\text{Eq. 2.9})$$

Finally, the total Gibbs free energy of mixing ΔG^m is the difference between the ideal mixing energy and the value obtained from the experimental isotherm data

$$\Delta G^m = \Delta G^{exc} - \Delta G^{id} . \quad (\text{Eq. 2.10})$$

A mixed state is energetically more stable than an unmixed state if the total Gibbs free energy ΔG^{exc} is negative.

Thus when excess area of mixing A^{exc} is negative, the Gibbs free energy of the mixed system is less than that predicted from the classical Gibbs free energy of mixing equation and the monolayer will be stable and mixed. When A^{exc} values are positive, the excess Gibbs free energy of mixing is positive and, depending on the magnitude of this excess Gibbs free energy relative to the classical contribution, amphiphiles in the spread films need not be in a molecularly mixed state [Gabrielli 1982, Jones 1999].

Similarly, ideality can also be tested by making surface pressure-composition plots at constant molecular area:

$$\pi_{id} = \pi_1 X_1 + \pi_2 X_2. \quad (\text{Eq. 2.11})$$

π_{id} = calculated surface pressure of ideal mixed monolayer

π_1, π_2 = surface pressure of single component monolayer

X_1, X_2 = mole fractions of components

As in the former relationship (Eq. 2.7), deviations from linearity of the function $\pi_{id} = f(X_i)$ indicate the existence of interactions while linearity proves either ideal mixture or complete immiscibility.

Also systems with more than two components can be investigated. By keeping the ratio X_1/X_2 constant and varying X_3 , one can determine the interactions.

Further insight on miscibility can be obtained by analysis of the surface pressure-area isotherms at the collapse pressure π_c . When the components are miscible, the value of π_c depends on the molar fraction of its components, lying between the collapse pressures of pure components. If the components are immiscible, two collapse pressures at constant value, corresponding to the pure components, are observed (Fig. 2.13).

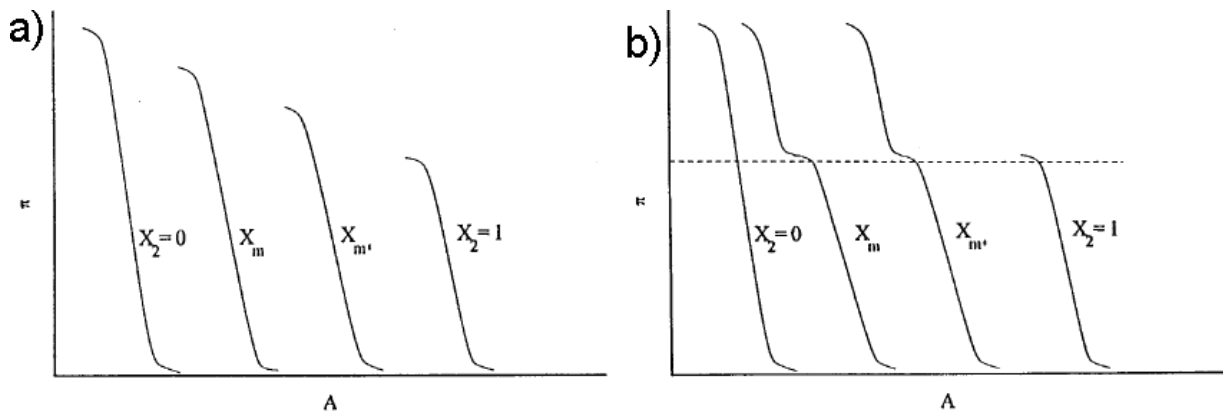


Figure 2.13. Dependence of surface pressure-area isotherms for mixed films with miscible (a) and immiscible (b) components [Dynałowicz-Łatka 1999].

It is known that the collapse pressure π_c of a film is characteristic of the degree of interaction between the film-forming components. If the two components are immiscible, then the $\pi - A$ isotherm would exhibit the following behavior:

The individual components would be present separately, and as the value of π reaches a value equivalent to $\pi_{c,1}$ (component 1 with the lower collapse pressure), one will observe a collapse state. The second component would then be ejected at the corresponding surface pressure [Birdi 1989].

This can be explained based on the Gibbs surface phase-rule principle [Defay 1966, Gaines 1966, Birdi 1989]

$$L = (C_v + C_s) - (F_v + F_s) + 3. \quad (\text{Eq. 2.12})$$

L = number of degrees of freedom (e.g. temperature, external pressure, surface pressure, monolayer composition....)

C_v = number of components in the bulk phase

C_s = number of components at the surface

F_v = number of bulk phases in equilibrium

F_s = number of surface phases in equilibrium

For a two component mixed monolayer the number of components in the bulk, C_v , is two (air and water), whereas the number of components at the surface is equal to two as well (two surfactants).

In case of miscibility there is one homogenous surface phase $F_s = 1$. At the collapse pressure there are three bulk phases $F_v = 3$ (air, water & collapsed monolayer). The number of degrees of freedom L is therefore 3. When temperature and external pressure are kept constant the degree of freedom equals one which means that collapse pressure directly depends on the composition of the mixed film.

In case of immiscibility, the number of surface phases at the collapse F_s equals 2. With three bulk phase $F_v = 3$ (air, water & collapsed monolayer) there are only two degrees of freedom, $L = 2$. At constant T and p the system has zero degrees of freedom and thus collapse pressure is constant for all mixtures.

Molecularly mixing two-component monolayers have been classified into several types according to their intrinsic $\pi - A$ and $\pi - X$ isotherms:

cigar-type mixed isotherms, modified cigar-type isotherms, positive azeotropic type isotherms, negative azeotropic type isotherms, eutectic type isotherms and complicated-type isotherms [Matuo 1981, Birdi 1989]. Du lieber Gott! Was so ein Mann nicht alles, alles denken kann! Beschämt nur steh' ich vor ihm da. Und sag' zu allen Sachen ja. Bin doch ein arm unwissend Kind, begreife nicht, was er an mir find't [Goethe].

Further approaches in describing the excess interactions between components in mixed Langmuir monolayers are given in the excellent review by Dynarowicz-Latka and Kita [Dynarowicz-Latka 1999]. For example information can be gained by analysing the surface pressure stability [Crisp 1949], by estimation of surface activity coefficients [Mestres 1992] or by expressing the interactions as excess thermodynamic functions (e.g. entropy, enthalpy, free energy) [Goodrich 1957, Costin 1975].

2.1.3.3. Surface elasticity

Elasticity is the ability of a material to change its physical dimensions when a force is applied to it and then to restore its original size and shape when the force is removed. In general, solid materials exhibit linear elastic properties for small deformations. This means that there is a linear relationship between the amount of deformation and the amount of response.

The film elasticity describes the differential change in surface tension with relative change in area (also termed surface elasticity, dilational elasticity, areal elasticity, compressional modulus, surface dilational modulus or modulus of surface elasticity). The compressibility is the inverse of film elasticity.

Compressibility is a measure of the relative volume change of fluid or solid as a response to an applied compressional stress.

$$C_s = -\frac{1}{V} \left(\frac{\partial V}{\partial P} \right)_T \quad (\text{Eq. 2.13})$$

The 2d compressibility C_s [m/mN] of mixed monolayers is calculated from [Dy-narowicz-Łatka 1999]

$$C_s = -\frac{1}{A_{12}} \left(\frac{\partial A_{12}}{\partial \pi_{12}} \right)_T, \quad (\text{Eq. 2.14})$$

where A_{12} is mean molecular area in \AA^2 and π_{12} is the surface pressure corresponding to that area in mN/m. Normally, in literature compressional moduli, C_s^{-1} [mN/m], are found:

$$C_s^{-1} = -A_{12} \left(\frac{\partial \pi_{12}}{\partial A_{12}} \right)_T. \quad (\text{Eq. 2.15})$$

If the modulus is plotted against the mean molecular area, peaks should be visible: the higher the peak the more organized the physical state of the monolayer, thus it is possible to discriminate the order regime of the phase. The approximate compressibility (or compressional modulus) values can be found in literature [Harkins 1992, Kita 2002] (Table 2.1).

Monolayer state	Approximate compressibility
gas (G)	above $4 \cdot 10^{-2}$ [m/mN]
liquid expanded (LE)	$2 \cdot 10^{-2}$ to $7 \cdot 10^{-2}$ [m/mN]
liquid condensed (LC)	$5 \cdot 10^{-3}$ to 10^{-2} [m/mN]
superliquid (LS)	$5 \cdot 10^{-4}$ to $1.7 \cdot 10^{-3}$ [m/mN]
solid (S)	$5 \cdot 10^{-4}$ to 10^{-3} [m/mN]

Table 2.1. Approximate compressibility values of monolayer states [Harkins 1992, Kita 2002].

Proper characterization of monolayer phases and transitions between them is of great importance. Investigation of the 2d compressibility allows in many cases better elucidation of phase transitions. The detectability of phase transitions can be increased significantly by plotting $C_s - A$ or $C_s - \pi$ curves instead of $\pi - A$ curves. In addition, the asymmetry of a peak indicates how many steps (molecular reorientations) contribute to a transition. Deconvolution of a peak directly yields the number of molecular orientations taking place during a phase change [Yu 2002].

2.1.4. Brewster angle microscopy

Brewster Angle Microscopy (BAM) is a technique that allows the in situ observation of ultrathin films at the gas/liquid or gas/solid interfaces or in general on transparent dielectric substrates. It was invented independently and almost simultaneously by two groups, that of Jacques Meunier in Paris, France and that of Dietmar Möbius in Göttingen, Germany [Hénon 1991, Hönig 1991].

It is named after Sir David Brewster a 19th century Scottish physicist, who investigated the reflection of light from polished surfaces (Fig. 2.14). In 1811 he discovered that reflected light is always partially polarized. In fact, at a particular angle of reflection, constant for a given interface, the reflected light becomes completely polarized (Fig. 2.15).

The light of the polarization with its electric field vector parallel to the surface (TE- or s-polarization) is always partly reflected and partly transmitted or absorbed. However at the Brewster angle, the light with its electric field vector parallel to the plane of incidence (TM- or p-polarized) is completely transmitted or absorbed. None of it is reflected. This angle is satisfying the relationship

$$\tan \theta = \frac{n_{\text{subphase}}}{n_{\text{superphase}}}, \quad (\text{Eq. 2.16})$$

where n is the refractive index of the corresponding phase.

Nevertheless this is only true for a Fresnel interface (an interface where the refractive index changes steeply). For a real interface, the reflected light intensity has a minimum at the Brewster angle, but does not vanish.

The principle of the Brewster angle microscope (BAM) is as follows:

A monolayer introduced in between two phases is extremely thin, approximately 0.5% of the wavelength of visible light. The relative effect it has on the electric field reflected from a water surface is therefore very small. However if the water surface is illuminated with p-polarized light at the Brewster angle, there is no reflection from the water surface and the background is completely dark. Due to the minimal changes of the optical properties through introduction of a thin film it is possible to make out the tiny effect of the monolayer.

The reflected intensity at the Brewster angle is strongly dependent on the interfacial properties and is particularly sensitive to monolayers at the interface. The reflectivity of a real interface at the Brewster angle for the mentioned polarization has three origins: (a) the

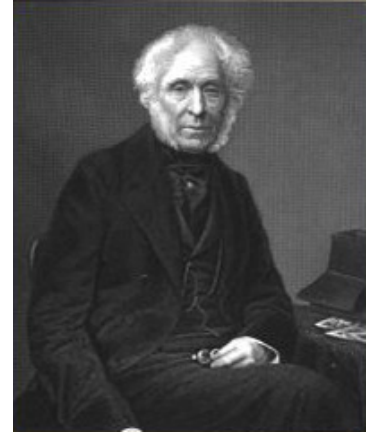


Figure 2.14. Sir David Brewster (1781-1868) [Intaglio].

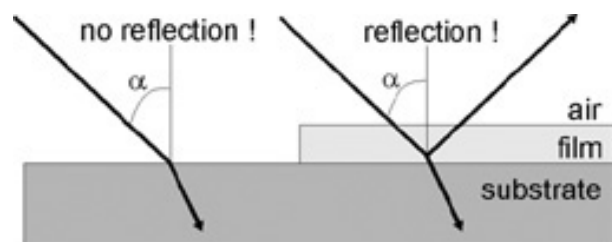


Figure 2.15. Reflection of polarized light at Brewster angle in absence and in presence of a thin film at the interface [Nanofilm].

thickness and density of the interface, (b) the roughness of real interfaces, and (c) the anisotropy of phase domains in monolayers.

A Brewster angle microscope (BAM) is comprised of a light source (laser), a set of one or two polarizing filters of which the first is responsible for the polarization of the beam prior to its reflection and the second is analyzing the polarization state of the reflected part of the beam and a light detector (a CCD camera) (Fig. 2.16).

The 'black background' of the Brewster Angle setup allows using the detector (CCD-camera) with the maximum of intensity. Typically, the resulting reflection due to a monolayer is only about a millionth of the incident intensity. The reflected light can be used to form a high contrast image of the lateral morphology of the layer.

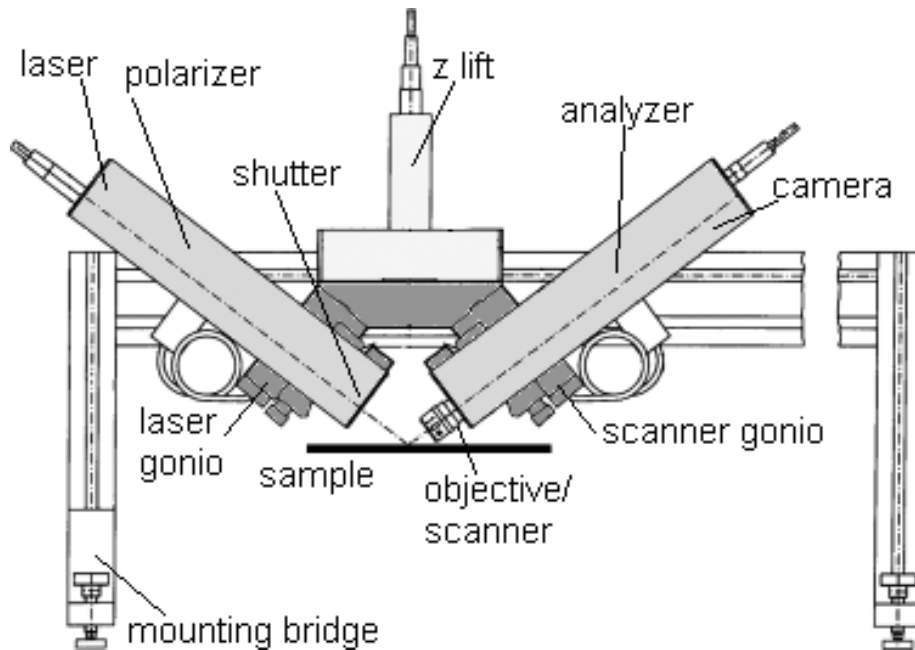


Figure 2.16. Schematic of a BAM setup [Nanofilm].

2.1.5. Langmuir-Blodgett films

Langmuir-Blodgett (LB) films consist of mono-molecular layers stacked sequentially onto a solid substrate. An appropriate solid substrate is lowered or raised from the subphase, breaking through the Langmuir film. The film attaches itself to the substrate, coating it with a mono-molecular layer (Fig. 2.17).

Once the first layer has been transferred, further layers will be deposited on each subsequent pass of the substrate through the air-water interface. Multilayers can therefore be built to produce a film of defined thickness. These transferred films can then be analyzed by surface topography techniques (e.g. AFM, reflectometry). LB films are unique systems allowing to precisely tailor the films in respect to molecular orientation, organization and thickness.

For a homogenous transfer the surface pressure needs to be kept constant. This is usually achieved by a computer controlled feedback system between the electrobalance and the barrier moving mechanism.

The LB deposition is traditionally carried out in the liquid-condensed or solid phase. The surface pressure is then high enough to ensure sufficient cohesion in the monolayer, i.e. the attraction between the molecules in the monolayer is high enough so that the monolayer does not fall apart during transfer to the solid substrate. This also ensures the build up of homogeneous multilayers. The surface pressure value that gives the best results depends on the nature of the monolayer and is usually established empirically.

When the solid substrate is hydrophilic (glass, mica, SiO_2 etc.) the first layer is deposited by raising the solid substrate from the subphase through the monolayer, whereas if the solid substrate is hydrophobic (HOPG, silanized SiO_2 etc.) the first layer is deposited by lowering the substrate into the sub phase through the monolayer.

There are several parameters that affect the type of LB film produced. These are the nature of the spread film, the subphase composition and temperature, the surface pressure during the deposition and the deposition speed, the type and nature of the solid substrate and the time the solid substrate is stored in air or in the subphase between the deposition cycles.

The quantity and the quality of the deposited monolayer on a solid support are measured by a so called transfer ratio TR. This is defined as the ratio between the decrease in monolayer area during a deposition stroke and the area of the substrate.

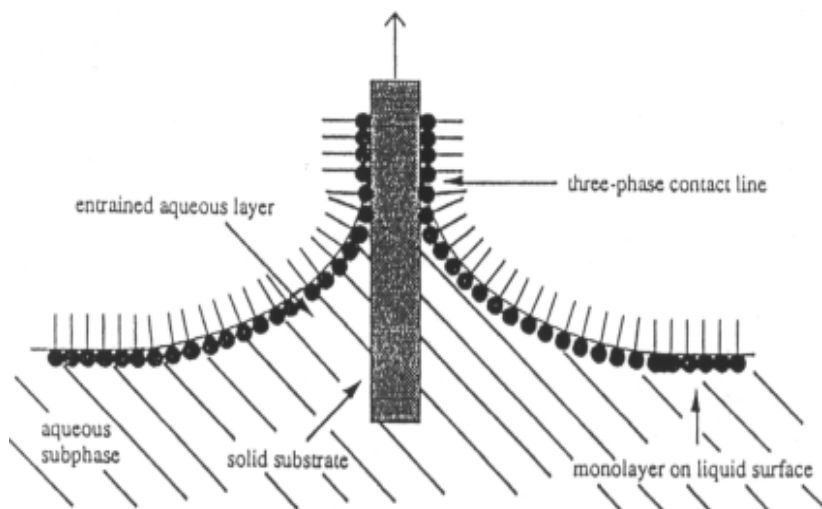


Figure 2.17. Schematic illustrations of deposition of a floating monolayer on a solid substrate [Binks 1991].

$$TR = \frac{\text{decrease in monolayer surface area}}{\text{total surface area of substrate}} \quad (\text{Eq. 2.17})$$

For ideal transfer the TR is equal to 1. However the acceptance of the value of unity as ideal reflects a strongly ingrained implicit assumption that the deposition process consists of simply transferring the molecules from the water surface to the substrate. This assumption is often correct but amphiphiles generally attempt to reach a new thermodynamic minimum as they experience interactions with the solid substrate. If the molecular packing density changes during transfer, then $TR = 1$ will not be the indicator of a defect-free film [Schwartz 1997].

Depending on the behavior of the molecule the solid substrate can be dipped through the Langmuir film until the desired thickness of the LB film is achieved. Different kinds of LB multilayers can be produced by successive deposition of monolayers on the same substrate. The most common one is the Y-type multilayer, which is produced when the monolayer deposits to the solid substrate in both up and down directions. When the monolayer deposits only in the up or down direction the multilayer structure is called either Z-type or X-type. Intermediate structures are sometimes observed for some LB multilayers and they are often referred to be XY-type multilayers (Fig. 2.18).

Such idealized film transfers are in general hardly achievable. The first layer may be different from subsequent layers since the molecules interact with the bare substrate instead of the headgroups or tails of the previous layer. The different energetics can affect the dynamics of the transfer as well as the structure of the first layer. During multilayer deposition, the upstroke and downstroke transfer are distinctly different primarily because of the necessity of water drainage during the upstroke. As a result the final structure is rarely a highly symmetrical multilayer – a synthetic crystal.

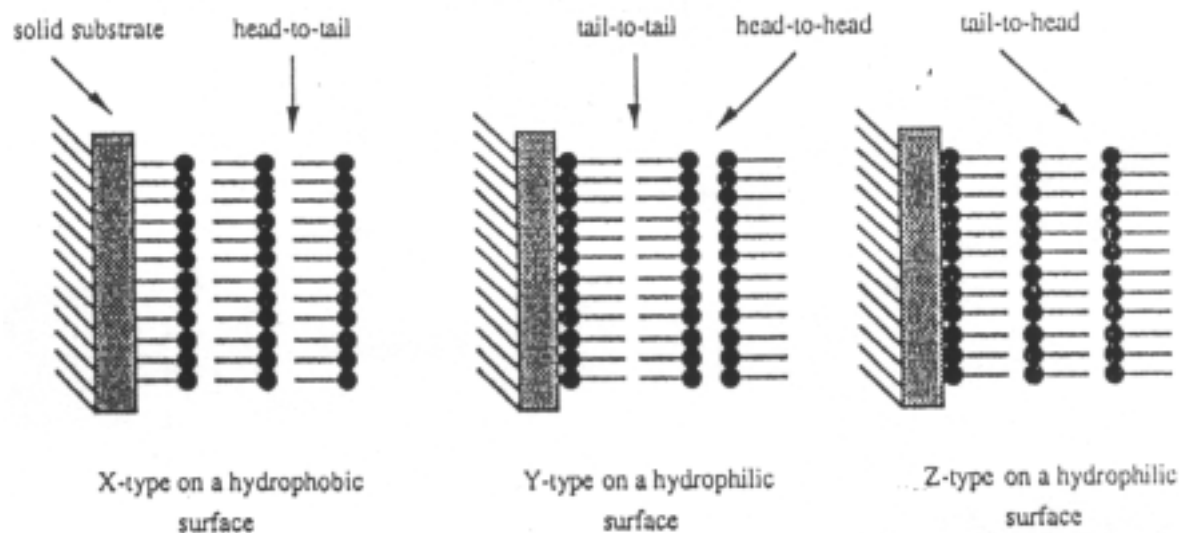


Figure 2.18. Schematic illustrations of different types of deposited LB films [Binks 1991].

Although the concept of LB transfers seems to be very simple, many practical problems may occur. Already Blodgett mentioned difficulties in finding the appropriate conditions for LB transfers in her original work [Blodgett 1935, 1937].

Depending on the properties of the amphiphiles used to build a monolayer, a number of determining factors like surface pressure, solid substrate and dipping speed need

to be optimized. The amount of intercalated water e.g. depends strongly on dipping speed and waiting time between individual strokes [Ariga 1994]. It was further observed, that drainage speed and cristallinity of transferred film is better for 'fresh' monolayers than for 'aged' ones [Peterson 1983]. For successful monolayer transfer interfacial free energies and the contact angle need to be considered as well, both being strongly dependent on surface pressure and substrate hydrophobicity [Gemma 1992].

Defects and anomalies of all sorts are present and various instabilities can result in thickness variation across a given sample. Extensive film reorganization and rearrangement has been observed for many systems yielding LB films in the form of trenches and terraces separated by bilayer or four-layer steps [Kopp 1975, Fuchs 1992, Schaper 1993], due to molecular repacking [Schwartz 1993, Zasadzinski 1994], head-to-head to head-to-tail conversion [Decher 1992], lamellar to columnar transitions [Tippmann-Krayer 1991, Albouy 1992], phase transitions [Rabe 1987, Rothberg 1987] or dewetting and desorption [Tippmann-Krayer 1992, Höhne 1994, Wu 1996].

2.1.6. Biological relevance of monolayers

All living cells use the bilayer self-assembly principle to build their membranes. The membrane is not just used passively by the cell as a barrier to retain important molecules, but also actively as a support and a highway to transport materials. The membrane holds captive many proteins used by the cell, and the force that keeps these membrane-bound proteins firmly anchored arises from the same hydrophilic-hydrophobic interactions which are responsible for the membrane's stability.

Strictly speaking, the above discussion only proves the biological relevance of bilayers. However for a number of experimental purposes, bilayers are quite inconvenient. They are always surrounded by water, and thus hidden away from a large number of surface-sensitive techniques. They float freely and hence do not stay put for observation at molecular resolution. There are many situations where it is highly desirable to tether the bilayer.

A monolayer is inherently tethered by the interface to which it is attached. The idea that one can look at a monolayer and get information about a bilayer is accepted by many researchers and is usually called the Principle of Equivalent States [*Peterson 1992, 1994*].

The most widely used models for bilayers, multilamellar or unilamellar bilayer dispersions, suffer from three significant limitations compared to monomolecular films at the air-water interface. First, the range over which the lipid composition can be varied without changing the surface curvature and phase state is limited [*Micol 1999*]. A second limitation is their inability to regulate lipid lateral-packing density and lipid composition independently. Lastly, the lipid composition and area exposed to the medium are not known unless the curvature of the lipid surface is negligible and the exact geometry of the dispersion is known [*Brockmann 1999*].

Monomolecular films exhibit the same thermodynamical properties as bilayers [*Feng 1999*]. Many experiments performed at the air-water interface give direct evidence of the behavior of a bilayer. Besides surface pressure-area isotherms [*Castano 1999*], electrical membrane potentials [*Brockman 1994*], microscopic visualization of lateral domains [*Denisov 1998*], vibrational spectroscopy [*Mendelsohn 1998*] and combinations of these methods [*Wu 1998*] yield a great deal of information directly transformable to the bilayer model.

Another aspect to consider is that basic bilayer methods are macroscopic and mostly provide information which is averaged over an area that is large relative to the size of a lipid. Contrary, a range of new sophisticated techniques are available which can be used to probe individual molecules or to visualize submicron domains in a monolayer (e.g. SNOM) [*Shiku 1999*].

However, caution needs to be taken in interpreting results achieved on monolayers. Membrane active macromolecules which do not only reside on or in one half of a bilayer but which are membrane spanning (e.g. membrane channels, porines) will not behave naturally in a monolayer and will not exhibit the same structural behavior and functionality at the air-water interface than in a natural lipid bilayer.

2.2. Biological surfactants

The term ‘lipid’ comprises a diverse range of relatively water-insoluble or nonpolar compounds of biological origin with nonuniform chemical structure, including waxes, fatty acids, triglycerides, fatty-acid derived phospholipids, sphingolipids, glycolipids and terpenoids, such as retinoids and steroids. Some lipids are linear aliphatic molecules, while others are cyclic or even polycyclic. Some are aromatic, while others are aliphatic. Some are flexible, while others are rigid.

Most lipids are amphiphilic molecules, implying that one structural part is polar or hydrophilic while the bulk of their structure is nonpolar or hydrophobic and will tend to self-assemble in polar solvents like water (Fig. 2.19) [IUPAC Glossary]. Molecular self-assembly is a process by which molecules spontaneously organize into ordered assemblies via non-covalent intermolecular forces, such as hydrogen bonds, electrostatic interactions, ion-ion interactions, ion-dipole interactions, hydrophobic interactions, etc. [Tandford 1978]. Self-assembly is one of the most universal strategies used in biology for the development of complex and functional structures: fascinating examples are biomembranes, viruses, oligomeric proteins and nucleic acid multiplexes. Inspired by these biological architectures, the design and synthesis of various molecules that are able to self-assemble spontaneously has become an active field of scientific research [Hamley 2003a].

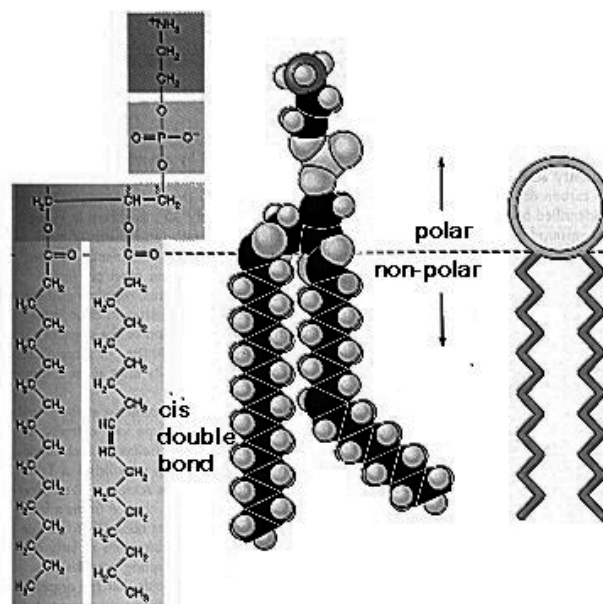


Figure 2.19. Molecular structure of a phospholipid with schematic representation of polar and non-polar segments [Wolfe 1993].

2.2.1. Phospholipids

Phospholipids or, more precisely, glycerophospholipids, are built on a glycerol core to which are linked two fatty acid-derived ‘tails’ by ester linkages and one ‘head’ group by a phosphate ester linkage. Fatty acids are unbranched hydrocarbon chains, either saturated or unsaturated, usually 10-24 carbon groups long. The head groups of the phospholipids found in biological membranes are phosphatidylcholine, phosphatidylethanolamine, phosphatidylserine and phosphatidylinositol, whose head group can be modified by the addition of one to three more phosphate groups. While phospholipids are the major component of biological membranes, other lipid components like sphingolipids and sterols are also found.

Lecithin is usually used as synonym for phosphatidylcholine (PC), a phospholipid which is the major component of a phosphatide fraction which may be isolated from either egg yolk (in Greek lekithos - λεκιθος) or soy beans. It is commercially available in high purity as a food supplement and for medical uses [Kuksis 1985, Prosis 1985]. PC is a mixture of differently substituted sn-glycerol-3-phosphatidylcholine backbones. As can be seen from Table 2.2, the structure of PC is variable and dependent on fatty acid substitution. Fatty acids of mainly 16-20 C in chain length dominate in egg PC. The sn-1-chain typically shows an average of 16 C, whereas the sn-2-chain shows an average of 18 C. Naturally occurring unsaturated fatty acids are almost entirely of all-cis-conformation [Gennis 1989]. In the sn-1-position saturated acyl-groups, and in sn-2-position unsaturated species are more common [Kuksis 1985].

%wt	sn-1 and sn-2-chain of PC or other component	chain length & saturation	abbreviation
38.2%	Palmitoyl/Oleoyl	16:0 / 18:1	POPC
21.8%	Palmitoyl/Linoleoyl	16:0 / 18:2	PLPC
11.2%	Stearoyl/Linoleoyl	18:0 / 18:2	SLPC
9.3%	Stearoyl/Oleoyl	18:0 / 18:1	SOPC
2.4%	Stearoyl/Arachidoyl	18:0 / 20:4	SAPC
0.7%	Di-Palmitoyl	16:0 / 16:0	DPPC
8.4%	Phosphatidylethanolamine		PE
3.0%	Lyso-Phosphatidylcholine		LPC
2.5%	Lyso-Phosphatidylethanolamine		LPE
2.5%	Sphingomyelin		SPM

Table 2.2. Main constituents of egg PC (in % wt/wt) [Kuksis 1985].

2.2.2. Lyotropic phase behavior

2.2.2.1. Amphiphilic properties of lipids

Lipids consist of a polar ‘head group’ and comparably nonpolar residues (Fig. 2.19). The molecules tend to self-organize in a distinct way, which is that lipophilic tails and hydrophilic head groups take a separate, packed arrangement. The state of order and the length of the lipophilic tail depends on the conformation of the carbon chains which preferably will be ‘all-trans’ in the case of saturated acyl-chains, since in this case a potential energy minimum occurs. Thus, the carbon chains become extended to a maximum, whereas in the case of a carbon-carbon bond taking on the gauche-conformation, a kink in the chain occurs (Fig. 2.20). A similar displacement can be observed if a cis-double-bond is located in the hydrocarbon chain (Fig. 2.21) [Wabel 1998].

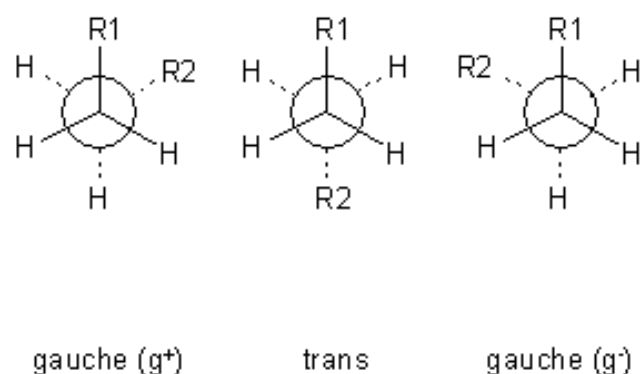


Figure 2.20. Newman projections of carbon-carbon bond rotation in an alkyl chain [Gennis 1989].

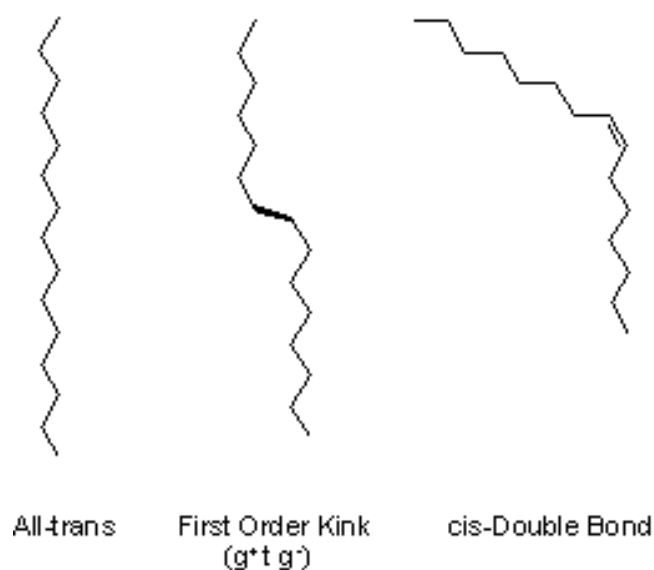


Figure 2.21. Alkyl chain configurations [Gennis 1989].

2.2.2.2. Lyotropic mesophases

Amphiphilic lipids typically often do not exhibit abrupt transitions from the solid to the liquid state, but do undergo 'intermediate' states, where properties of solid crystals and of liquids can be observed [Lee 1977]. Therefore these 'intermediate' states are also known as 'mesophases' or 'liquid crystalline phases'. This so-called mesomorphic behavior can be attributed either to temperature changes when e.g. heating causes 'chain melting' which means transformation of the alkyl chains into a less ordered state owing to increased occurrence of thermodynamically unfavorable chain kinks and consequently increased chain space requirement ('thermotropic phase transition'), or changes in hydration state owing to the fact that only the polar head groups bind to water and become hydrated, which increases their respective space requirements and eventually results in changes in molecule packing ('lyotropic phase change'). In Table 2.3, the resulting mesophases are listed according to IUPAC nomenclature using the following abbreviations which describe long-range and short-range orders in lipid-water phases [Marsh 1990]:

Long-range order regimes	
L	Lamellar (one-dimensional)
H	Hexagonal (two-dimensional)
P	Oblique or centred (two-dimensional)
Q	Cubic or viscous isotropic
R	Rhombohedral
C	Crystalline (three-dimensional)
M	Micellar (disordered)
Short-range order regimes	
α	Disordered (fluid)
β	Partly ordered, untilted (gel-state)
β'	Partly ordered, tilted
δ	Partly ordered, helical
I	Oil-in-Water Type
II	Water-in-Oil Type

Table 2.3. IUPAC nomenclature of lipid-water phases [Marsh 1990]

The following phases are most commonly encountered in lipid-water systems [Hamley 2000]:

Lamellar liquid crystalline phase (L_{α})

Molecules are located in a two-dimensional order, but acyl chain-regions show considerable disordered (fluid) state. This phase represents the most common arrangement of phospholipids in biological membranes.

Lamellar gel phase (L_{β})

At lower temperatures the molecules become more tightly packed and the acyl chains become more ordered (all-trans). In lipids with larger head groups, acyl chains are found in tilted positions denoted by a prime (L_{β}').

The density and the bilayer thickness of gel phases are slightly larger compared to the liquid crystalline state.

Hexagonal I phase (H_I)

Lipids are organized in the form of cylinders with the polar 'head groups' outside, facing the water. The cylinders themselves are packed in a hexagonal array.

Hexagonal II phase (H_{II})

In this case the acyl chains face the outer side of the cylindrical shapes, whereas on the inside the polar groups are located facing a continuous area of water.

Cubic I phase (Q_I)

Discontinuous phase consisting of spherical micelles with head groups facing a continuous phase of water at the outside.

Cubic II phase (Q_{II})

Bicontinuous phase, representing an intermediate state between lamellar and hexagonal phase.

The interdependence of lyotropic and thermotropic phase transitions of lipid-water systems is summarized in Figure 2.22. It shows that certain preferences in phase behavior according to substitution and temperature exist, which in most cases are reversible. It must be stressed, however, that the thermal 'history' of the lipid plays also an important role at which phase changes occur. Similarly, in the case of phospholipid-water mixtures, occurrence of thermotropic or lyotropic phase changes is known.

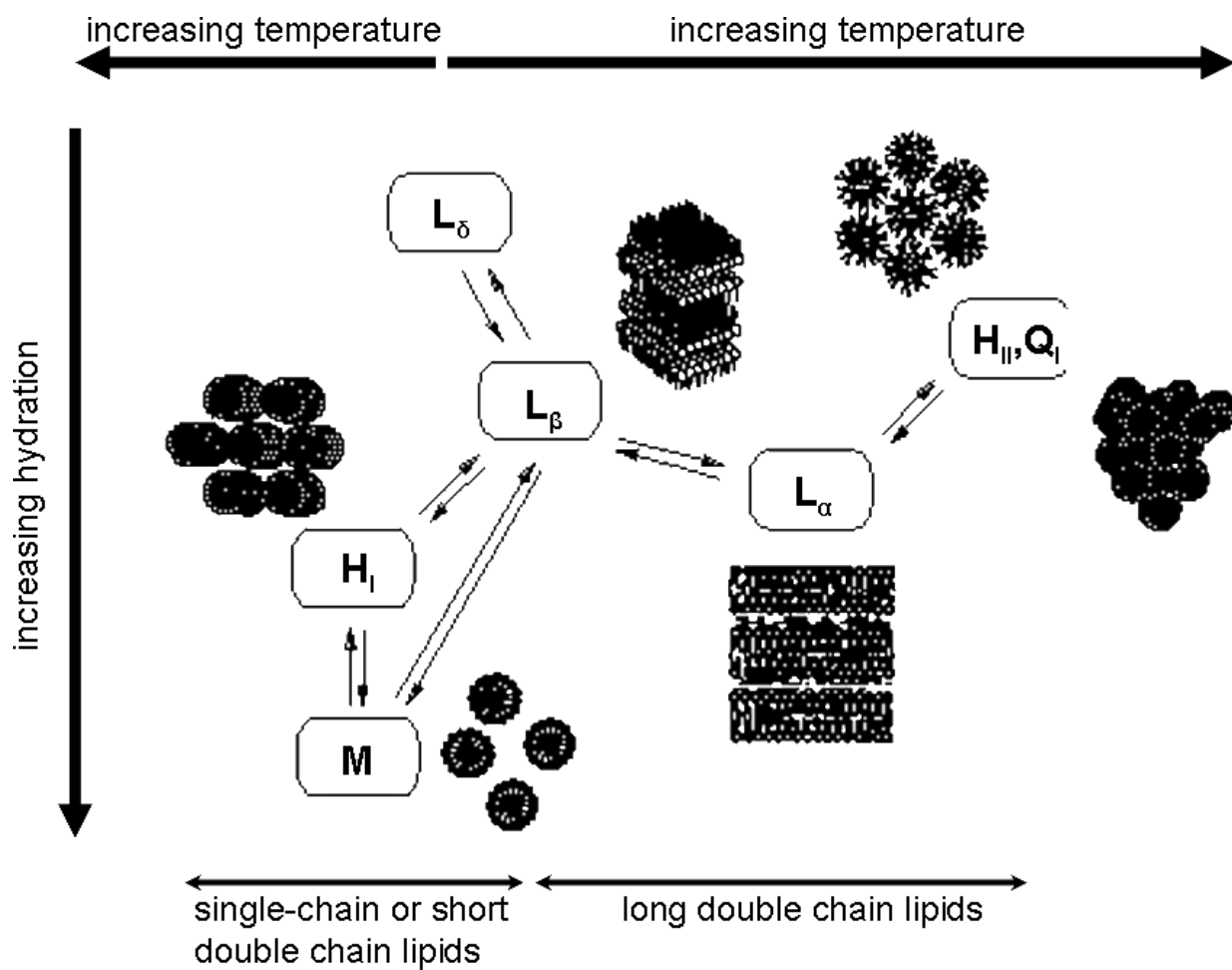


Figure 2.22. Dependence of phase transitions of lipid-water mixtures on hydration and temperature (hexagonal (H_I), hexagonal inverse (H_{II}), lamellar liquid crystalline (L_α), lamellar gel (L_β), lamellar helical (L_δ), micellar (M), cubic (Q_I)) [Brown 1979, Gennis 1989, Marsh 1990].

2.2.2.3. Morphology of self-assembled structures

The lyotropic phase behavior of amphiphiles and therefore the shape of self-assembled structures can be described by two types of models. The first is based on the shape of the amphiphile molecules themselves. The second is based on the curvature of a surfactant film at an interface.

In the model based on molecular shape, typical packing adaptations are explained by means of the 'critical packing parameter' (CPP or surfactant packing parameter), which is the ratio of the hydrophobic volume V divided by the interfacial area of the hydrophobic volume A and the chain length normal to the interface L .

$$CPP = \frac{V}{AL} \quad (\text{Eq. 2.18})$$

The CPP determines the preferred association structures assumed for each molecular shape [Israelachvili 1992]. A summary of packing determined phospholipids phases is summarized in Table 2.4, where examples of typical molecular shapes, phase arrangements and CPPs are shown for the most prominent phospholipids.

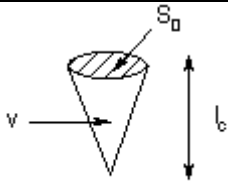
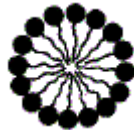
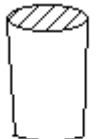
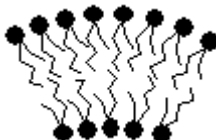


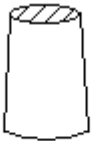
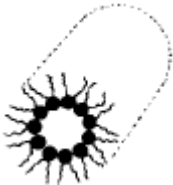
Critical packing shape	CPP	Phase formed	Lipid examples
 <p>Cone</p>	$< 1/3$ (spheres) $1/3$ to $1/2$ (rods)		Lysophospholipids, free fatty acids
 <p>Truncated cone</p>	$1/2$ to 1 (lamellar, vesicles)		Double-chained lipids with large head group areas and fluid chains
 <p>Cylinder</p>	~ 1 (lamellar, planar bilayers)		Double-chained lipids with small head group areas, anionic lipids and saturated chains
 <p>Inverted truncated cone</p>	> 1 (hexagonal H_{II})		Double-chained lipids with small head group areas, non-ionic lipids and polyunsat. chains

Table 2.4. Molecular shapes and association structures of phospholipids [Cevcs 1987, Genis 1989].

In the model for interfacial curvature of a continuous surfactant film, results from differential geometry of surfaces are applied [Hamley 2000, Lasic 2001]. A surface can be described by two fundamental types of curvature: mean curvature H and Gaussian curvature K_G . Both can be defined in terms of the principal curvatures

$$\kappa_1 = \frac{1}{R_1} \text{ and } \kappa_2 = \frac{1}{R_2}, \quad (\text{Eq. 2.19})$$

where R_1 and R_2 are the radii of curvature. The mean curvature is

$$H = \frac{\kappa_1 + \kappa_2}{2}, \quad (\text{Eq. 2.20})$$

whilst the Gaussian curvature is defined as

$$K_G = \kappa_1 \kappa_2. \quad (\text{Eq. 2.21})$$

According to Hyde [Hyde 1990], the interfacial curvature is related to the critical packing parameter as follows:

$$CPP = \frac{V}{AL} = 1 - HL + \frac{K_G L^2}{3}. \quad (\text{Eq. 2.22})$$

Apart from forming vesicles, amphiphilic membranes are also capable to curve differently: saddle-shaped deformations arise from the 'frustration' experienced by the two monolayers because of their inability to curve with their natural curvature. Especially interesting in this context are minimal surfaces, whose mean curvature H is always zero, and the Gaussian curvature K_G is negative, as presented in Figure 2.23, yet in this case, morphologies different from vesicles should be expected: saddle-splay deformations generally lead to bicontinuous phases. The mean and Gaussian curvatures of various amphiphile aggregates are listed in Table 2.5.

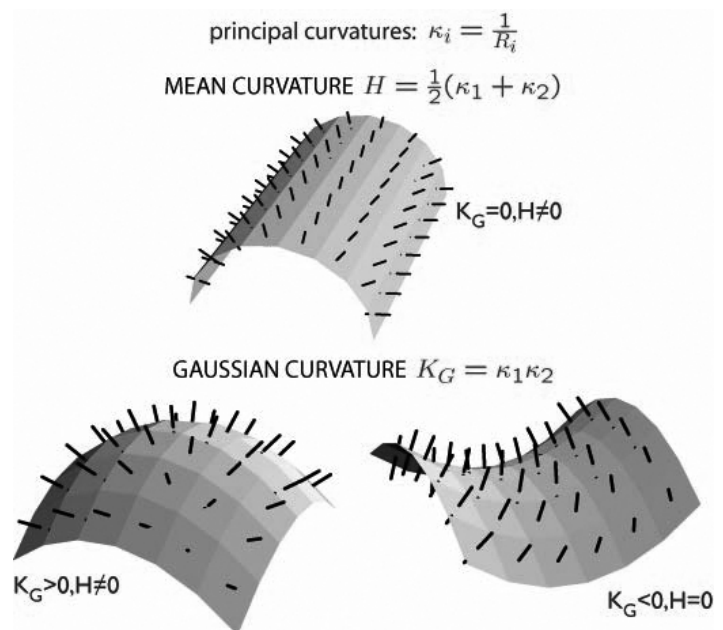


Figure 2.23. Complex morphologies obtained with different mean curvature (H) and Gaussian curvature (K_G) [DiDonna].

Structure / Phase	Mean curvature H	Gaussian curvature KG
Spherical micelles or vesicles	R^{-1}	R^{-2}
Cylindrical micelles	$(2R)^{-1}$	0
Bicontinuous cubic phases	0 to $(2R)^{-1}$	R^{-2} to 0
Lamellar phases	0	0
Inverse bicontinuous cubic phases	$-(2R)^{-1}$ to 0	$-R^{-2}$ to 0
Inverse cylindrical micelles	$-(2R)^{-1}$	0
Inverse spherical micelles or vesicles	$-R^{-1}$	$-R^{-2}$

Table 2.5. Mean and Gaussian interfacial curvature for common aggregate shapes. Here R denotes radius of curvature [Hamley 2000].

2.2.3. Lamellar phases from phospholipids

Lamellar lecithin phases show increasing inter-bilayer spacing upon uptake of water ('swelling') to form myelins, which on further dilution form closed bilayer vesicles. These so called 'liposomes' show diverse size and number of bilayers (lamellae) [New 1990]. Curvature of the phospholipid bilayers, which is determined by packing geometries, limits the smallest possible size of the bilayer and is also the reason for different distribution of the phospholipid molecules in the inner and outer bilayers [Vance 1991].

Oriented amphiphilic molecules in vesicle membranes are able to move freely in the tangential direction (along the boundary between the polar and non-polar regions of a nanoparticle) and are only restricted in their movement along the normal. Therefore, vesicles can be viewed as liquids (two-dimensionally) and solid bodies (one-dimensionally). Owing to their two-dimensional fluidity multiple non-spherical shapes such as prolate, oblate, nanotubes etc. can be achieved [Kita-Tokarczyk 2005a]. In Figures 2.24-2.26, a variety of liposomes, made from egg yolk PC are presented.

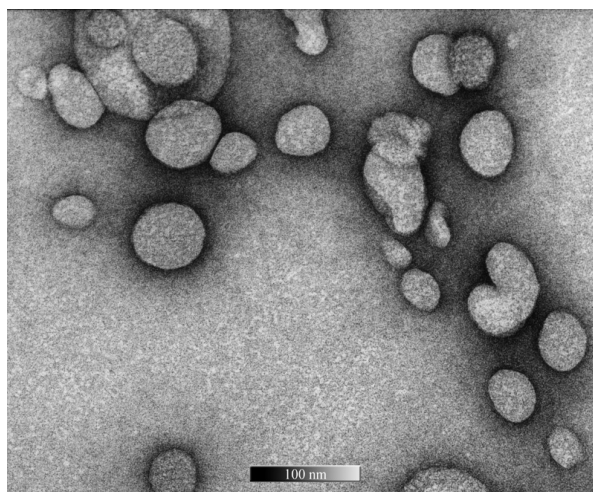


Figure 2.24. TEM micrograph of small unilamellar liposomes from egg yolk PC obtained by film rehydration (negative stained, scalebar 100nm).

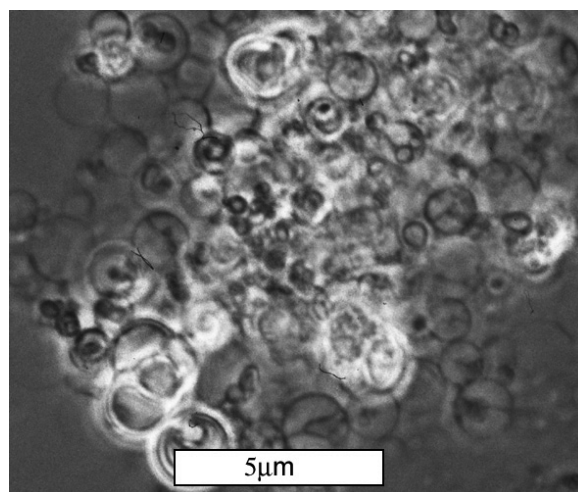


Figure 2.25. Phase contrast micrograph of giant unilamellar liposomes from egg yolk PC obtained by electroformation (scalebar 5µm).

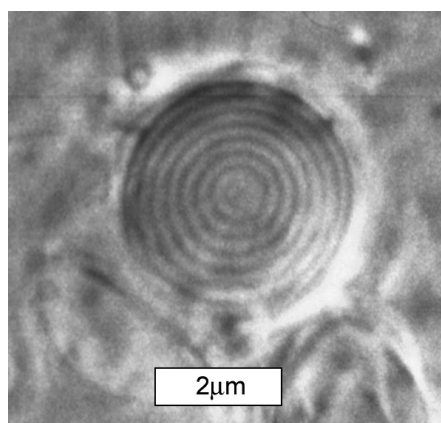


Figure 2.26. Phase contrast micrograph of a giant multilamellar onionlike liposome from egg yolk PC obtained by film rehydration (scalebar 2µm).

2.3. Ampiphilic polymers

2.3.1. Macromolecules

The term macromolecule or polymer (greek: poly = many; meros = part) describes a molecule of a high molecular mass, the structure of which essentially comprises the multiple repetition of units derived, actually or conceptually, from molecules of low molecular mass [Lechner 2003]. The constitutional units of the structure of a macromolecule are provided by polymerization of monomer molecules.

Addition or subtraction of small numbers of subunits has a negligible effect on the properties of the macromolecule. A constitutional unit or constitutional structural element is therefore the smallest, periodically repeating unit which describes entirely the structural composition of the polymer. These constitutional units are interconnected through covalent, ionic or hydrogen bonds.

Macromolecules can be classified, similarly to low molecular weight chemistry, into organic and inorganic polymers according to the chemical nature of the monomers. Organic polymers can be further divided into natural biopolymers and chemically modified or synthetic polymers. The complexity and diversity of biopolymers is the prerequisite for life. Polynucleotides, polypeptides, polysaccharides and polydienes are the constituents of all living organisms.

Since the invention and fabrication of the first synthetic polymer, polymers attracted a growing interest resulting in one of the most important classes of today's materials. In the 21st century, life without plastics is incomprehensible. They have become one of the most used materials in industrial and commercial life. Plastics are broadly integrated into today's lifestyle and make a major, irreplaceable contribution to virtually all product areas.

Whilst plastics are thought of as 'new' materials there is nothing further from the truth. Polymers have a long and full history with references as ancient as the Old Testament about natural materials used as fillers, adhesives, coatings, and the like. For a detailed historical timeline of the evolution and development of polymers and plastics see Appendix B.

2.3.1.1. Polymer constitution

Polymers built of only one sort of monomer are called uni- or homopolymers. A polymer consisting of several different types of subunits is called hetero- or copolymer or in respect to the number of monomer sets a bi- ter- or quaterpolymer for two, three or four different comonomers [Lechner 2003].

Depending on the sequence of the comonomers, a copolymer is further divided into four constitutional subgroups:

Statistical copolymers

The comonomers are distributed statistically along the polymer chain, e.g. for a bi-polymer of subunits A and B:



Alternating copolymers

The comonomers alternate in a regular repeating order, either one by one (alternating) or sequence by sequence (periodic):



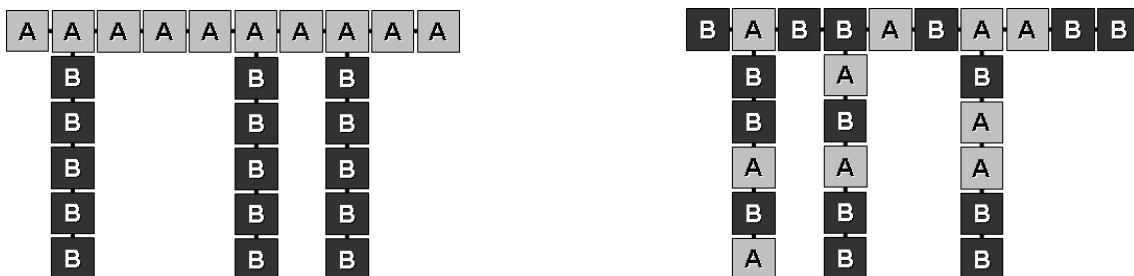
Block copolymers

Linear block copolymers are built from individual blocks of monomers of the same kind:



Graft copolymers

Graft copolymers are branched polymers consisting of a backbone on which side chains are grafted. The side chains and the backbone can be either homopolymeric, statistical or a combination:



2.3.1.2. Polymer architecture

If a monomer exhibits more than two reactive functional groups, the polymer can have a more complex architecture [Lechner 2003]. The following architectures can be achieved:

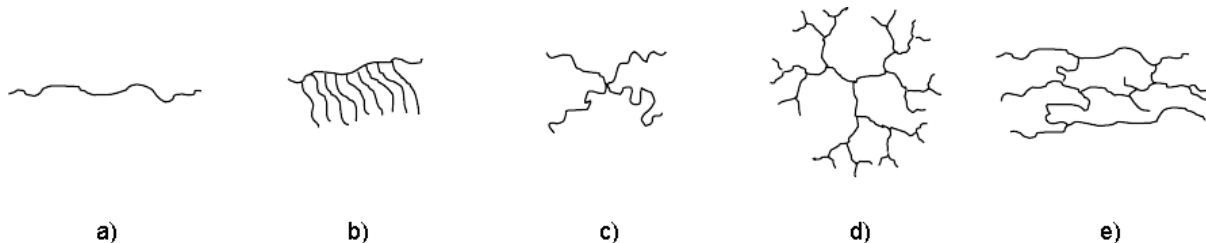


Figure 2.27. Schemes of different polymer architectures

Linear polymers

A linear polymer (Fig 2.27a) is obtained if the monomers have only two reactive groups and can therefore only arrange as a linear chain. As a special case are cyclic ring polymers where both chain ends are attached to each other.

Comb polymers

A comb polymer (Fig 2.27b) is a macromolecule comprising a main chain with multiple trifunctional branch points from each of which a linear side-chain emanates. The branch points may either be equidistant or statistical and the side chains may be of uniform or varying length. If at least some of the branch points are of functionality greater than three, the macromolecule may be termed a brush macromolecule.

Star polymers

Star polymers (Fig 2.27c) possess one central branch point from which several side chains of uniform or varying length originate. Tree polymers are a subset of star polymers where the side chains are further branched. A special case of tree polymers are dendrimers (Fig 2.27d) in which all generations of branched side chains are of uniform size resulting in a spherical symmetrical tree.

Polymer networks

Individual polymer chains and molecules can be interconnected resulting in a network (Fig 2.27e), a so called giant macromolecule. The bonds between the polymer chains can be of chemical nature (covalent, ionic) or of physical character (loops, hooked).

2.3.2. Amphiphilic block copolymers

In macromolecules even weak repulsions between monomers are magnified due to the large number of repeats, so many blends of polymers are highly immiscible and tend to separate into distinct phases (macrophase separation).

Block copolymers exhibit the features and properties of all individual blocks [Goodwin 2004, Hadjichristidis 2004]. Due to the fact that the blocks are linked covalently no macroscopic demixing takes place. The antagonistic properties of the blocks can be e.g. plastic-elastic, rough-smooth, rigid-flexible or hydrophilic-hydrophobic. Usually the blocks become less miscible as the temperature is lowered, i.e. the system exhibits an upper critical ordering temperature (UCOT) below which phase separation occurs. However, in contrast to blends of statistical polymers, the length-scale for phase separation is restricted by the connectivity of the blocks (microphase separation). The transition from an ordered microphase to the homogenous polymer melt at high temperatures occurs at the order-disorder transition (ODT) [Hamley 2000]. Microphase separation leads to the formation of a variety of ordered structures, illustrated in Figure 2.28, which shows an idealized phase diagram for a diblock copolymer. In the microphase-separated state the structure will have some characteristic length scale that arises from a competition between surface energy and the free energy associated with the stretching of the chains. If block copolymers are very asymmetrical, e.g. one block is much shorter than the other, lamellar morphology will impose unequal stretching constraints on each block. The asymmetry is conveniently parameterised by the ratio of length of one block to the total length of the copolymer, f ; as this changes away from a value of 0.5 an intrinsic interfacial curvature is imposed on the system, leading to different shapes of the microdomains [Jones 1999].

It needs to be mentioned that this idealized phase diagram is only correct if it is assumed that both blocks have identical conformational properties. For real block copolymers this is not the case; one block is likely to be stiffer than the other and this will make the phase diagram asymmetrical [Bates 1994].

In the case of amphiphilic block copolymers, at least one block is hydrophilic and at least another block is hydrophobic. The thermodynamic properties of amphiphiles in solution are controlled by the tendency for the hydrophobic region to avoid contact with the water, which is a result of the hydrophobic effect. Therefore amphiphilic block-copolymers spontaneously self-assemble at sufficiently high concentrations into ordered structures called lyotropic liquid crystalline phases (also known as mesophases). A liquid crystalline phase is denoted a phase that lacks the full three-dimensional translational order of molecules on a crystal lattice. Lyotropic refers to the fact that such phases are formed by amphiphiles as a function of concentration (in addition to temperature dependence).

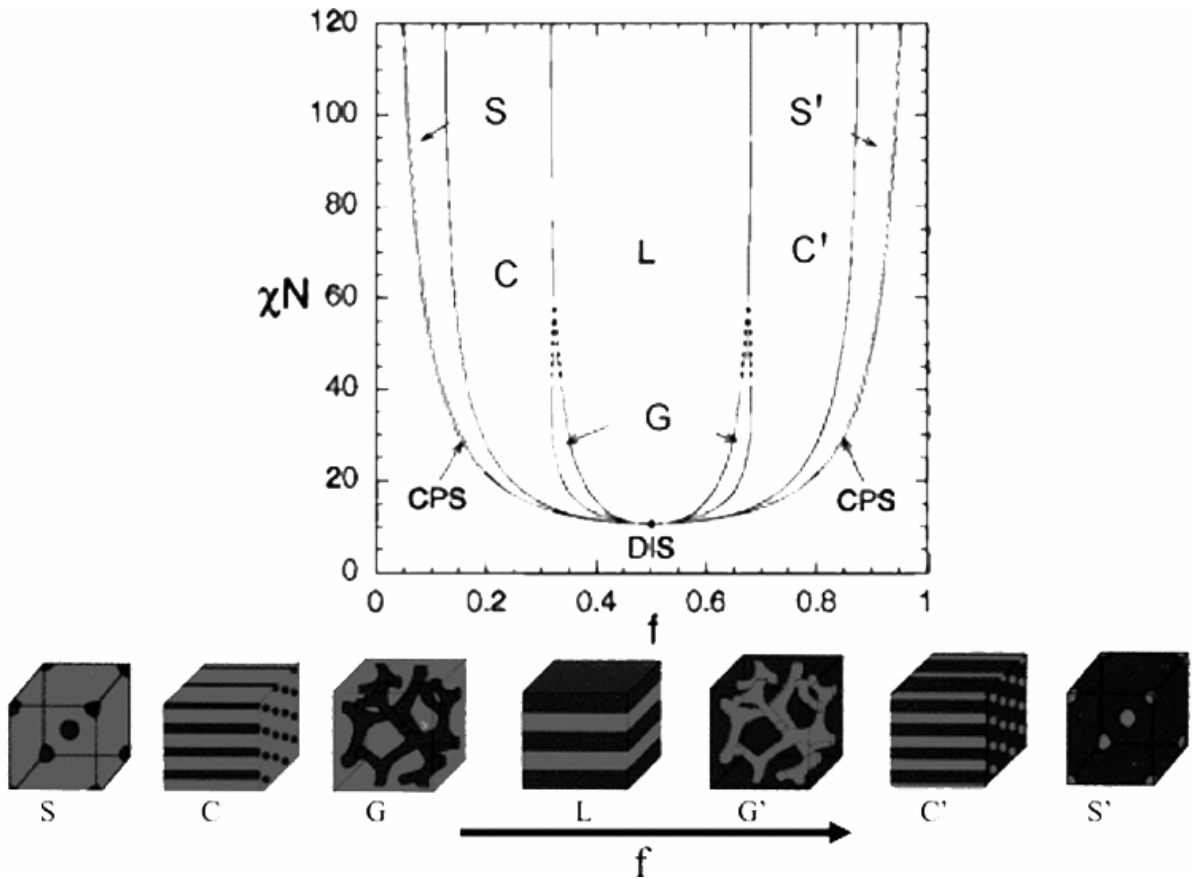


Figure 2.28. Schematic phase diagram for an ideal diblock copolymer depicting the different morphologies as a function of the Flory-Huggins interaction parameter, χ , degree of polymerization N and block length fraction f . χN is inversely proportional to temperature, therefore temperature increases from top to bottom. At high temperature entropy dominates and the polymer falls into the disordered state (DIS). The resulting morphologies at lower temperatures are described as close packed spheres (CPS), body-centred cubic (S), hexagonal-packed cylinders (C), gyroid (G), lamellar (L), and their respective inverses (represented by S', C', and G'). Abbreviations are not according to IUPAC [Hamley 2000, Hadjichristidis 2004].

2.3.2.1. Lyotropic hase behavior of amphiphilic block copolymers

Block copolymers comprised of two or more chemically incompatible and dissimilar blocks can microphase separate into a variety of morphologies [Kawakatsu 1993, Jenekhe 2000, Huang 2004]. This self-assembly process [Tandford 1978, Di Mario 1999] is driven by an unfavorable mixing enthalpy and a small mixing entropy, while covalent bonds between the blocks prevent macrophase separation. Depending on the polymers used and their volume fractions, various microphase separation morphologies are formed: spheres, lamellae, inverse spheres and several more complex shapes [Klok 2001, Kita-Tokarczyk 2005a].

The definitions of these mesophases of amphiphilic block-copolymers and the models to deduce the shape and structure of the respective phase are identical to the ones obtained for low molecular weight surfactants such as lipids. All explanations and definitions in this context given in Chapter 2.2.2. therefore also apply for amphiphilic block copolymers.

Similarly to lipids, amphiphilic block copolymers aggregate in solution producing a variety of morphologies [Zhang 1995, Regenbrecht 1999, Shen 1999, Meier 2000, Nardin 2000a, Maskos 2001], in which the insoluble blocks are shielded as far as possible by the soluble ones from the surrounding medium. Depending on block length ratio, the hydrophilic-to-hydrophobic balance (HLB), concentration, temperature, preparation method, etc., different morphologies can be observed in solution [Won 1999, Stoenescu 2004].

A typical phase diagram of an amphiphilic ABA triblock copolymer and the respective structures found at each order regime is given in Figure 2.29.

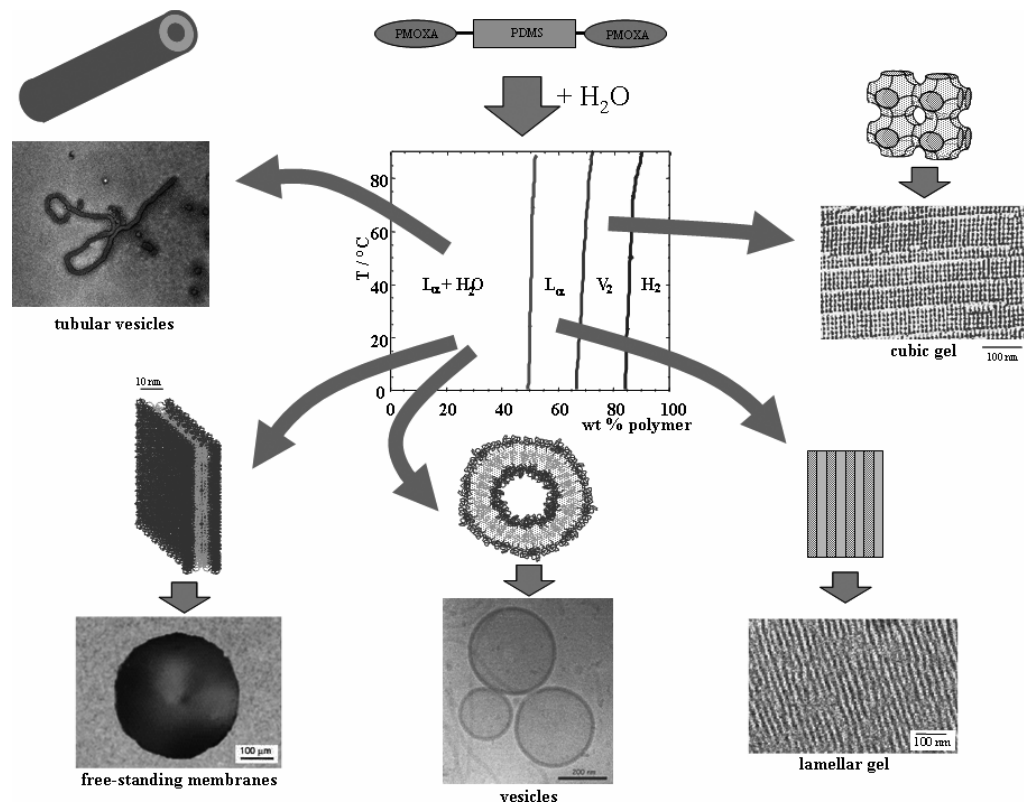


Figure 2.29. Phase diagram of an amphiphilic PMOXA-PDMS-PMOXA triblock copolymer (PMOXA hydrophilic, PDMS hydrophobic) and the respective morphologies formed at each phase [Nardin 2001a].

Even though the stability of lipid and polymer vesicles will inevitably vary due to their different chemical composition, the principle of their formation remains essentially the same: both are held together solely by non covalent interactions [Kita-Tokarczyk 2005a]. Amphiphilic block copolymers can be referred as high molecular weight homologues of common surfactants although the self-assembled polymeric superstructures are far more stable than structures formed by surfactants [Förster 2003]. This is mainly due to stronger hydrophobic interactions because of the increased molecular weight and therefore increased thickness of lamellar structures (Fig. 2.30) [Lee 2002]. The increase in membrane stability is restricted to a limit set by the interfacial tension γ that drives membrane formation. Additionally an increase in molecular weight decreases membrane permeability (due to increased membrane thickness) and further decreases mobility of individual polymer molecules in the membrane (associated with entangling chains) (Fig. 2.31) [Discher 2000, 2002].

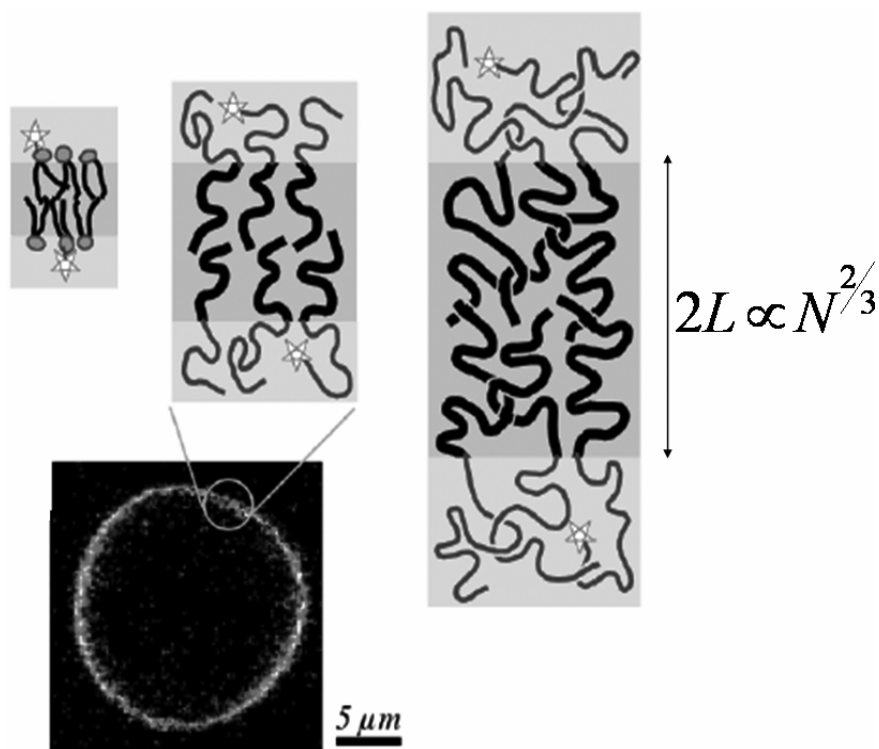


Figure 2.30. Thickness of block copolymer membrane drawn to scale; the chains in the bilayer are highly stretched and core dimensions of a given chain length L scale as $N^{2/3}$ [Lee 2002].

Almost unlimited possibilities exist for producing individually tailored amphiphilic block copolymers for specific applications: composition, constitution and architecture of individual blocks, and further hydrophilic-to-hydrophobic balance (HLB) of the copolymer define the structures and properties of block copolymer self-assemblies absolutely [Förster 2002]. Moreover polymers can be easily modified with reactive groups, and therefore the resulting structures can be further stabilized by e.g. crosslinking polymerization [Nardin 2000a]. Another alternative of endgroup functionalisation is the attachment of dye molecules enabling easy detection by microscopy or spectroscopy [Stoescu 2004].

Nevertheless the most potent method of functionalisation of self-assembled block copolymer membranes is the incorporation of membrane proteins, serving various purposes in biological membranes. Details of membrane protein action are given in the subsequent chapter. There already exist a few literature reports proving successful incorporations of proteins into purely polymeric membranes, including evidence of protein functionality in such an artificial environment [Nardin 2000b, 2001b, Graff 2002, Hamley 2003b, Ho 2004]. Even though membranes built from amphiphilic block copolymers can be several times thicker than natural lipid bilayers functional membrane integration is achievable. Pata and Dan [Pata 2003] proved theoretically that protein insertion into polymer membrane at least two-fold thicker than lipid bilayers is possible. This is mainly due to the fact that polymer molecules are very flexible and can be compressed considerably (Fig. 2.32). The chains in the unperturbed bilayer are highly stretched. As a result, the requirement to match the thickness of much shorter proteins can be achieved without significant compression in comparison to the free chain radius of gyration. Thus, matching a protein, whose thickness is half that of the bilayer, is easily obtained. The increase in the local surface energy is compensated by a decrease in the stretching energy.

In addition synthetic block copolymers exhibit a certain polydispersity of molecular weight. Thus shorter chains are allowed to segregate around a membrane protein easing the membrane insertion process (Fig. 2.33).

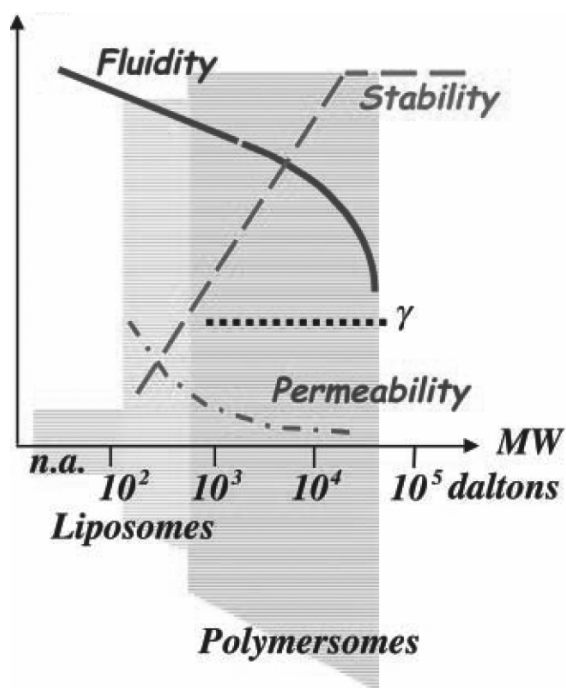


Figure 2.31. Increase of stability, decrease of permeability and decrease of fluidity due to increasing molecular weight of amphiphile [Discher 2002].

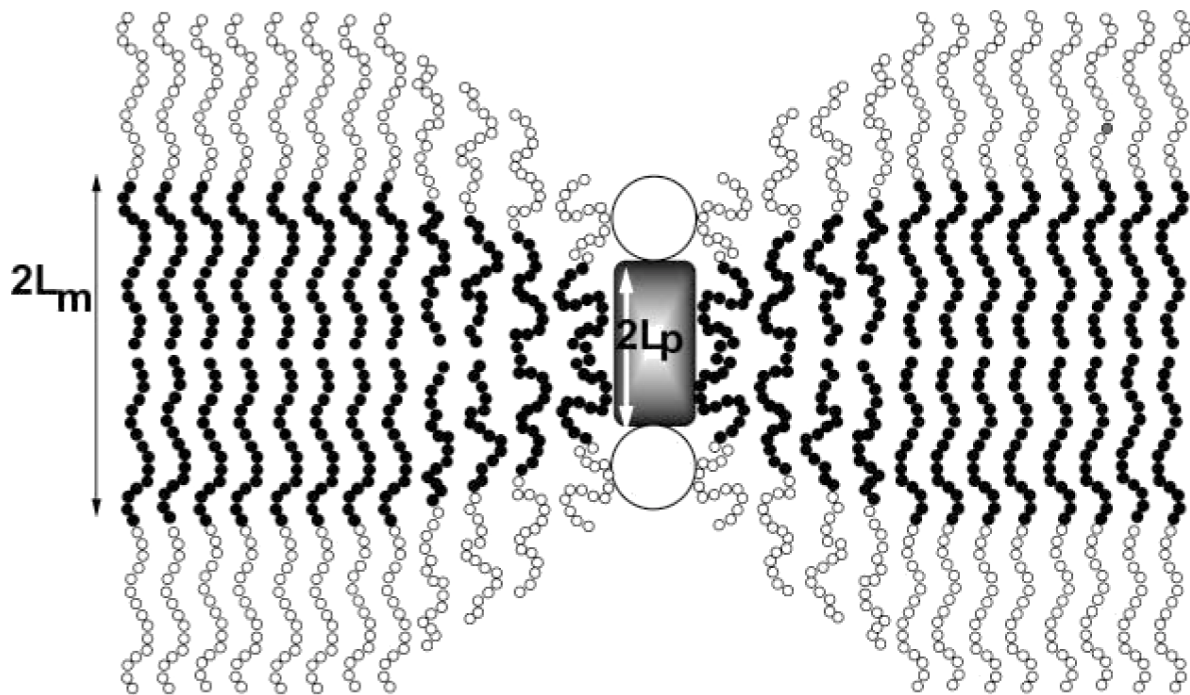


Figure 2.32. Conformation of polymer chains near an inclusion of a membrane protein in a polymeric bilayer: $2L_m$ is the thickness of the hydrophobic segments of a flat bilayer

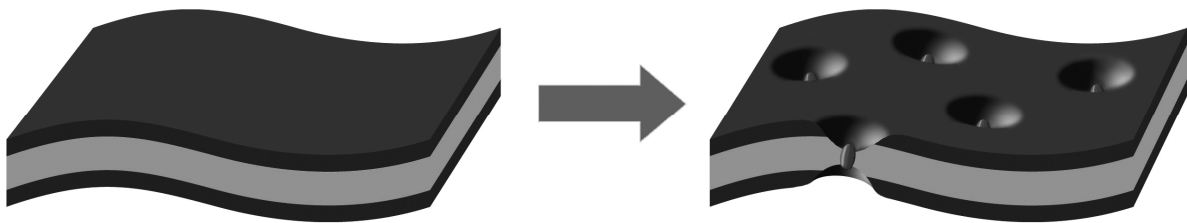


Figure 2.33. Schematic of an insertion of membrane proteins in a membrane built from amphiphilic block copolymers [Streich 2004].

2.3.2.2. Isothermal phase behavior of amphiphilic block copolymers

Insoluble molecular layers at interfaces have been the subject of many experimental and theoretical studies since the pioneering work of Langmuir [Langmuir 1916, 1917a, 1917b]. These studies have been performed on small amphiphilic molecules such as surfactants and lipids at the gas-liquid or solid-liquid interface. More recently the structure of quasi 2d layers of long polymer chains at interfaces has been examined theoretically and experimentally [Fauré 1998].

Investigations have been reported employing block copolymers, graft copolymers, lipopolymers and blends of polymers with different properties. Homopolymers in general do not form stable monolayers at the air-liquid interface. As subphase not only water is employed but also a variety of organic solvents or mercury to tailor the solubility of the investigated macromolecules.

Low relative molecular mass materials display a very rich monolayer phase behavior. In opposition it has been reported that spread polymer films do not show the same range of isotherm behavior and that generally only two phase regimes are encountered, namely liquid expanded and condensed films [Jones 1999]. This finding is scrutinized by the work of Halperin suggesting a rich variety of phase transitions involving grafted and block copolymers [Halperin 1992].

Numerous surface pressure-area isotherms have been reported for many different polymers and polymer mixtures but their discussion has been mainly of a qualitative nature and confined to the reporting of limiting surface areas. Although in recent years the interpretation of surface pressure isotherms has become a little more quantitative, there is currently no general theory of organization of polymers at the air-water interface which can be compared with experimental data. Since Alexander's pioneering work in 1977 [Alexander 1977], many attempts have been taken to describe the monolayer behavior of polymers by scaling, computational and other approaches [Bouchaud 1987, Zhulina 1991, Halperin 1992, Ligoure 1993, Srinivas 2004a].

Nonetheless, certain general questions can be addressed; these include queries regarding the thickness and morphology of the spread films and the influence of the surface concentration on these parameters. Where the spread polymer film has an amphiphilic nature questions concerning the distribution in space of the hydrophobic and hydrophilic regions arise.

It is impossible to review and mention all systems which have been investigated so far. Detailed overviews on the research performed with polymer films at the air water interface can be found in Jones [Jones 1999] and Birdi [Birdi 1989].

Examples of homopolymers of which the monolayer behavior is described are e.g. poly(ethylene oxide) (PEO) [Henderson 1993], poly(vinyl acetate) (PVAC) [Ober 1977], poly(methacrylate) (PMAA) [Takahashi 1982] and poly(methyl methacrylate) (PMMA) [Vilanove 1980].

The blends of the following homopolymers have been studied at the air-liquid interface: poly(methacrylate)/poly(vinyl acetate) (PMAA/PVAC) [Gabrielli 1982] poly(methyl methacrylate)/poly(vinyl acetate) (PMMA/PVAC) [Gabrielli 1982] and poly(dimethyl siloxane)/ polyhedral oligomeric silsesquioxane (PDMS/POSS) [Hottle 2004].

The air-liquid interfacial properties of the following linear diblock and triblock copolymers were reported: poly(dimethyl siloxane)-b-poly(styrene) (PDMS-PS) [Kent 1992], poly(ethylene oxide)-b-poly(ethyl ethylene) (PEO-PEE) [Wesemann 2003], poly(ethylene oxide)-b-poly(methyl methacrylate) (PEO-PMMA) [Rochford 1995], poly(ethylene oxide)-b-poly(styrene) (PEO-PS) (Fig. 2.34) [Bijsterbosch 1995, Fauré 1998], poly(vinyl acetate)-b-poly(styrene) (PVAC-PS) [Ikada 1980], polyester-b-poly(ethylene oxide)-b-polyester (UP-PEO-UP) [Myrvold 1996] and poly(ethylene oxide)-b-poly(propylene oxide)-b-poly(ethylene oxide) (PEO-PPO-PEO) [O'Connor 1999, Muñoz 2000].

An example where grafted block copolymers were employed for monolayer experiments is poly(vinyl acetate)-g-poly(styrene) (PVAC-PS) [Ikada 1980]. I must not fear. Fear is the mind-killer. Fear is the little-death that brings total obliteration. I will face my fear. I will permit it to pass over me and through me. And when it has gone past I will turn the inner eye to see its path. Where the fear has gone there will be nothing. Only I remain [Herbert 1968].

The isothermal behavior of many lipopolymers has also been described, such as dioctadecanoyl glycerol-poly(methyl oxazoline) (DC₁₈Gly-PMOXA) [Baekmark 1999], dioctadecanoyl glycerol-poly(ethyl oxazoline) (DC₁₈Gly-PEOXA) [Baekmark 1999], dimyristoyl phosphatidylcholine-poly(methyl oxazoline) (DMPC-PMOXA) [Gutberlet 2000] and distearoyl phosphatidylethanolamine-poly(ethylene oxide) (DSPE-PEO) [Barkmark 1995, 1999, Majewski 1997].

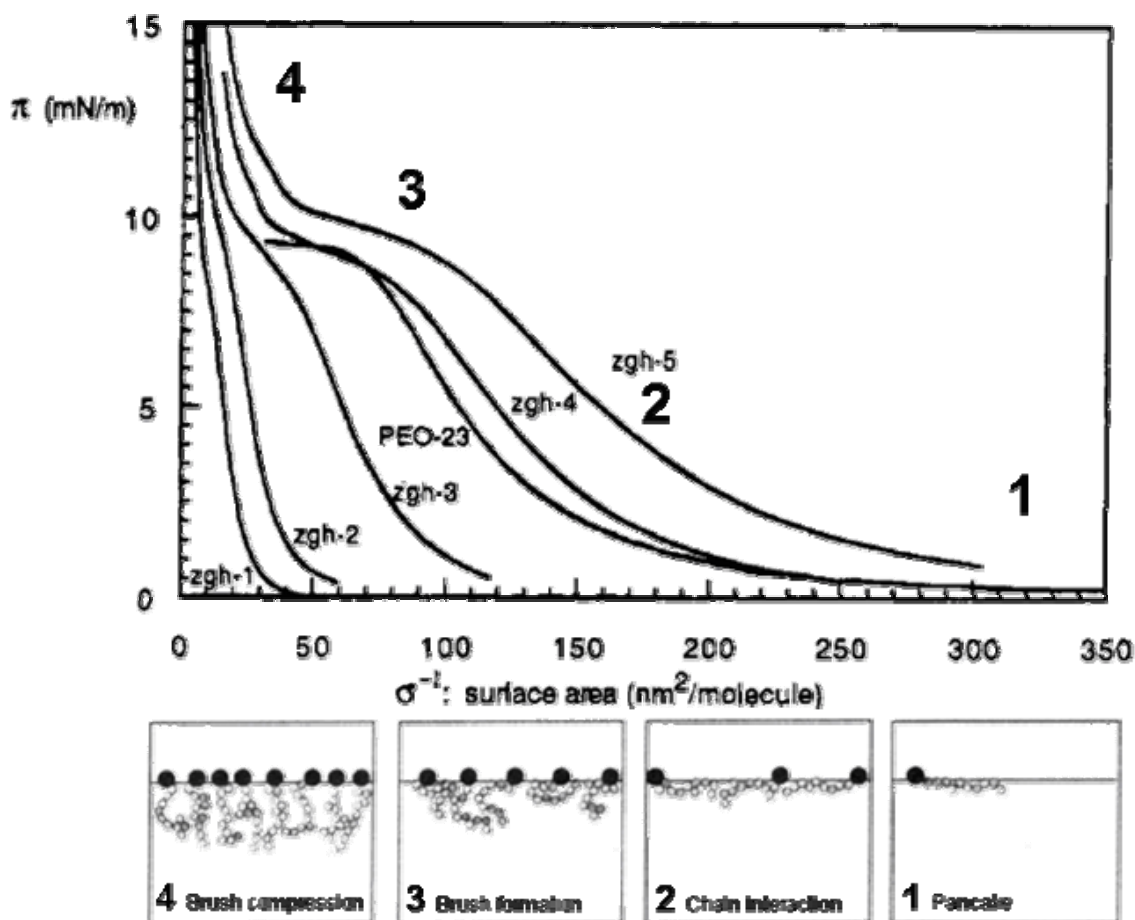


Figure 2.34. Surface pressure-area isotherms of different PS-PEO block copolymers (zgh-1 – PS₄₀₀₀PEO₃₉₅₀, zgh-2 – PS₄₀₀₀PEO₆₅₀₀, zgh-3 – PS₄₀₀₀PEO₁₁₀₀₀, zgh-4 – PS₄₀₀₀PEO₁₉₆₀₀, zgh-5 – PS₄₀₀₀PEO₃₀₈₀₀, PEO-23 – PEO₂₃₀₀₀) and sketch of diblock copolymer phase behavior at the respective surface pressures [Bijsterbosch 1995].

2.4. Membrane active peptides

2.4.1. Membrane proteins

More than 3 billion years ago, primitive replicating forms became enveloped in a lipid film, a diffusion barrier that separated the living cell from its environment. Although this lipid membrane had the advantage of retaining vital cell components, it would have prevented the access of necessary substances and the loss of waste products. Thus new transport and signaling mechanisms had to evolve hand-in-hand with the appearance of the membrane [*Hille 2001*].

One universal feature of all cells is an outer limiting membrane called the plasma membrane. In addition, all eukaryotic cells contain elaborate systems of internal membranes which set up various membrane-enclosed compartments within the cell. The plasma membrane is built from lipids, carbohydrates and proteins and serves as the interface between the machinery in the interior of the cell and the extracellular fluid [*Alberts 1994*].

A membrane protein is a protein molecule that is attached to, or associated with the membrane of a cell or an organelle. Membrane proteins can be classified into two groups, based on their attachment to the membrane, integral and peripheral membrane proteins.

2.4.1.1. Integral membrane proteins

Integral membrane proteins are firmly attached to the membrane. In most cases, the protein spans the entire membrane (a transmembrane protein) but in all cases, the protein is anchored in the membrane's hydrophobic region. A detergent is necessary to disrupt the lipid bilayer and solubilize the protein. A hydrophobic domain of the protein resides in the lipophilic core of the membrane, while hydrophilic domains protrude into the aqueous environment inside and outside the cell or compartment. Transmembrane proteins often have their N-terminal on the exoplasmic face and their C-terminal on the cytoplasmic face. Many transmembrane proteins have multiple membrane spanning segments which anchors them to the membrane. Most transmembrane proteins have an internal topogenic sequence.

Most commonly the function of integral membrane proteins is to act as a transporter for various molecules that would otherwise not be able to move across the cell membrane (ion channels, porins). When used as a transporter, its most common configuration is to have an extra-cellular domain and a cytoplasmic domain separated by a non-polar region that holds it tightly in the cell membrane.

Examples of other functions of integral membrane proteins include the identification of the cell for recognition by other cells (transmembrane receptors), the anchoring of one cell to another or to surrounding media (linkers, markers, cell adhesion molecules), and the initiation of intracellular responses to external molecules (enzymes) (Fig. 2.35).

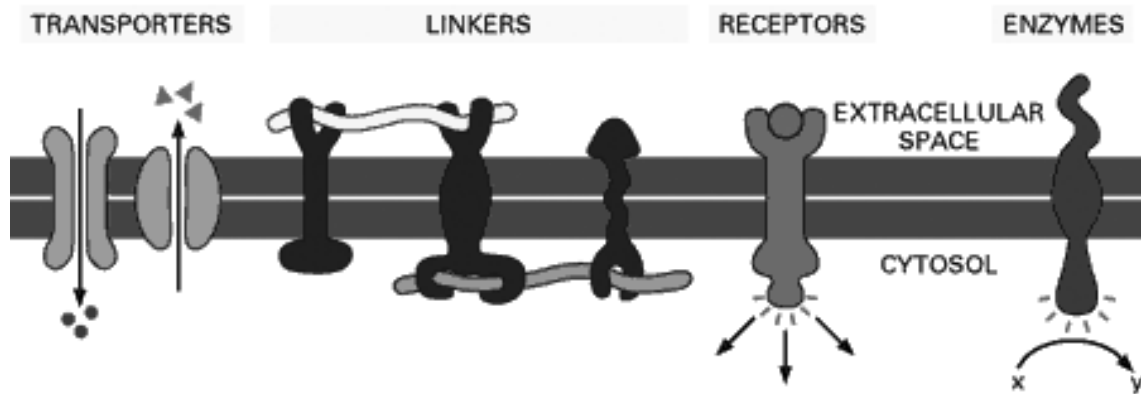


Figure 2.35. Schematic of a variety of integral membrane proteins and their intrinsic functions [Alberts 1998].

2.4.1.2. Peripheral membrane proteins

Peripheral membrane proteins are proteins that adhere only loosely to the biological membrane with which they are associated. These molecules do not span the hydrophobic core of the membrane, but attach indirectly, typically by binding to integral membrane proteins, or by interactions with the lipid polar head. Therefore the so-called regulatory protein subunits of many ion channels and transmembrane receptors, for example, may be defined as peripheral membrane proteins. These proteins, in contrast to integral membrane proteins, tend to collect in the water-soluble fraction during protein purification.

2.4.2. Antimicrobial peptaibols

Gene-encoded peptide antibiotics are ubiquitous components of host defenses in the plant and animal kingdom [Martin 1995]. The first antimicrobial peptide to be discovered was alamethicin in 1967 [Meyer 1967]. Whereas the animal antibiotic peptides often exhibit a wide range of antibacterial, antifungal, virucidal, and tumoricidal activities, exclusively antifungal properties have been described for most plant defensins [Broekaert 1997]. Because the activation and deployment of pathogen-specific immune responses occur slowly relative to the potential kinetics of microbial proliferation, epithelial surfaces and phagocytic cells are equipped with various antimicrobial substances that act rapidly to neutralize a broad spectrum of pathogenic microbes. Small endogenous antimicrobial peptides are stored in granules or vesicles which can be released or fused quickly into a phagosome, or they can be synthesized and excreted very rapidly after induction in certain types of cells, thus allowing them to play an important role in the initial phases of resistance to microbial invasion [Huang 2000]. Antimicrobial peptides are typically 20-40 amino acids in length, with a folded size approximating the membrane thickness. All evidence indicates that antimicrobial peptides act by disturbing the bilayer integrity, either by disruption or pore formation. The resulting openings in the lipid bilayer lead to a collapse of the transmembrane electrochemical gradient, killing the cell [Boman 1994]. The action does not involve stereospecific protein receptors; it is the result of direct interaction with the lipid matrix of the membranes. However, such interactions are generally considered to be nonspecific. The target cell selectivity is probably regulated by electrostatic interactions [Lohner 1997]. Bacterial membranes contain negatively charged lipids on the outer leaflet, whereas the outer leaflets of eukaryotic cell membranes are predominantly neutral [Gennis 1989]. Despite their diversity in structure, most antimicrobial peptides are positively charged. Alamethicin is one of the rare exceptions being not cationic.

Although their secondary structures differ remarkably, the overall shape of each antimicrobial peptide, with the side chains filling the space, is roughly cylindrical. An important characteristic of these peptides is that the folded cylindrical structures are hydrophobic on one side along the cylindrical axis and hydrophilic on the other. Thus, the minimum free energy configuration of a single peptide by itself is adsorbing on the bilayer's hydrophilic-hydrophobic interface with the cylindrical axis more or less parallel to the plane of the bilayer [Huang 2000].

2.4.2.1. Molecular structure of alamethicin

Alamethicin (alm, U22324) ($M = 1964 \text{ g mol}^{-1}$) is a linear peptide antibiotic, produced in vivo by the fungus *trichoderma viride*. This fungus is a common inhabitant of soils and its secretions (including alamethicin) are believed to affect the quality of pasture land through effects on the bacterial contents of ruminant animal stomachs [Jen 1987]. The in vivo synthesis is nonribosomal so that production of the peptide using recombinant DNA methods is not possible [Kleinkauf 1987].

Alm consists of 19 amino acids and 1 amino alcohol. Although cyclic structures and different peptides sequences have been proposed [Payner 1980, Martin 1076], there is now general consensus on the molecular structure. Two native forms occur, the R_f30 form with a Glu residue at position 18 and the R_f50 form in which this Glu is replaced by a Gln, making the peptide electrically neutral [Pandey 1977, Fox 1982]:

The 20 AA peptide sequence (R_f30) is (Fig. 2.36):

Ac – Aib – L-Pro – Aib – L-Ala – Aib – L-Ala – **L-Gln** – Aib – L-Val – Aib – L-Gly – L-Leu – Aib – L-Pro – L-Val – Aib – Aib – **L-Glu** – **L-Gln** – L-Phl

(Ac = acetyl, Phl = phenylalaninol, hydrophilic residues in bold, L denotes chirality of respective amino acid)

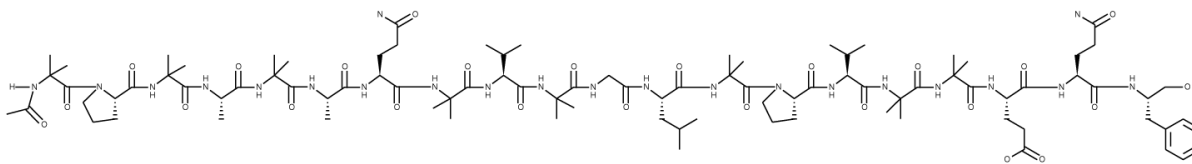


Figure 2.36. Molecular structure of the amino acid sequence of alamethicin.

Alamethicin contains the non-proteinogenic amino acid 1-amino isobutyric acid (Aib, or α -methylalanine) and the preponderance of this rather unusual amino acid is the reason for the peptide's name [Woolley 1992]. The amino terminus is acetylated and the C terminal residue is an amino alcohol. Alamethicin and naturally occurring analogues have been termed 'peptaibols' since these peptides all contain Aib residues and a C-terminal amino alcohol.

The Aib residues restrict the conformational space so that an α -helical peptide structure is preferred [Nagaraj 1981]. Due to the fact that Aib is achiral, left- and right-handed helical conformations are likely, however the presence of L-amino acids confers a preference for right-handed helices [Jung 1988].

The central Gly-X-X-Pro motif forms a molecular hinge between the two α -helical segments to the left and to the right (Fig. 2.37) [Franklin 1994].

The α -helical dimensions of alm were determined from crystal structure to be 3.2 nm in length parallel to the helix axis and 1 nm in diameter [Fox 1982].

Alamethicin is amphiphilic because its hydrophilic groups are at the C-terminus or delineate a narrow longitudinal hydrophilic sector (residues Gln7, Gly11, Gln18, and exposed backbone of Aib10 and Gly11 because of the kink). The majority of the amino acid residues, including the N-terminus, are of hydrophobic nature [White 1998].

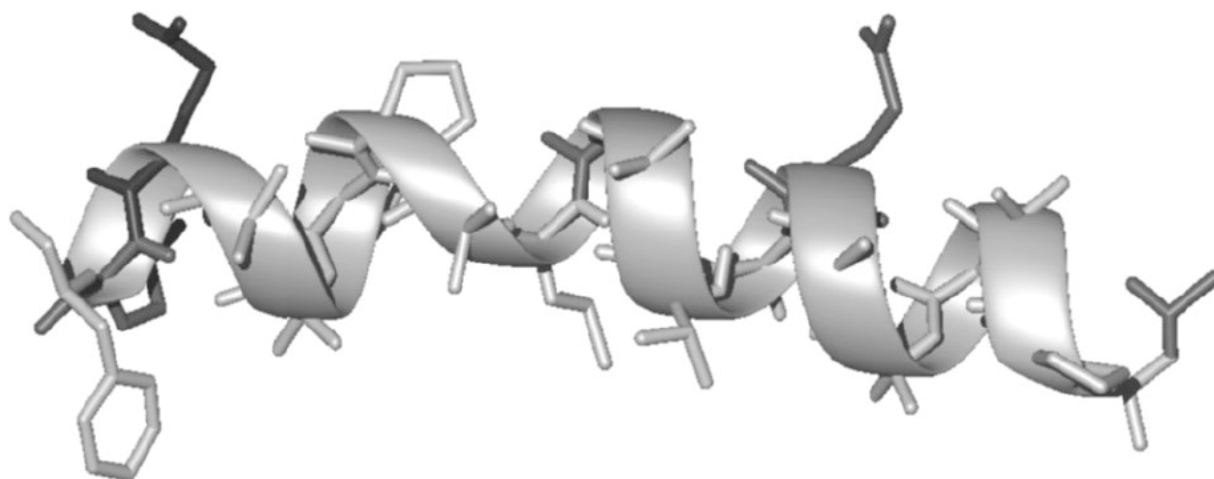


Figure 2.37. Representation of an alamethicin α -helix with kink determined by crystal structure analysis [Bechiner 2004].

2.4.2.2. Structure of ion channels and mechanisms of pore formation

The voltage-gated channel forming properties of alamethicin have been described already in 1968 by Mueller & Rudin [Mueller 1968]. The α -helix has an excess of negative charge at the C-terminus and positive charge at the N-terminus due to alignment of the dipole moments of individual peptide bonds [Hol 1981]. Thus, a peptide in the α -helical conformation may be thought of as a macro-dipole with a large dipole moment (54.1 D [Chugh 2002]). The molecular origin of voltage-dependent conductance has been a fundamental problem in biophysics for many years.

Although hundreds of publications have been written on alamethicin, its channel forming properties in cell membranes could not be fully elucidated yet. Different mechanisms were and are proposed. One of the first concepts claimed that alamethicin forms gramicidin-like head-tail n-mers with a central cavity for the ions to pass through [Payne 1970, Ovchinnikov 1971, 1974, Martin 1975]. While this model soon was recognized as impossible, other mechanisms emerged which are still under discussion.

In the so-called barrel-stave model, a channel is formed by aggregation of 4 to 12 parallel perpendicular oriented α -helices, polar faces at the center of the bundle and nonpolar residues to the exterior in contact with the lipid membrane. (Fig. 2.38 & 2.39) [Gordon 1976, Nagaraj 1981, Mathew 1982, Duclohier 2001, Tieleman 2001b].

This model provides a straightforward explanation for the strong peptide-concentration dependence of channel formation. The discrete conductance multi-levels in single ion-current measurements can be explained by a discretely varying pore radius due to addition or removal of peptide monomers [Sansom 1993a]. Several modes of action have been proposed for the voltage-gated molecular mechanism of channel formation [Woolley 1992].

In the 'surface to transbilayer reorientation model', it is proposed that alm molecules are adsorbed to the membrane surface in the absence of an electric field but are tilted into the membrane by application of a voltage [Baumann 1974].

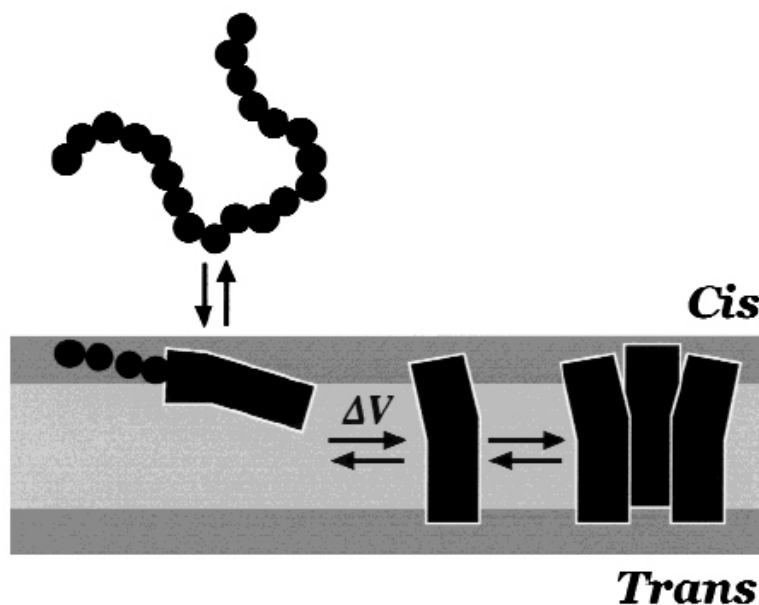


Figure 2.38. Pathway of channel formation according to the barrel-stave model. Upon secretion individual alm helices adsorb at the membrane interface. An electrical field or an increased concentration drives the individual molecules to build oligomeric perpendicular pores [Duclohier 2001].

In a more recent 'two-state model' it is assumed, that at low peptide-to-lipid ratios, the peptide tends to adsorb in the lipid headgroup region in a functionally inactive state. At a certain threshold concentration of peptide, a multiple-pore state is formed [Huang 2000].

The 'pre-aggregate and conformational change model' proposes that a preaggregate of alamethicin molecules exists which changes conformation and becomes conducting when a voltage is applied [Fox 1982, Hal 1983, Barranger-Mathys 1996].

Boheim proposed the 'flip-flop model' which does not require a conformational change. Alamethicin monomers form aggregates in an antiparallel fashion. A voltage causes monomers to flip in the membrane so that all dipoles become aligned with the field [Boheim 1983].

The 'voltage dependent partitioning model' describes, that alm helices can aggregate also in the absence of a potential. If a sufficient concentration of peptide is reached, conducting aggregates may form. An electric field eases alamethicin association [Rizzo 1987].

The commonly accepted barrel-stave model has recently been confronted with a different explanation by Ionov et al., who proposed a lipid-covered ring model (Fig. 2.40 & 2.41). The model includes a plate-like peptide ring covered with a lipid monolayer, an arrangement that imparts structural asymmetry to the channel. Thus the α -helical axis within the alamethicin aggregate are oriented perpendicular to the pore axis and hence parallel to the membrane/water interface. The alm helices form stable two-dimensional aggregates, with a central hydrophilic ring-like cavity formed by the polar hydrophilic C-terminal amino acid residues. The radius of the pore could vary discretely by the addition or subtraction of helical monomers.

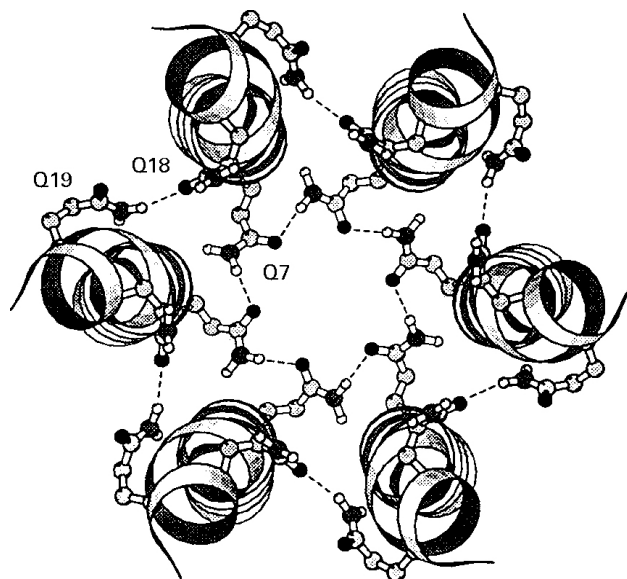
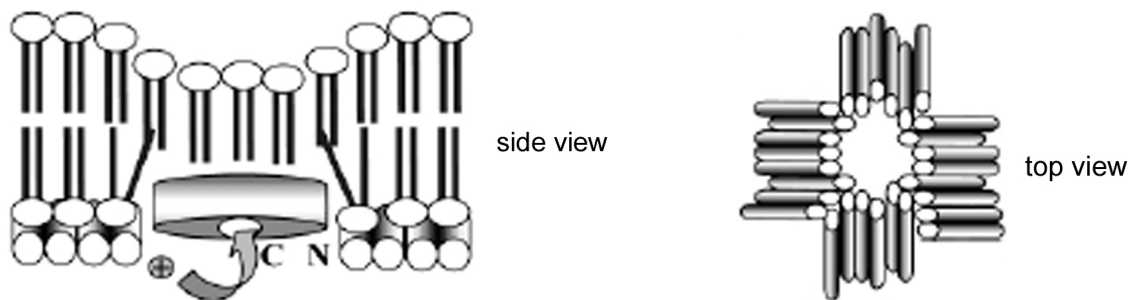


Figure 2.39. Model of a hexameric helical barrel. The alamethicin molecules are oriented such that their N-terminal helices are parallel. Possible channel-stabilizing hydrogen bonds involving the side chains of residues Gln-7, Gln-18 and Gln-19 are indicated [Sansom 1993b].



Figures 2.40 (left) & 2.41 (right). Scheme of lipid covered ring model of plate-like surface adsorbed alamethicin aggregates (side view and top view) [Ionov 2004].

The polar surface of the peptide helix is oriented toward the water phase (cis-side) whereas the hydrophobic part is pointed toward the hydrocarbon chains of the adjacent monolayer of the membrane (trans-side). This orientation of the helices is energetically highly favorable.

Upon the application of a weak positive electrical field to the cis-side, cations enter the hydrophilic cavity of the ring and disturb the relatively fluid hydrophobic tails of the phospholipids of the trans-monolayer. Strong positive electrical fields are able to open the channel because of the force applied by the cation to the trans monolayer.

If the applied field is of opposite sign (i.e. a negative field applied to the cis-side), the energy of anions should be sufficient to overcome both potential barriers, the one of the cavity and the one of the trans-side monolayer. Therefore, a higher negative voltage would be necessary to open the channel and to allow anions to pass [*Ionov 2000, 2004*].

All of these proposed modes of action of pore formation are under discussion but clear elucidation is complex because of problems to distinguish unequivocally between free aqueous alm, closed channels and open channels with classical experimental methods (crystallography, NMR, XRD, FTIR, CD, Langmuir isotherms, BAM). In recent years many computational approaches were accomplished to get further insight into the dynamics and mechanism of alm aggregation and pore formation in lipid bilayers with or without applied electrical field [*Breed 1997, Tieleman 1999, 2001a, 2001b, Kessel 2000, Cantor 2004*].

It is generally agreed that ions from the electrolyte are not involved in the gating mechanism of alamethicin since an extremely wide variety of ions can be used as charge carriers with little difference in voltage gating [*Gordon 1975*]. Other environmental conditions like peptide-lipid ratio, lipid-type or lipid-mobility have a major influence on channel formation [*Kikukawa 2002*].

It is generally established that alm forms ion channels that transport small mono- and divalent cations and anions [*Gordon 1976, Nagaraj 1981, Mathew 1982, Smith 1999*]. Ion selectivity is minimal although cations are somewhat preferred over anions [*Eisenberg 1973, Starostin 1999*].

*Wir werden vom Schicksal
hart oder weich geklopft;
es kommt auf das Material an!*

Marie v. Ebner-Eschenbach

CHAPTER 3

MATERIALS AND METHODS

3. Materials and methods

Unless mentioned all manipulations were performed at room temperature.

3.1. Materials

3.1.1. Reagents

The following reagents were obtained from Fluka AG, Buchs/CH:

Benzophenone (purum), calcium hydride (technical 95%), chloroform (puriss. p.a.), 5-cholesten-3 β -ol (>99.0%), dihexadecyl phosphate (purum), dipotassium hydrogen phosphate (puriss. p.a.), ethanol (puriss. or technical 96%), ethyl acetate (puriss.), hexadecane (purum), hexane (puriss. p.a.), 4-(2-hydroxy-ethyl) piperazine-1-ethanesulfonic acid (>99.0%), methanol (puriss. p.a.), 2-methyl-2-oxazoline (purum), molecular Sieve UOP Type 4A (rods), potassium dihydrogen phosphate (puriss. p.a.), potassium chloride (puriss. p.a.), triethylamine (purum), trifluoromethanesulfonic anhydride (purum)

Other reagents were purchased as follows:

Alamethicin (Sigma, St. Louis/MO & Biomol Research Laboratories Inc., Plymouth Meeting/PA), deuteriochloroform (Aldrich Inc., Milwaukee/WI, 99.96% D, 0.03% (V/V) TMS), 5-(4,6-dichlorotriazinyl) aminofluorescein (Molecular Probes, Eugene/OR), ethanol (Schweizerhall Chemie AG, Basel/CH, technical 96%), Hellmanex II (Hellma GmbH, Müllheim/D), L- α -phosphatidylcholine (Sigma, St. Louis/MO, ~99%), bis(hydroxyalkyl) terminated poly(dimethylsiloxane) (M = 1941 g mol⁻¹, Wacker-Chemie GmbH, München/D), α,ω -bis(3-hydroxypropyl) poly(dimethylsiloxane) (M = 5600 g mol⁻¹, Aldrich Inc., Milwaukee/WI), potassium hydroxide (Riedel-de Haën, Seelze/D, technical 85%), tetramethylrhodamine-5-carbonyl azide (Molecular Probes, Eugene/OR), tripotassium phosphat (Riedel-de Haën, Seelze/D, puriss.)

Unless mentioned, the reagents were used without any further purification.

3.1.2. Triblock copolymer synthesis

The amphiphilic block copolymers used in this work were two hydroxy terminated poly(2-methyloxazoline)-block-poly(dimethylsiloxane)-block-poly(2-ethyloxazoline) triblock copolymers (PMOXA₁₆-PDMS₇₄-PMOXA₁₆, $M_n = 8360 \text{ gmol}^{-1}$ and PMOXA₁₃-PDMS₂₃-PMOXA₁₃, $M_n = 4150 \text{ gmol}^{-1}$, further referred to as A₁₆B₇₄A₁₆ and A₁₃B₂₃A₁₃, respectively, Figure 3.1). The main difference between the two polymers is the length of the hydrophobic block, whereas the hydrophilic part is essentially of very similar size.

For specific investigations and applications, further triblock copolymers were used, namely fluorescently labeled and amino functionalized polymers.

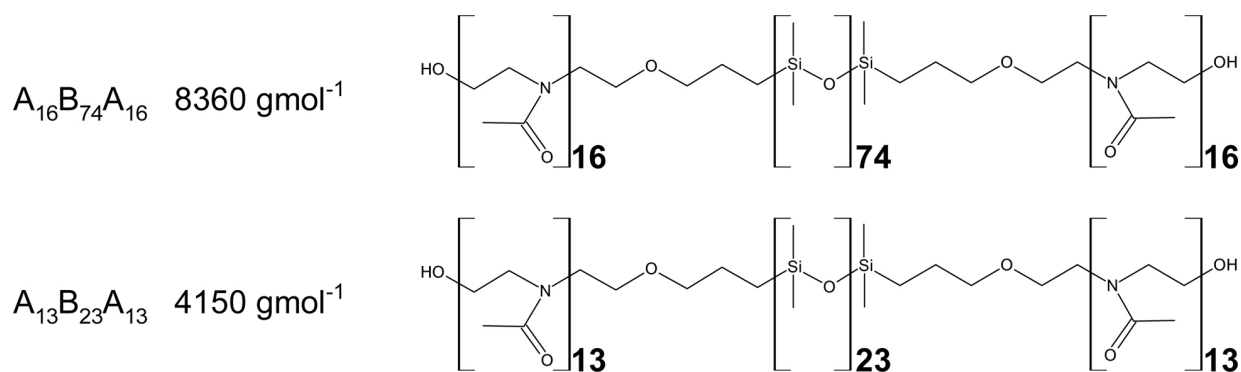


Figure 3.1. Chemical structure of the investigated polymers.

3.1.2.1. $PMOXA_{16}$ - $PDMS_{74}$ - $PMOXA_{16}$

Hydroxy terminated poly(2-methyloxazoline)-block-poly(dimethylsiloxane)-block-poly(2-methyloxazoline) triblock copolymer ($PMOXA_{16}$ - $PDMS_{74}$ - $PMOXA_{16}$, $M_n = 8360 \text{ g mol}^{-1}$, further referred to as $A_{16}B_{74}A_{16}$) was synthesized according to the method described by Nardin [Nardin 2000a] through cationic ring opening polymerization of 2-methyl-2-oxazoline with activated bis(hydroxyalkyl) terminated poly(dimethylsiloxane) (Fig. 3.2) [Saegusa 1976, Kobayashi 1984, 1990].

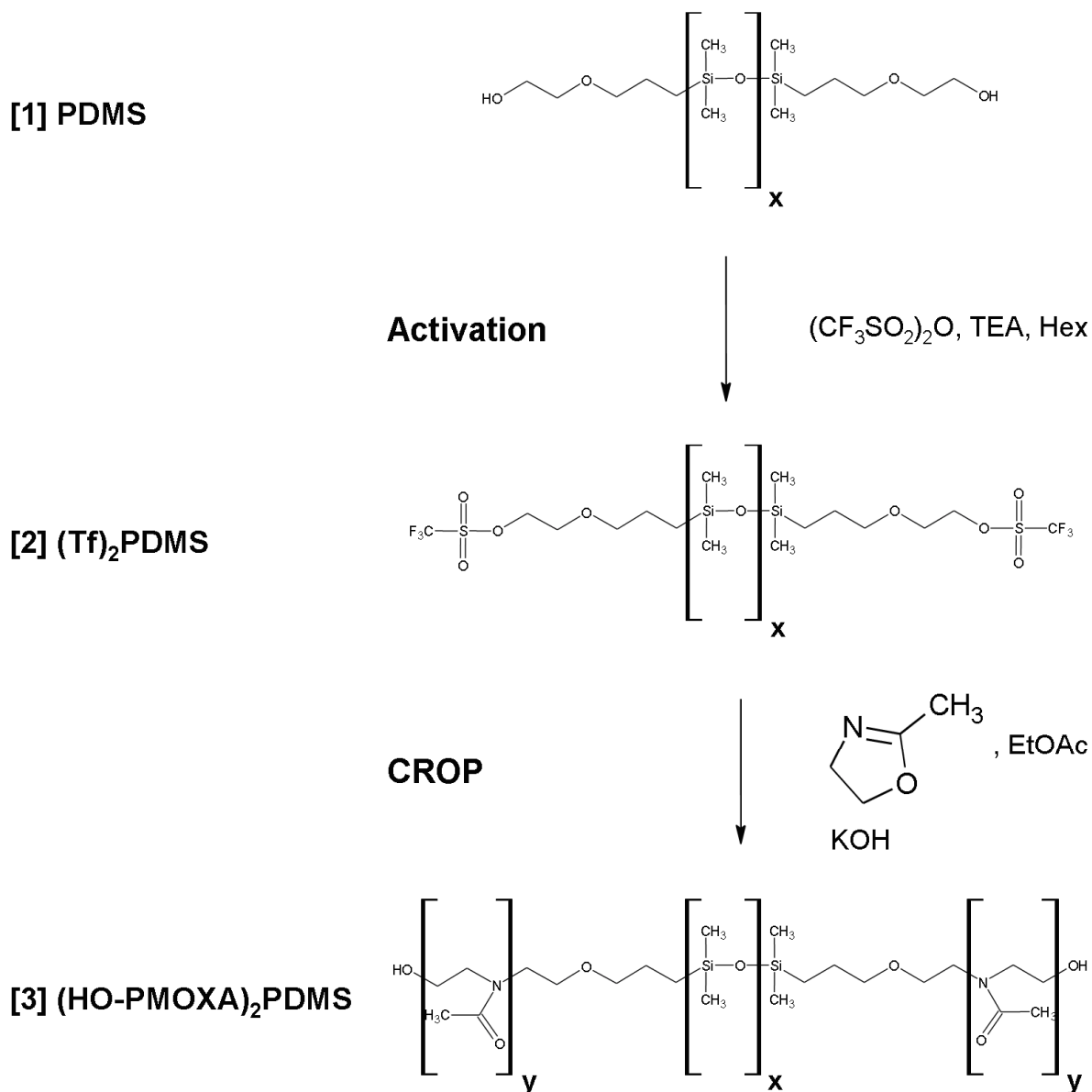


Figure 3.2. Reaction scheme of $PMOXA$ - $PDMS$ - $PMOXA$ synthesis.

3.1.2.1.1. Activated Poly(dimethylsiloxane)

In a 500 ml round-bottom flask with a Soxhlet extractor (filled with molecular sieve 4 Å), 20.58 g (3.68 mmol) α,ω -bis(3-hydroxypropyl) poly(dimethylsiloxane) [1] ($M = 5600 \text{ g mol}^{-1}$, Aldrich Inc., Milwaukee/WI) was dissolved in 100 ml absolute hexane and refluxed for 24 h in nitrogen atmosphere. Subsequently, 1.19 ml (8.45 mmol) of dry triethyleamine were added at room temperature and the solution was stirred for 30 min at 0 °C. Then, 1.28 ml (7.73 mmol) of trifluoromethanesulfonic acid anhydride in 8 ml absolute hexane were added dropwise to the PDMS solution for 30 min and the mixture was stirred for 1 h at 0 °C. After removal of the solvent under high vacuum, 70 ml of distilled hexane were added and the solution was cooled at 0 °C for 12 h. The resulting suspension was filtered under vacuum at 0 °C using a G4 glass filter funnel. The solvent was evaporated under high vacuum.

The yield was 19.72 g (3.36 mmol, 91.4 %) of clear colorless oil [2].

$^1\text{H NMR}$ (CDCl_3 , 400 MHz, ppm): 0.02 (s, $\text{CH}_3\text{-Si}$), 0.51 (m, $\text{-CH}_2\text{-CH}_2\text{-Si}$), 1.8 (m, $\text{-CH}_2\text{-CH}_2\text{-CH}_2\text{-}$), 4.4 (m, $\text{CF}_3\text{SO}_3\text{-CH}_2\text{-CH}_2\text{-}$).

3.1.2.1.2. Hydroxy terminated triblock copolymer

19.72 g (3.36 mmol) of bifunctional PDMS [2] were dissolved in 150 ml absolute ethyl acetate. 12.60 ml (148.04 mmol) of freshly distilled 2-methyl-2-oxazoline were added and the solution was refluxed for 60 h at 40 °C. At room temperature, 14.78 ml (7.39 mmol) of potassium hydroxide were added. After 3 h of stirring the solvent was removed yielding 27.99 g colorless solid polymer. The triblock copolymer was purified by ultrafiltration (water:ethanol = 5:1) and afterwards lyophilised yielding 26.23 g (3.14 mmol, 93.4 %) of white glassy solid [3]. The molecular weight was determined by $^1\text{H NMR}$.

$^1\text{H NMR}$ (CDCl_3 , 400 MHz, ppm): 0.02 (s, $\text{CH}_3\text{-Si}$), 0.51 (m, $\text{-CH}_2\text{-CH}_2\text{-Si}$), 1.62 (m, $\text{-CH}_2\text{-CH}_2\text{-CH}_2\text{-}$), 2.19 (m, $\text{CH}_3\text{-CON}<$), 3.55 (m, $>\text{N-CH}_2\text{-CH}_2\text{-N}<$), 3.71 (m, $\text{-CH}_2\text{-CH}_2\text{-CH}_2\text{-}$).

FT-IR (KBr , cm^{-1}): 3461 (m, δ O-H), 2975 (m, ν C-H), 1630 (s, ν C=O), 1420 (m, δ_s CH_2), 1255 (s, δ_s $\text{Si}(\text{CH}_3)_2\text{-O}$), 1025 (s, δ_s $[\text{-Si}(\text{CH}_3)_2\text{-O-}]_n$), 790 (s, δ_s $\text{Si}(\text{CH}_3)_2$).

3.1.2.2. $\text{PMOXA}_{13}\text{-PDMS}_{23}\text{-PMOXA}_{13}$

$\text{PMOXA}_{13}\text{-PDMS}_{23}\text{-PMOXA}_{13}$, $M_n = 4150 \text{ g mol}^{-1}$, further referred to $\text{A}_{13}\text{B}_{23}\text{A}_{13}$, was synthesized by Dr. Jörg Widmer according to Nardin [Nardin 2000a] through cationic ring opening polymerization of 2-methyl-2-oxazoline (Fluka AG, Buchs/CH, purum) with activated bis(hydroxyalkyl) terminated poly(dimethylsiloxane) ($M = 1941 \text{ g mol}^{-1}$, Wacker-Chemie GmbH, München/D) [Widmer 2000].

3.1.2.3. Amino terminated triblock copolymers

Amino terminated triblock copolymers were synthesized by Dr. Roxana Timmermans-Stoenescu according to a method described by Furukawa et al. [Furukawa 1960]. In the terminal step after the polymerization, ammonia was added instead of potassium hydroxide to yield an amino terminated $\text{H}_2\text{N-PMOXA}_{30}\text{-PDMS}_{75}\text{-PMOXA}_{30}\text{-NH}_2$ [Stoenescu 2004].

3.1.2.4. Dye labeled triblock copolymers

Fluorescent dye labeled triblock copolymers were synthesized by Dr. Roxana Timmermans-Stoenescu [Stoenescu 2004]. The azide dyes were reacted with the hydroxy terminated poly(2-methyloxazoline) ends of triblock copolymers with intermediate isocyanates to form carbamic acid esters [Curtius 1915]. 5-(4,6-dichlorotriazinyl) aminofluorescein (DTAF) and tetramethyl rhodamine-5-carbonyl azide (TAMRA) were employed because of their high reactivity against alcohol groups and their fluorescent properties.

3.1.2.4.1. DTAF labeled polymers

5-(4,6-dichlorotriazinyl) aminofluorescein (DTAF) – single isomer dye was purchased from Molecular Probes and was used without further purification. The conjugation of asymmetric triblock copolymer with a fluorescein derivative was performed according to a literature procedure [Balestrieri 1996, Ahmed 2001]. The labeled triblock copolymer was purified using size exclusion chromatography on Sephadex G-50 in the dark.

3.1.2.4.2. TAMRA labeled polymers

The rhodamine conjugated triblock copolymers were synthesized by employing tetramethyl rhodamine-5-carbonyl azide (TAMRA) by an adapted procedure [Tan 1993, Gingell 1994]. The labeled polymer was purified by ultrafiltration through membranes with 3 kD cut off.

3.2. Methods

3.2.1. Langmuir monolayers

For surface pressure-area (π -A) isotherms either a Langmuir-Blodgett minitrough (surface area 273 cm²) or a BAM trough (surface area 432 cm²) was used (both from KSV Instruments Ltd., Helsinki/SF; solid PTFE/Teflon[®] troughs equipped with two symmetrically moving hydrophilic Delrin barriers and a Wilhelmy plate film balance).

Prior to experiments, the trough was thoroughly cleansed with chloroform and ethanol, rinsed with water (double-distilled or ultrapure from ELGA, resistivity 18 M Ω cm, pH 5.5) and filled with the aqueous subphase (either pure water or a phosphate buffer saline (50 mM Na₂HPO₄, 10 mM KCl, pH 7.4)). No difference was noticed concerning the mean molecular area or the isotherm patterns whenever PBS buffer was used compared to ultrapure water as subphase. The barriers were cleaned with ethanol and rinsed with water. The Wilhelmy plate (made of chromatography paper, ashless Whatman Chr 1, perimeter 20 mm) was allowed to equilibrate for at least 30 minutes. The surface was cleaned repeatedly through compression - aspiration - expansion cycles and checked for impurities.

For each mixture series, the same number of molecules (typically 10¹⁵-10¹⁶) was spread dropwise from chloroformic or ethanolic stock solutions of 0.02-0.1 % (wt/wt) on the surface. The solvent was allowed to evaporate for 10 minutes, and the monolayers were compressed at a rate of 1-15 mm/min. After each measurement, the surface was cleaned and checked for impurities. All experiments were performed at 20°C in a dust-free room; for additional protection from impurities the trough was housed in a Plexiglas cabinet.

3.2.2. Brewster angle microscopy(BAM)

A BAM2plus Brewster angle microscope (Nanofilm Technologie GmbH, Göttingen/D) with a Nd-YAG laser at 532 nm, Nikon 10x Plan Epi SLWD objective (N.A. 0.30) and monochrome CCD camera attached to real-time frame grabber) was used, mounted over the Langmuir trough. The images were captured either as single frames or in line scan mode and corrected for geometry and contrast.

Owing to the fact that the intensity of light (I) reflected from an optically isotropic molecular film at the Brewster angle of the subphase depends on the film thickness (d) as $I = C \cdot d^2$, where C is an instrument constant [Azzam 1992], it is possible to estimate the relative thickness of the investigated monolayers. The gray level of the camera was converted into absolute intensity values after calibration was performed as described by Rodriguez Patino and co-workers [Patino 1999].

3.2.3. Langmuir-Blodgett (LB) film transfers

For LB film transfers, the above described KSV mini trough was employed equipped with a software controlled and automatic film deposition system (KSV Instruments Ltd., Helsinki, Finland). The surface pressure was kept constant by a computer controlled feedback system between the electrobalance, measuring the surface pressure, and the barrier motor.

Due to the fact, that only hydrophilic solid substrates were used and only single layers were deposited, the cleansed or etched solid substrate was attached on the dipper and placed in the subphase prior to spreading the Langmuir film on the air-water surface. The monolayers were deposited at various surface pressures (liquid expanded to super liquid regime) by dipping the hydrophilic solid substrate (e.g. mica) from the subphase through the monolayer at a typical dipper speed of 0.5-1 mm/min.

3.2.4. Contact angle measurements

Contact angles were measured on a homemade setup, built by Thomas Kaufmann, Biocentre of the University of Basel. A droplet of 4 μ l MilliQ water (18M Ω) was added on the sample substrate and a total of six images were acquired per droplet by two perpendicularly arranged CCD-cameras. Image analysis and mean contact angle calculation was performed by an algorithm written by Thomas Kaufmann [*Kaufmann*].

3.2.5. Preparation of polymersomes

All methods reported for liposome preparation work in general also for self-assembled vesicular structures of amphiphilic polymers (polymersomes) [*Kita-Tokarczyk 2005a*]. Preparation methods can be divided in two groups: solvent free techniques and ones using organic solvents. In the first group the amphiphile is brought in contact with the aqueous media in a dry state and is subsequently hydrated to yield vesicles. This offers the advantage, that no organic solvents is present in the system what can be mandatory for certain applications.

In the second group the block-copolymer is first dissolved in an appropriate organic solvent and then mixed with water. The organic phase is subsequently excluded with an appropriate technique. This leads only to virtually solvent free conditions. It is not possible to completely get rid of all solvent. Solvent residues may interfere in biological and galenical applications and further they fluidize membranes leading to decreased vesicle stabilities and promoted aggregation [*Meng 2003*].

Due to this fact, only solvent free preparation methods were used to make polymersomes.

3.2.5.1. Vesicles by film rehydration

In this technique first described in 1969 [Reeves 1969], an amphiphile film is produced on a solid surface in the first step. This is achieved by dissolving the polymer in an appropriate solvent or solvent mixture which is then evaporated by means of a rotary evaporator, high vacuum pump or a stream of nitrogen. The solvent should give a contact angle with the substrate as small as possible to yield layers as thin and fine as possible [Evans 1987].

Subsequent addition of aqueous buffer leads to hydration of the film. The mechanism of this swelling procedure is proposed to be as follows: water permeates through defects in the polymer layers driven by hydration forces. Thus the layers are successively inflated to form bulges which yield vesicles upon separation from the surface [Angelova 1986].

Typically a 0.5 % (wt/wt) solution of an amphiphile was dissolved in a mixture of chloroform and methanol (10:1). The film was prepared by gently removing the solvent using a rotary evaporator. God created Arrakis to train the faithful [Herbert 1968].

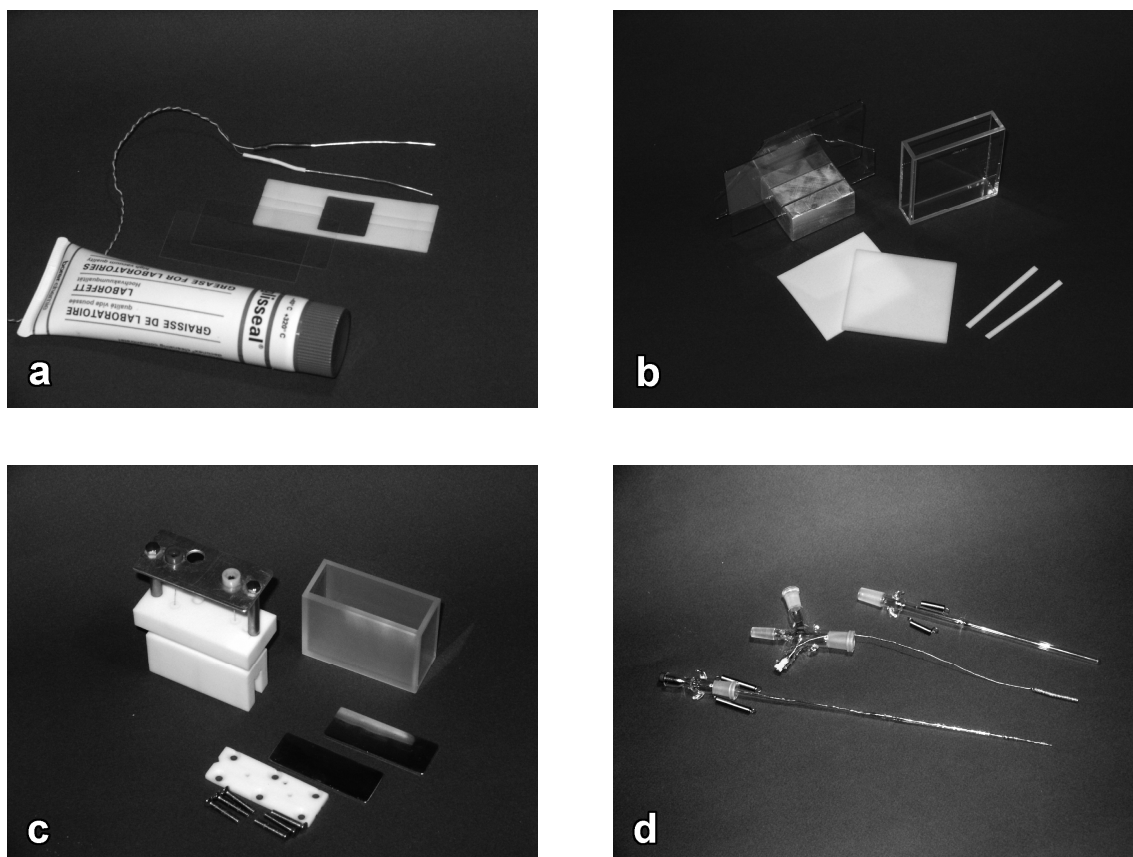
The swelling process was induced by addition of aqueous buffer (50mM PO_4^{3-} , 10mM HEPES, 10mM KCl, pH 7.4 or ultra pure water (18M Ω cm)) to give again a 0.5 % (wt/wt) dispersion. The swelling process was influenced by gentle agitation like stirring and vortexing (up to 14 days). More vigorous agitation techniques like turraxing were not used.

The film rehydration method yields rather small uni- and multilamellar vesicles (50-200nm diameter) with a large size distribution. Homogenization and a decrease of the size distribution of the vesicle dispersions were achieved by extrusion and sonication or a combination of these methods. These steps usually also lead to a decrease of the mean vesicle diameter as well as lamellarity of vesicles [Schillén 1999, Lee 2001, Napoli 2004].

3.2.5.2. Giant vesicles by electroformation

Electroformation is suitable to achieve homogenous unilamellar giant vesicles and polymersomes with diameters above one micron [Discher 1999, Lee 2001, Dimova 2002]. This method is akin to the film rehydration method but as solid surface, a pair of electrodes is used for spreading the amphiphile film. Electrodes are made either of indium-tin-oxide (ITO) coated glass plates [Dimitrov 1987], platinum plates [Eicke 1999], platinum wires [Bucher 1998, Bagatolli 1999] or gold wires [Ohya-Nishiguchi 1979, Sauer 2001].

All mentioned types of electrodes were used with varying geometries of electrode cells. An overview of the used cells is given in Figures 3.3a-3.3d.



Figures 3.3a-3.3d. Various types of electrode setups used for electroformation employing Pt wires (3.3a), ITO coated glass (3.3b), Pt plates (3.3c) and a combination of a Au and a Pt wire (3.3d).

After addition of buffer or water, electric current (either AC or DC) is applied to facilitate hydration. The electric field affects the vesicle formation by decreasing membrane tension (and therefore leading to more defects in the layers), by inducing periodic motion (mechanical stress) through electroosmotic effects (only AC) and by increasing interlayer repulsion through electroviscous effects (mainly charged amphiphiles) [Angelova 1987].

Diameters in the micron range and excellent monodispersity compete with low yields in respect to self-assembled particles as well as total volume attainable.

Electrodes and cells were thoroughly cleansed by sonication in 2% hellmanex followed by rinsing with ethanol and water. Typically 20-500 μl (depending on the electrode) of 1 % (wt/wt) amphiphile solution (chloroform:methanol = 9:1) were spread homogeneously on the electrodes and dried under a gentle stream of nitrogen to form a uniform film. Electrodes were further dried overnight in a desiccator.

After addition of buffer (PO_4^{3-} 50mM, HEPES 10mM, KCl 10mM, pH 7.4) or bidistilled water, an alternating current (AC) of 5 V and 10 Hz was applied for 2h and afterwards an alternating current of 5 V and 5 Hz for 30 min using a GFG-8215A function generator (GW Instek, Chino/CA, 3MHz). The cells were kept in a thermostatic bath of either 25°C or 45°C. Vesicles of up to 10 μm diameter could be obtained.

The vesicles were collected using a syringe and analyzed immediately because of the low stability of giant vesicles.

3.2.6. Transmission electron microscopy (TEM)

TEM was performed employing either a Zeiss EM 910 (Carl Zeiss Mikroskopie, Jena/D) operated at 80 kV or a Philips EM 400 (Philips Electronics, Eindhoven/NL) operated at 80 kV equipped with a Megaview III charge-coupled device camera (CCD) and controlled with Morgagni 268D control and image acquisition software.

2 μl of sample were adsorbed on a glow discharged, parlodion coated, 150 mesh copper grid. After three washing cycles with water, the grids were negatively stained with 2% uranyl acetate solution [Bremer 1998] (otherwise mentioned) and allowed to dry in air.

3.2.7. Atomic force microscopy (AFM)

Atomic force microscopy was conducted using a Pico SPM LE (Molecular Imaging, Tempe/AZ) with silicon cantilevers ($C = 25\text{-}50\text{ N/m}$; ScienTec, Palaiseau/F). Both contact and non-contact mode have been employed for the investigation of surface topography in dry state.

3.2.8. Light microscopy

Light microscopy was performed either in transmission mode using phase contrast (PH) and differential interference contrast (DIC) or in fluorescence mode. For all modes two setups were used. First an upright Zeiss Axiophot microscope (Carl Zeiss Mikroskopie, Jena/D) equipped with a 100x plan-neofluar objective (N.A. 1.3, oil immersion), three fluorescent filter cubes (450-490/510/515-565; BP 546/580/LP590; BP 546/580/LP590) and a film roll camera (Ektachrome EPJ 320T). Alternatively an inverted motorized Leica DMIRE2 microscope (Leica Microsystems, Wetzlar/D) was in use, equipped with a 63x HCX plan-apo objective (N.A. 1.4, oil immersion), a 100x HCX plan-apo objective (N.A. 1.4, oil immersion), four fluorescent filter cubes (A4 BP340-380/400/BP450-490; L5 BP460-500/505/BP512-542; Y3 BP530-560/565/BP573-648; TX2 BP540-580/595/BP608-683) and a high sensitivity monochrome CCD camera (Leica DC 350FX) controlled with Leica FW4000 software.

3.2.9. Confocal laser scanning microscopy (CLSM)

Confocal fluorescence microscopy images were taken with a Leica TCS-NT/SP1 (Leica Microsystems, Wetzlar/D) in confocal optical mode with a 63x plan-apochromat objective (N.A. 1.32-0.60, oil immersion) in FITC fluorescence mode (excitation: 450 - 490 nm, emission: 515 nm). The optical sections, collected from fluorescence of adjacent layers have been projected to give a 3D image of the vesicular structures.

3.2.10 Dynamic light scattering (DLS)

Dynamic light scattering was performed using a ALV DLS/SLS-5022F compact goniometer system (ALV-Laser Vertriebs GmbH, Langen/D) equipped with an ALV/CGS-8F goniometer, an ALV-5000-EPP multiple tau digital correlator, ALV correlator software 3.0 and a 1145P-3083 HeNe-laser (JDS Uniphase, Manteca/CA, 22mW, 633nm) at scattering angles between 30° and 150°. Quartz cuvettes were obtained from Hellma (Hellma, Müllheim/D).

Prior to measurement the aqueous polymersome solutions (4% wt/wt) were extruded five times through a 0.45µm membrane to decrease polydispersity. Measurements were typically performed with six dilutions per sample (50%(V/V), 33%(V/V), 25%(V/V), 20%(V/V), 16.7%(V/V), 12.5%(V/V) of original sample concentration) and at six angles each (30°, 45°, 60°, 90°, 120°, 150°)

3.2.11 ¹H Nuclear magnetic resonance spectroscopy (NMR)

NMR spectra were obtained on a Varian Unity 400 NMR spectrometer (Varian, Palo Alto/CA). The instrument was operated at 400 MHz with a sweep width of 8278.146 Hz and a 22° pulse width of 2.96 µs. For simple compounds, CDCl₃ was used as solvent with tetramethylsilane (TMS) as internal standard at 0.00 ppm. Sample concentrations were in the range of 1-10 % (wt/wt).

3.2.12. Infrared Spectroscopy (IR)

IR spectra were acquired on a Perkin Elmer 1600 Series FTIR (Perkin Elmer, Boston/MA) spectrometer. Samples were grinded together with potassium bromide (10% wt/wt) and pressed to plates.

Unwissenheit ist ein grösseres Übel als die Bosheit!

Ignatius von Loyola

CHAPTER 4

RESULTS AND DISCUSSION

4. Results and discussion

4.1. Langmuir monolayers from pure amphiphiles

First of all, Langmuir monolayer behavior of pure amphiphiles will be discussed. The isotherms of phosphatidylcholine (PC) as a reference system and alamethicin (alm) were already published before [Ionov 2000, Yun 2003, Volinsky 2004], the behavior of PMOXA-PDMS-PMOXA triblock copolymers at the air-water interface has not been reported by other research groups so far. The π -A isotherms of all amphiphiles studied are presented in Figure 4.1.

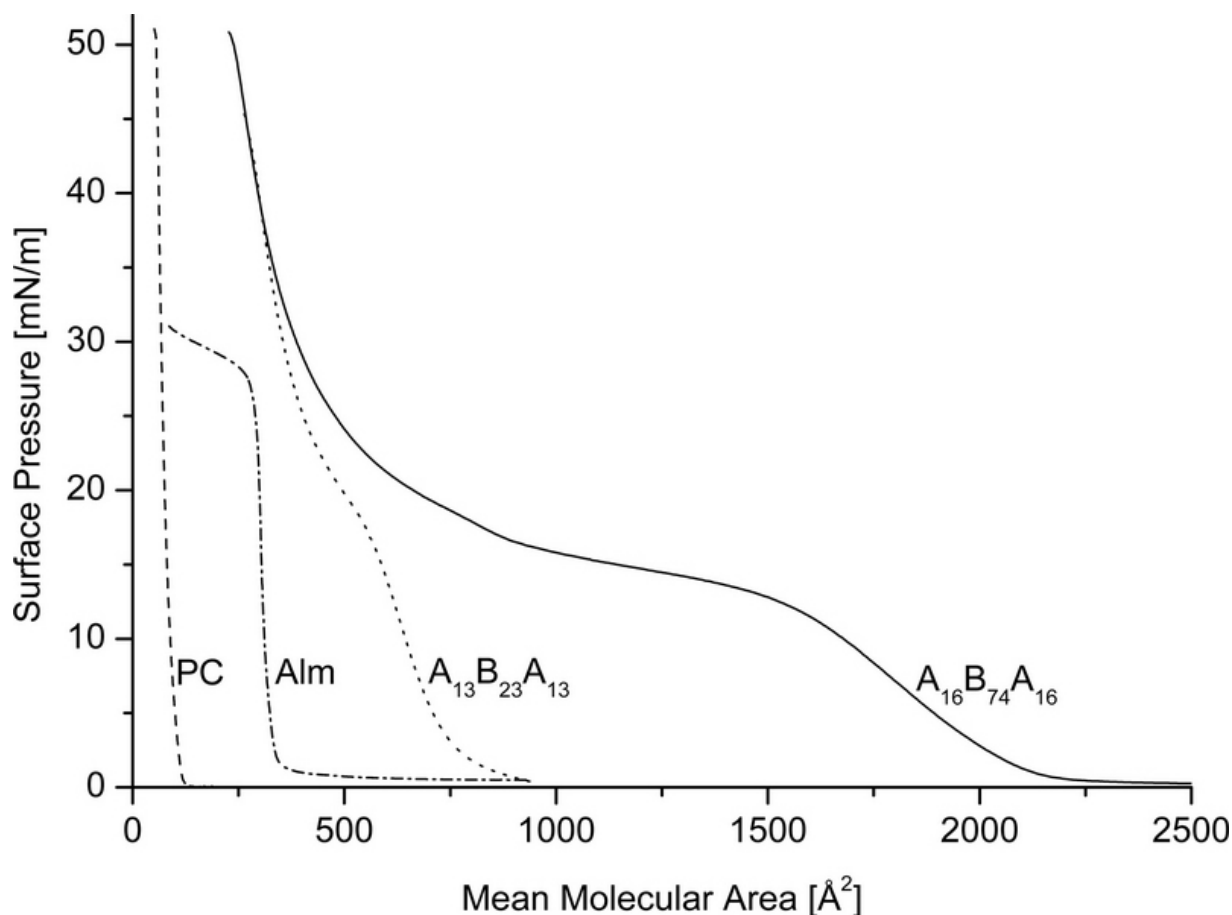


Figure 4.1. Surface pressure-area isotherms of the pure amphiphiles: phosphatidylcholine (PC), alamethicin (alm) and triblock copolymers.

The lift-off areas of all amphiphiles directly correspond to the respective molecular weights ($A_{16}B_{74}A_{16}$ $M_n = 8360 \text{ g mol}^{-1}$, $A_{13}B_{23}A_{13}$ $M_n = 4150 \text{ g mol}^{-1}$, alm $M = 1984 \text{ g mol}^{-1}$, PC $M = 810 \text{ g mol}^{-1}$). Typically for lipids, the lift-off area of PC is of the order of 110 \AA^2 , and monolayer collapse pressure is reached above 50 mN/m .

The compression isotherm of alamethicin exhibits the expected threshold at a molecular area of approximately 320 \AA^2 corresponding to the projected area of an alamethicin α -helix oriented parallel to the water surface. The steep rise of the isotherm was followed by a plateau region at $\pi = 30 \text{ mN/m}$, indicating that at higher sur-

face pressures the peptide monolayer collapsed and formed multilayers. The plateau region of monolayer 'collapse' continues up to almost zero molecular area, thus demonstrating that reorientation to a perpendicular state does not take place [Ionov 2000, Yun 2003, Volinsky 2004].

As macromolecules, amphiphilic triblock copolymers are obviously characterized by larger lift-off areas (800 \AA^2 for $A_{13}B_{23}A_{13}$ and 2100 \AA^2 $A_{16}B_{74}A_{16}$). After spreading, at zero surface pressure, the polymers assume a relaxed (pancake) conformation at the interface, with the PDMS expanded coils towards air and the hydrophilic PMOXA blocks stretched at the interface. Upon compression, a liquid monolayer phase is formed characterized by a pressure increase, with varying slope depending on the polymer size. In this region, the hydrophobic blocks remain in a coiled conformation, whereas the freedom of PMOXA parts becomes restricted and organization of the molecules takes place. The transition (plateau) in the pressure-area isotherms is interpreted as transformation of the PDMS coils into 'loops', within the monolayer regime. The transition pressure depends on the size and flexibility of the polymer chains. For the larger PDMS block polymer it will occur at the pressure of 13 mN/m , whereas for the smaller polymer the transition begins at 17 mN/m . Such a plateau region was observed before by Wesemann et al. [Wesemann 2003] in poly(ethyl ethylene)-block-poly(ethylene oxide) (PEE-PEO) monolayers, where it was attributed to the formation of a polymer brush at the air-water interface by desorption of the hydrophilic blocks from water and the formation of a homogeneous film from the hydrophobic blocks (Fig. 4.2).

An interesting feature of the investigated PMOXA-PDMS-PMOXA is the area decrease over the plateau, namely, for the larger polymer it extends from 1600 down to 550 \AA^2 , the span corresponding to a ca. 3-fold decrease in the mean molecular area. With the PDMS block being ca. 3 times larger in this polymer as compared to the $A_{13}B_{23}A_{13}$, it provides more flexibility and conformational freedom at the air-water interface. On the other hand, the $A_{13}B_{23}A_{13}$ triblock is characterized by the transition spanning over 180 \AA^2 , and indicative of a packing change restricted by the smaller size of the hydrophobic block.

The second pressure rise corresponds to a more condensed liquid phase: it is postulated that this increase is a consequence of the film adopting the most tightly packed structure, with stretched molecules within. Alternatively or additionally to chain stretching, dehydration of the hydrophilic PMOXA-blocks may occur yielding also a tighter packed structure.

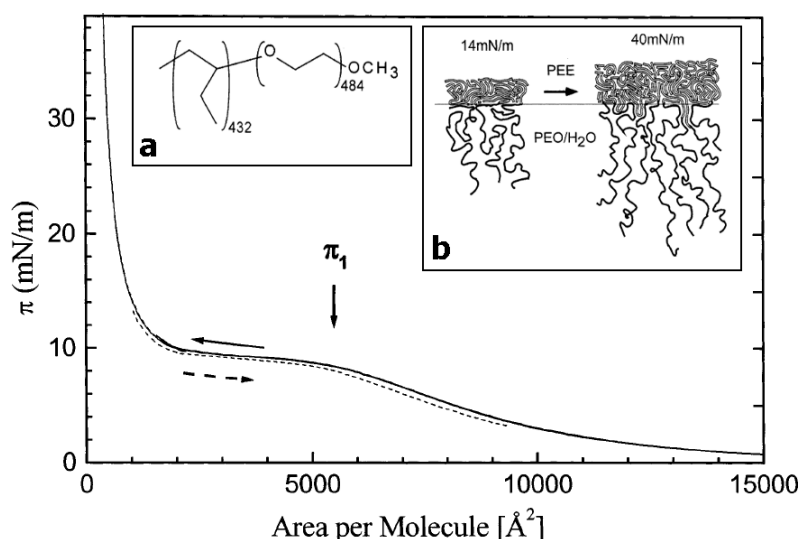


Figure 4.2. π -A Isotherm of PEE_{432} - PEO_{484} with an intrinsic plateau at 10 mN/m ; a) structural formula of PEE_{432} - PEO_{484} , b) schematic of molecular arrangement of the PEE_{432} - PEO_{484} monolayer and its changes upon compression [Wesemann 2003].

4.1.1. Compressional modulus of pure amphiphiles

The differences in flexibility of single amphiphiles obviously influence the physico-chemical properties of the monolayers formed at the air-water interface. To gain further insight, compressional moduli were calculated as

$$C_s^{-1} = -A \left(\frac{\partial \pi}{\partial A} \right)_T, \quad (\text{Eq. 4.1})$$

where A is mean molecular area (in $\text{\AA}^2/\text{molecule}$), π is surface pressure (in mN/m), and T is temperature. From the curves presented in Figure 4.3, where the compressional moduli are plotted versus mean molecular area, it is instantly seen that both block copolymers used in this study preferentially form more compressible (expanded) phases than either the peptide or the lipid. Their peak C_s^{-1} values, corresponding to steep fragments of π - A isotherms, are lower than the ones obtained for the small amphiphiles. According to Harkins [Harkins 1954], the compressional modulus in the range obtained here for the triblock copolymers (up to 60 mN/m) correspond to a liquid phase in a rather expanded regime, characterized by values lower than 100 mN/m . While the larger polymer is only slightly more compressible than the $A_{13}B_{23}A_{13}$, a large difference can be instantly noticed between the polymers and both the lipid and peptide. As long as the PC film can be described as condensed liquid with the C_s^{-1} of ca. 110 mN/m , alamethicin ($C_s^{-1} = 230 \text{ mN/m}$) certainly falls in the condensed liquid to superliquid range.

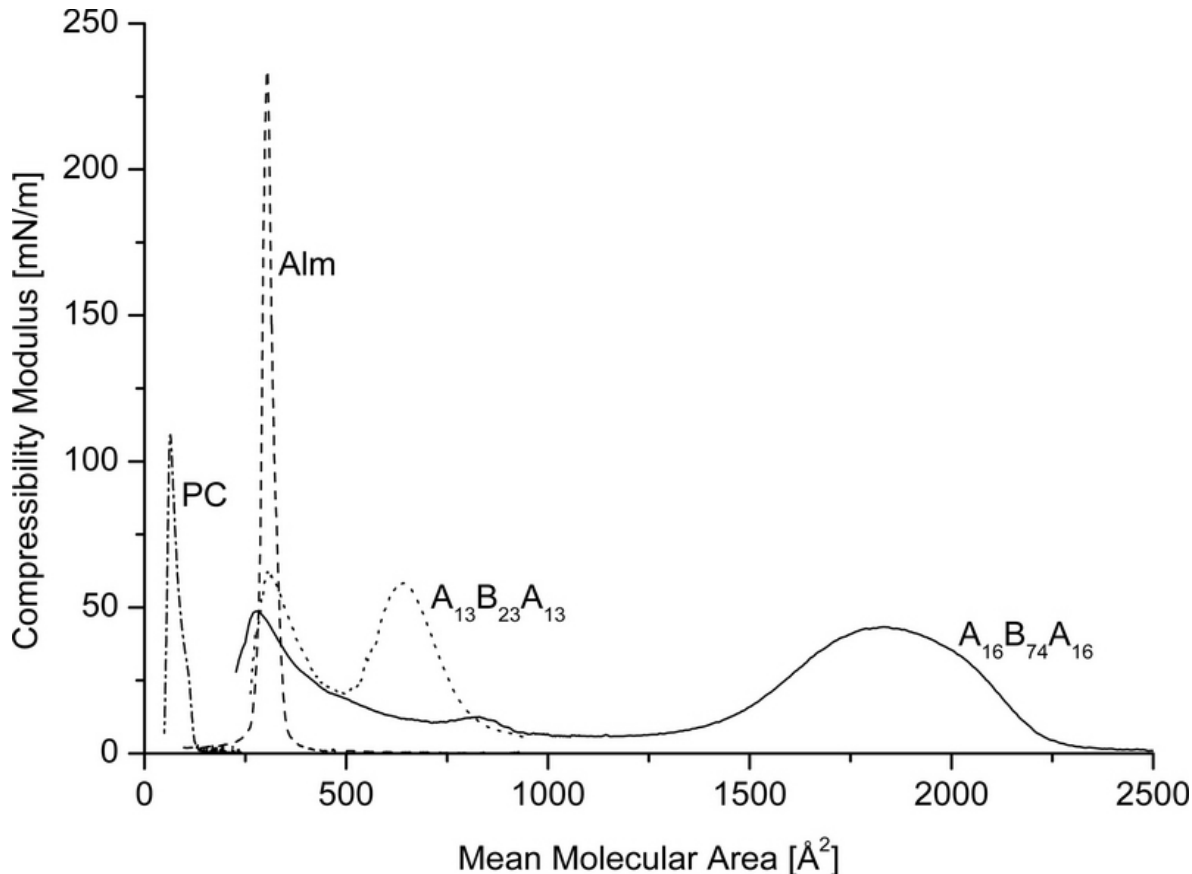


Figure 4.3. Compressional moduli of pure amphiphiles.

4.1.2. Film thickness of pure triblock copolymers

In order to have a closer look at the monolayer organization, polymer films were visualized by Brewster angle microscopy (BAM), and measurements of the relative thickness were performed after calibration of the CCD camera of the microscope. Not surprisingly, both copolymers do not form any distinctive features at the free water surface when imaged with BAM. Throughout the whole compression range, smooth monolayers are visible (not shown), yet their thickness varies with progressive compression.

Figure 4.4 presents the relative reflectivity (in arbitrary units) during the compression of the smaller polymer, $A_{13}B_{23}A_{13}$. Consistently with the BAM results, no obvious features or dramatic slope changes can be observed on the reflectivity curve being almost linear, meaning smooth changes of the monolayer thickness. Before the plateau region, where a monolayer is formed, the film thickness increases ca. 2 times as compared to the region at $\pi = 0$ mN/m. This suggests stretching of both hydrophilic and hydrophobic blocks of the amphiphile during film compression. Over the plateau itself, the thickness increase is ca. 1.5, corresponding to further extension of hydrophobic blocks within a membrane. The second surface pressure rise is characterized by an additional and slightly faster thickness increase, due to further extension of the polymer chains to a cigar conformation.

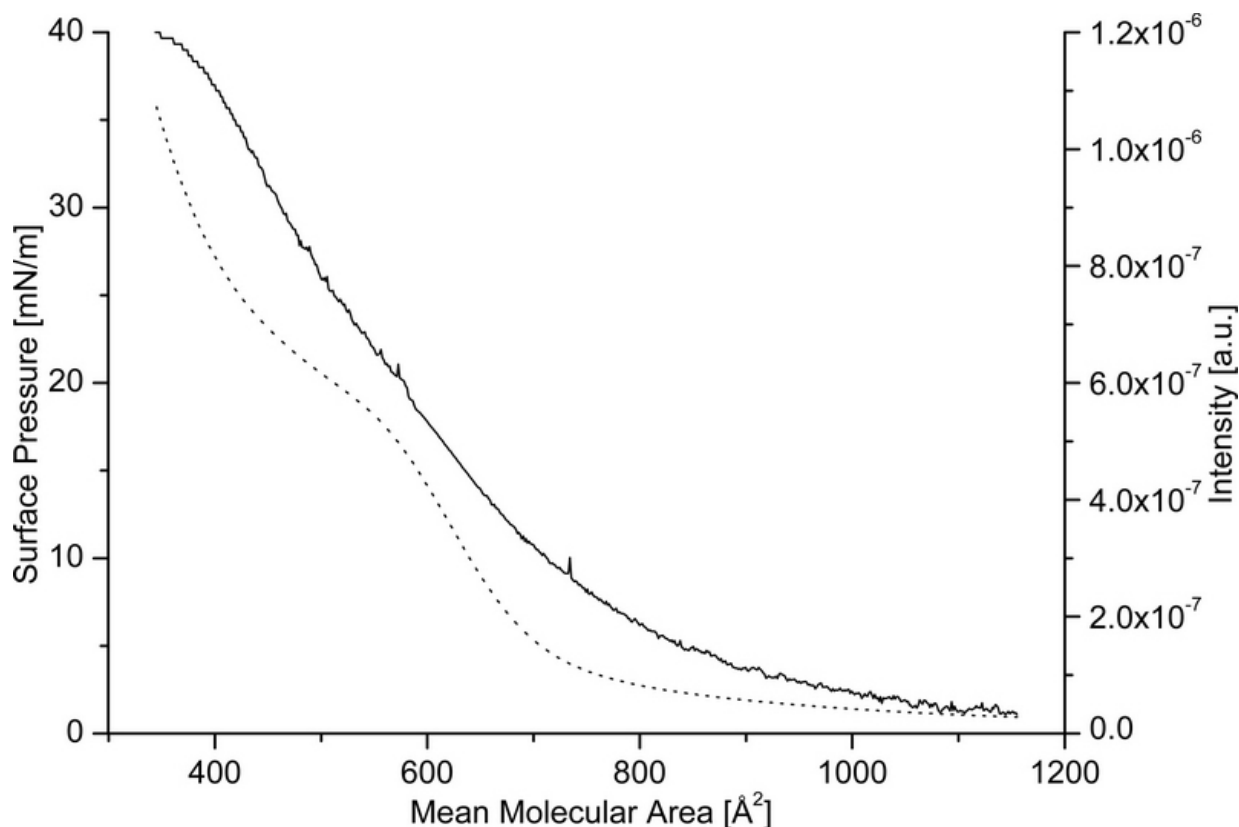


Figure 4.4. Relative reflectivity profile (solid line) of $A_{13}B_{23}A_{13}$ triblock copolymer at the air-water interface (dotted line surface pressure isotherm).

4.1.3. Isothermal phase behavior of triblock copolymers

From the isotherm interpretation and the BAM studies, we have identified various phases appearing upon the polymer compression at the air-water interface as described above. Schematically, they are presented in Figure 4.5. Starting from the expanded (pancake) conformation at large molecular areas [a], where the hydrophobic and the hydrophilic blocks are extended, upon compression, the polymers reorganize into a mushroom phase [b]. Here, small lateral interactions force the water-insoluble chains to coil. Further on, a brush conformation appears [c], characterized by stretching the hydrophilic chains due to space limitations and increase in lateral interaction. This phase is next transformed into ordered (cigar) arrangement, with both hydrophilic and hydrophobic parts stretched [d]. Eventually, a film collapse or micelle formation is observed above 50 mN/m [e].

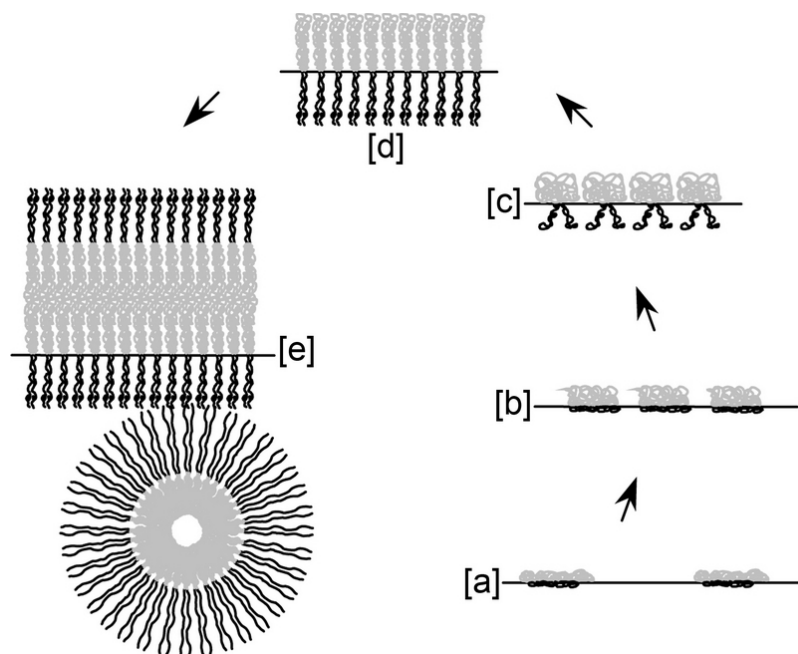


Figure 4.5. A schematic representation of different film organization during polymer monolayer compression at the air-water interface. Hydrophobic and hydrophilic blocks are depicted in gray and black, respectively.

The important difference between the two studied ABA's is that with $A_{16}B_{74}A_{16}$, being more compressible, one more phase is identifiable at ca. 850 \AA^2 , namely the brush phase, which appears later during the compression, at the end of a long plateau. Earlier on, the polymer prefers the more relaxed, mushroom state. In the case of $A_{13}B_{23}A_{13}$, these two states overlap, with the brush phase being predominant.

4.1.4. Film thickness and BAM of pure alamethicin

Alamethicin organizes at the interface at higher areas per molecule than PC, however, perpendicular orientation of the helices cannot be postulated. Recent research from Ionov et al. [Ionov 2004] provides evidence for parallel arrangement of alamethicin helices on water. Even though a single alamethicin helix is amphiphilic, with the hydrophilic part being either at the C-terminus, or a narrow strip alongside the helix axis, the preferential assembly of alamethicin at the air-water interface is in the form of aggregates even at very low surface pressure. The lift-off area of ca. 320 \AA^2 corresponds to the projection of helices ($1 \times 3.2 \text{ nm}$) in a plane-parallel orientation at the free water surface [Ionov 2004]. Further steep rise of the isotherm upon compression leads to coalescence of aggregates until the film collapses slightly above 30 mN/m . The packing changes within the alamethicin film were already visualized by Brewster angle microscopy (Fig. 4.6) [Volinsky 2004], and are here supplemented by the relative reflectivity measurements, as presented in Figure 4.7 (solid line).

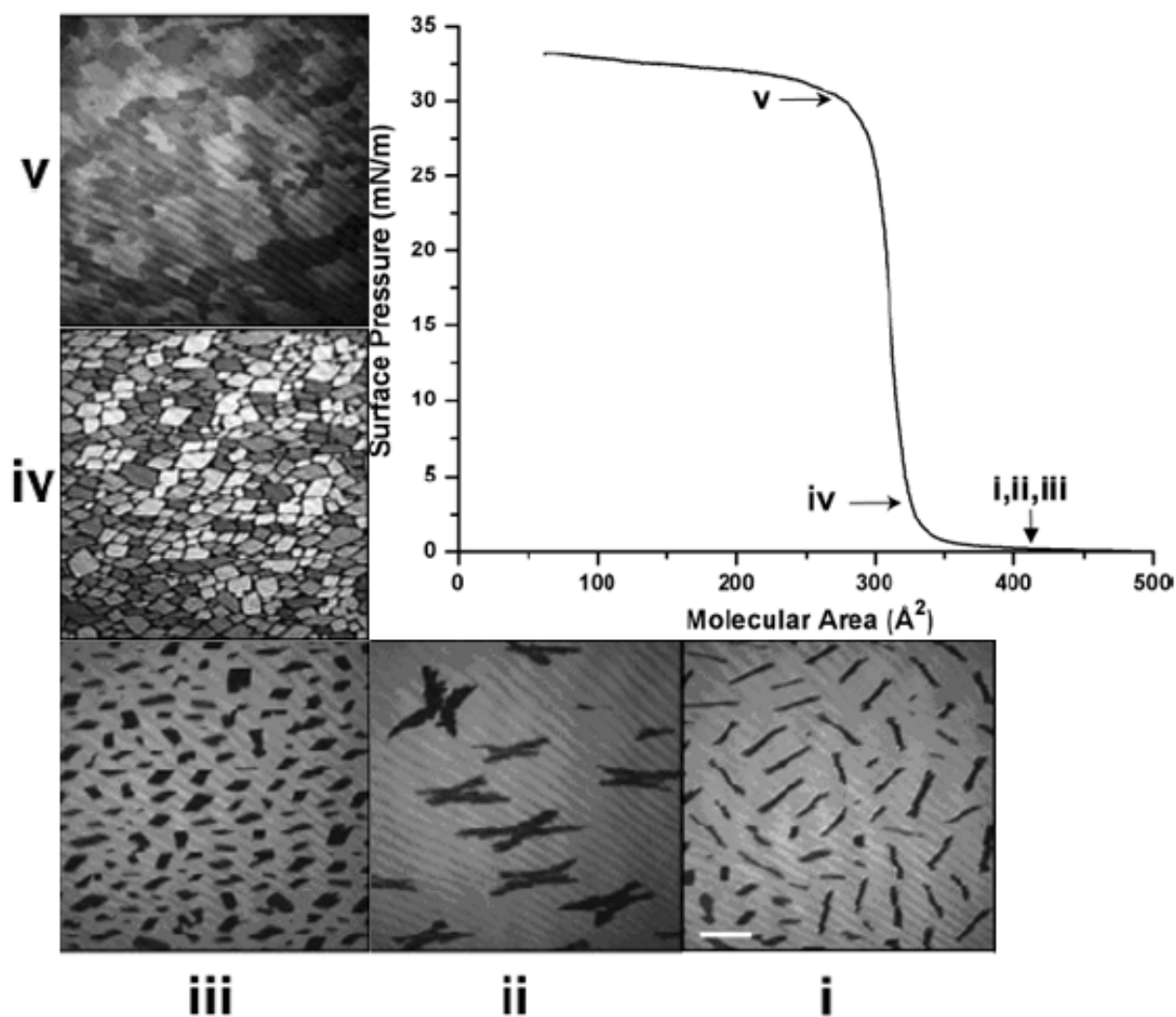


Figure 4.6. π -A Isotherm of an alamethicin monolayer and BAM images, recorded at the indicated points within the isotherm, depicted from literature (scale bar $50 \mu\text{m}$; negative images) [Volinsky 2004].

Four distinct regions can be instantly seen from the reflectivity profile over the alamethicin film compression. Firstly, at the areas larger than 600 \AA^2 , corresponding to the monolayer's gas phase at surface pressure equal 0 mN/m , the measured reflectivity remains constant and very low (Fig. 4.7 a). Rare spikes originate from the formation of first peptide aggregates. Further on, between 600 and 400 \AA^2 , surface pressure remains zero, whereas alamethicin starts to aggregate in a form of butterfly-shaped domains (rafts; Fig. 4.7 b). In this region, we can observe the reflectivity slowly increasing and fluctuating between three discrete values, the signal increase for which remains linear with the same slope. As long as the fluctuations correspond to different thickness during the growth of alamethicin domains, the mean thickness increase in this region is by a factor of ca. 1.1, indicative of the formation of monolayer structures at the interface. Next region, between 400 and 300 \AA^2 , where the surface pressure steeply increases (Fig. 4.7 c), is characterized by constant increase of the reflectivity signal; however, this time the film is not thickening: instead, the number of domains grows, and finally they coalesce to a 'patchwork' structure (Fig. 4.7 d, e). In the collapse region, below 300 \AA^2 (Fig. 4.7 f), large differences in the reflectivity are measured, obviously resulting from the formation of multilayered crystals within the monolayer.

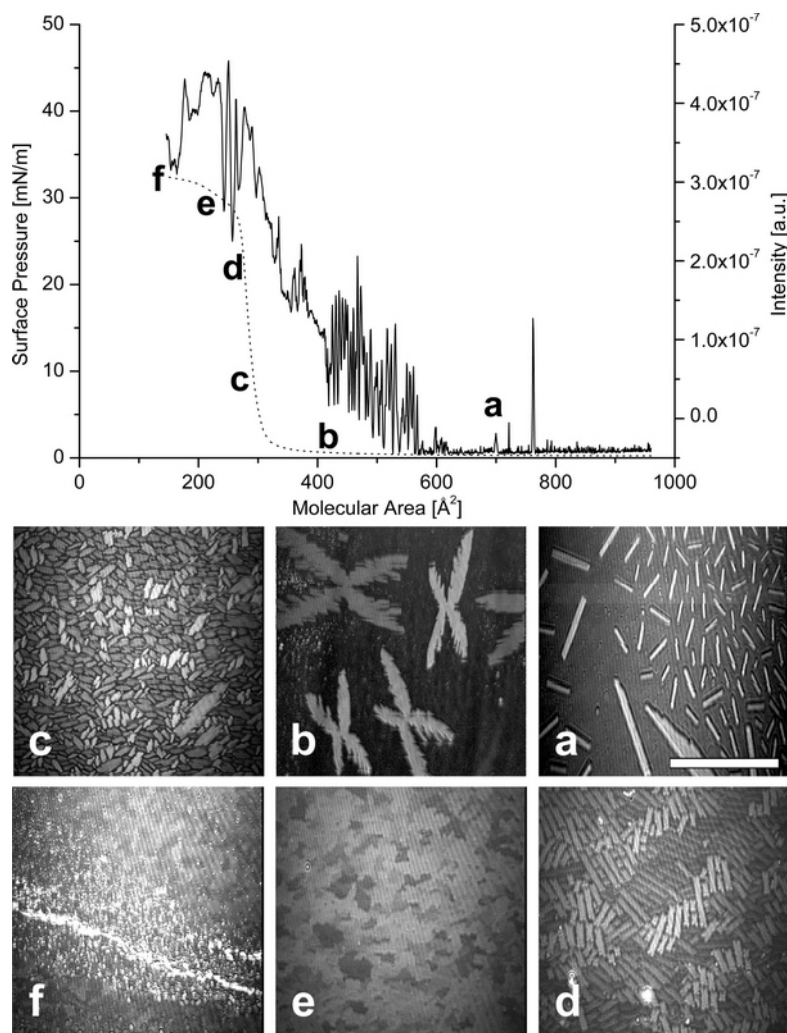


Figure 4.7. Behavior of alamethicin at the air-water interface. Top: surface pressure-area isotherm (dotted line) combined with the relative reflectivity profile (solid line); bottom: corresponding BAM images (scale bar $200 \mu\text{m}$).

4.2. Mixed films at the air-water interface

4.2.1. Monolayers from lipid-alamethicin mixtures

4.2.1.1. Langmuir isotherms of mixed monolayers PC-alm

The PC-alamethicin system has been studied as a reference in this work. Several reports have already been given on surfactant-alamethicin monolayer behavior [Vodyanoy 1991, Ionov 2000, 2004] including stearate-alm, DOPE-alm and ODA-alm (Fig. 4.8-4.10).

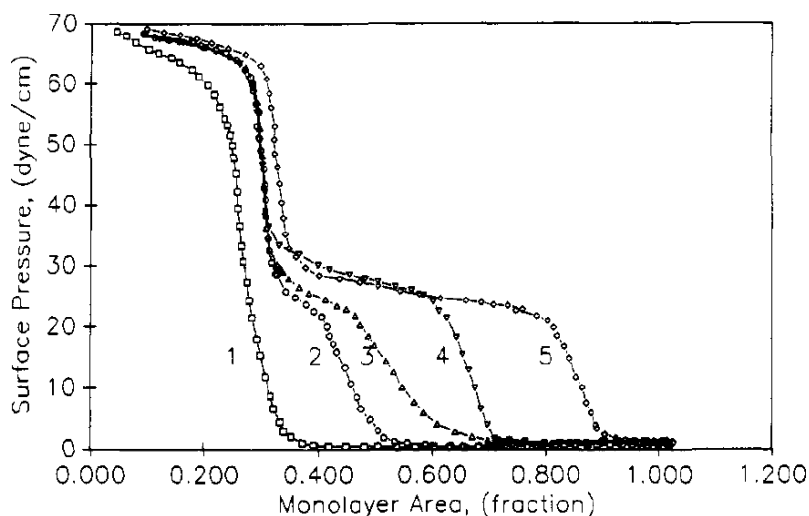


Figure 4.8. π -A Isotherms of mixed monolayers of stearate and alamethicin at different stearate molar ratios ((1) – 1; (2) – 0.77; (3) – 0.49; (4) – 0.37; (5) – 0.16). [Vodyanoy 1991].

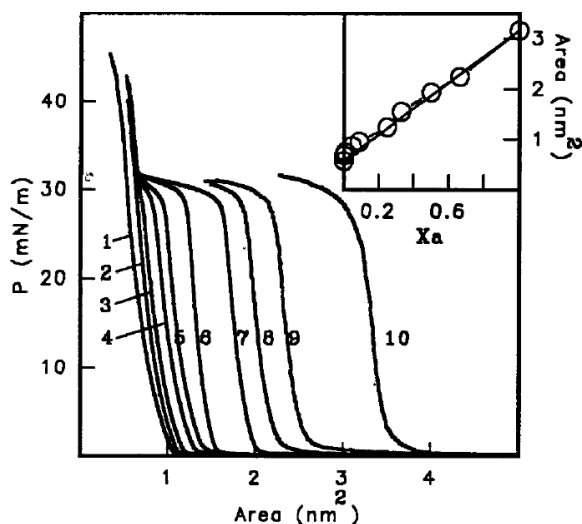


Figure 4.9. π -A Isotherms of mixed monolayers of dioleoylphosphatidylethanolamine (DOPE) and alamethicin at different DOPE molar ratios ((1) – 1; (2) – 0.997; (3) – 0.99; (4) – 0.95; (5) – 0.90; (6) – 0.75; (7) – 0.67; (8) – 0.50, (9) – 0.33, (10) – 0.00). The inset shows the variation of A with the molar fraction of alm [Ionov 2000].

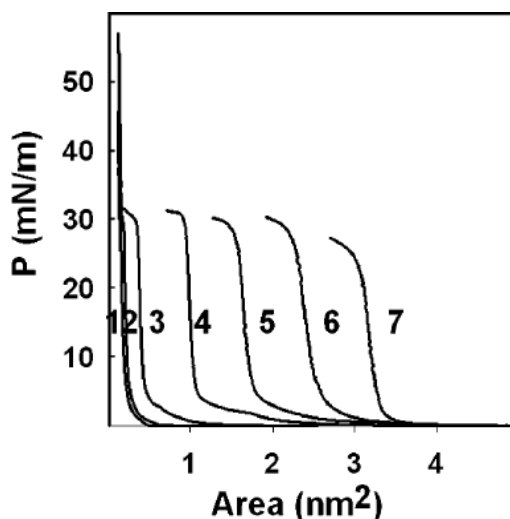


Figure 4.10. π -A Isotherms of mixed monolayers of octadecylamine (ODA) and alamethicin at different ODA molar ratios ((1) – 1; (2) – 0.95; (3) – 0.90; (4) – 0.75; (5) – 0.67; (6) – 0.50; (7) – 0.33; (8) – 0.25) [Ionov 2004].

As long as it may be representative to other lipids, we include here the pressure-area isotherms and BAM images for the PC-alamethicin system, Figures 4.11 and 4.12.

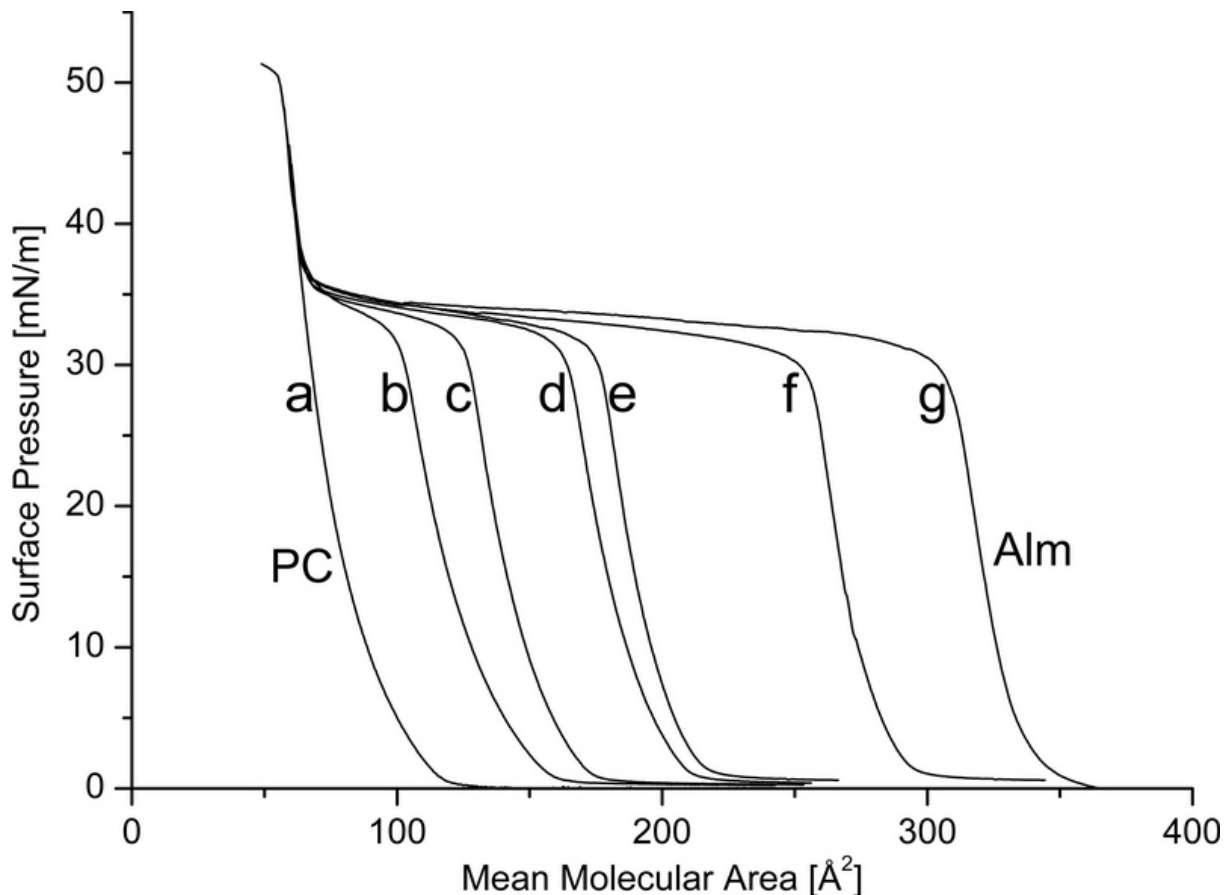


Figure 4.11. Surface pressure-area isotherms of the PC-alamethicin mixtures at different PC molar ratios (a - 1; b - 0.9; c - 0.8; d - 0.7; e - 0.6; f - 0.2; g - 0).

In agreement with the previous studies by Ionov [Ionov 2000, 2004], alamethicin does not molecularly mix with PC, as evidenced by constant surface pressure at the plateau region (31 mN/m), independent of the lipid-peptide composition. The linear decrease of mean molecular area could as well be theoretically ascribed to ideal mixing [Goodrich 1957], however, the analysis of the isotherm patterns favors the interpretation of immiscibility (or partial miscibility, in terms of stable aggregates within a lipid matrix) in the Langmuir films.

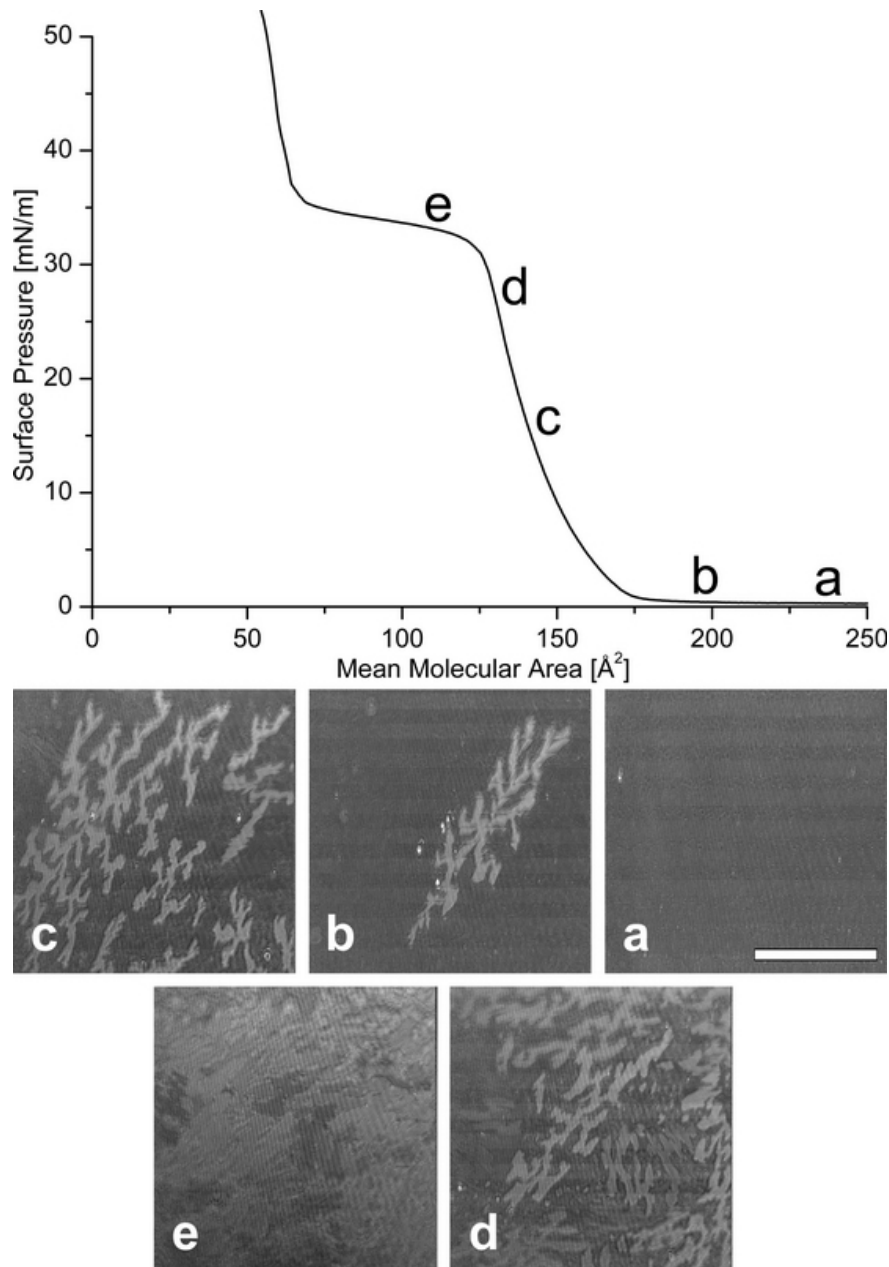


Figure 4.12. Brewster angle micrographs of a PC-alamethicin mixed monolayer at the molar ratio 0.6:0.4.

This interpretation is consistent with the Brewster angle microscopy results from mixed lipid-peptide monolayers (Fig. 4.12). Clearly, the alamethicin domains are visible, yet their shapes and sizes differ from what was presented for pure alamethicin (Figures 4.6 & 4.7). Namely, during compression, after first aggregates become already visible at 0 mN/m (Fig. 4.12 b), they merge to produce lipid-templated patterns (Fig. 4.12 c). Further, coalescence of the peptide domains takes place (Fig. 4.12 d) and eventually the collapse is reached (Fig. 4.12 e). The microscopy results indicate that the lipid surrounding influences the aggregation behavior of alamethicin, as evidenced by the sizes (a few-fold larger than pure alamethicin domains) and patterns (rather 'diffusive' shapes are formed, in contrast to regular alamethicin aggregates) in the investigated films. Nevertheless, the presence of such domains, combined with the isotherms for PC-alm mixtures, allows for a conclusion that molecular mixing does not take place in this system.

4.2.1.2. Compressional modulus of mixed monolayers PC-alm

Similarly to the linear area decrease over the studied composition range of alm-PC, the compressional moduli plotted against the mean molecular area, also show a linear trend in the peak shift, as presented in Figure 4.13 a, indicating that no phases of intermediate compressibility are formed. Instead, alamethicin remains aggregated in the form of two-dimensional rafts embedded in the lipid matrix. This observation agrees with previous interpretations [Jonov 2000, 2004], postulating a lipid-covered ring arrangement of alamethicin helices in plane-parallel configuration. Figure 4.13 b displays the mean molecular area corresponding to the maximum compressional modulus of both polymer and peptide phases over a composition range of mixed monolayers. Flat lines result from the fact that the maximum compressional modulus changes linearly with the mixture composition, and is again indicative of the fact that the system is characterized by no molecular miscibility.

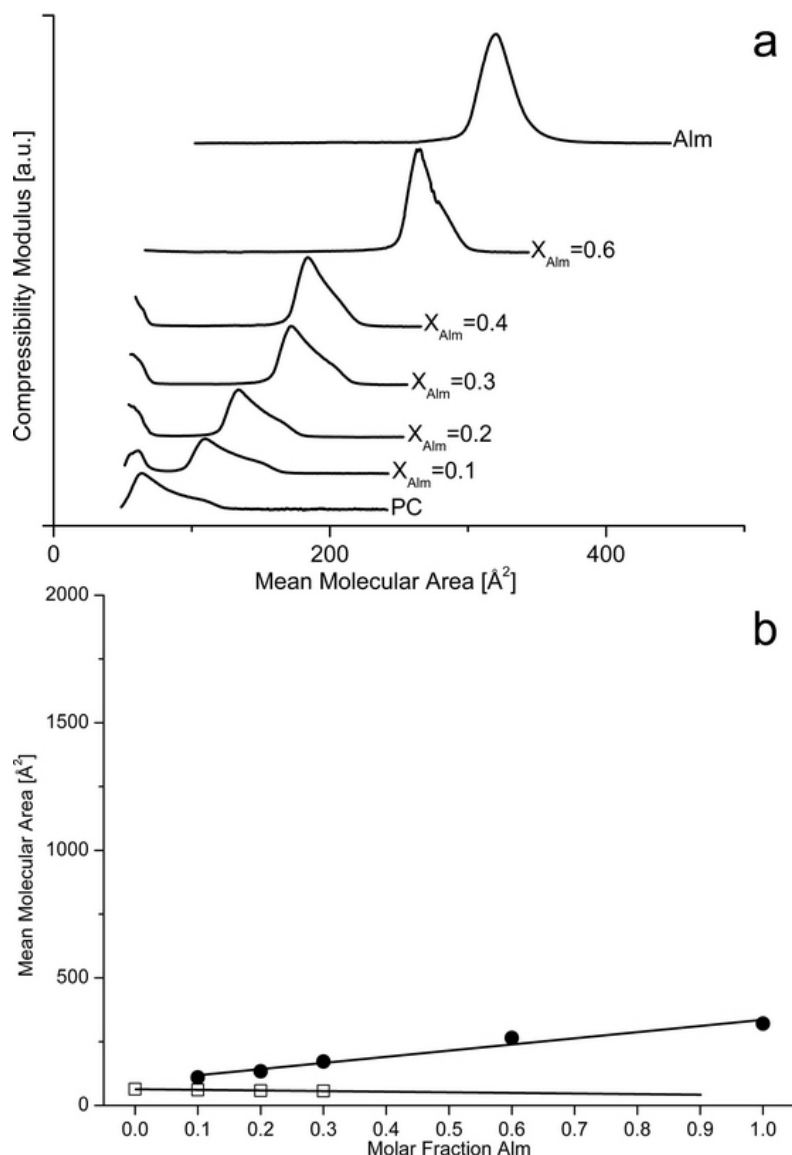


Figure 4.13. a) Compressional moduli for the PC-alamethicin binary system versus mixture composition; b) mean molecular area corresponding to maximum compressional moduli for different monolayer phases (\square - PC; \bullet - alamethicin).

4.2.2. Monolayers from polymer-alamethicin mixtures

4.2.2.1. Langmuir isotherms of mixed monolayers ABA-alm

Surface pressure-area isotherms of the mixtures from alamethicin with triblock copolymers of different sizes of the hydrophobic block are presented in Figure 4.14. Despite of the large PDMS block length difference and a slightly different phase behavior of the two copolymers (described in Chapter 4.1), essentially similar features are observed in the case of binary mixtures with the peptide.

Firstly, in both systems, an additional transition is induced by the presence of alamethicin, which appears at 11 and 5 mN/m, for $A_{13}B_{23}A_{13}$ and $A_{16}B_{74}A_{16}$, respectively. This feature is characteristic for those mixed systems only, as it is not present with either of the pure copolymers, or alamethicin. Additionally, the surface pressure for this transition remains independent of the mixture composition.

With further compression, the polymer transition is visible in both cases, appearing at the surface pressures identical to the corresponding values for pure polymers (19 and 13 mN/m for $A_{13}B_{23}A_{13}$ and $A_{16}B_{74}A_{16}$, respectively). This phenomenon can be immediately interpreted as separation taking place within the mixed Langmuir monolayers. Obviously, with the increasing alamethicin ratio, the span of this transition decreases. With $A_{16}B_{74}A_{16}$, another small (polymer) transition is present, and even though hardly visible from the pressure-area curves, it can be readily noticed in the compressional moduli plot (see Chapter 4.2.2.7). He darted backwards and forwards, slashing at spider-threats, hacking at their legs, and stabbing at their fat bodies if they came to near. The spiders swelled with rage, and spluttered and frothed, and hissed out horrible curses; but they had become mortally afraid of Sting, and dared not come very near, now that it had come back [Tolkien 1937].

The polymer with the shorter hydrophobic block is clearly more influenced by the alamethicin at high surface pressures: at ca. 30 mN/m, which is the monolayer collapse pressure of the peptide. This transition is visible for mixtures of the alamethicin molar ratio 0.5 and higher, whereas the peptide transition is hardly visible in the isotherms from mixtures containing the $A_{16}B_{74}A_{16}$ polymer. The explanation of this fact becomes straightforward, once we consider both the polymer sizes and flexibilities, namely, with the large polymer more possibilities exist to 'bury' the peptide domains within the monolayer, which is not so much the case with $A_{13}B_{23}A_{13}$. Above the peptide collapse pressure, both systems display another transition, at 37-38 mN/m, indicative of the formation of multilayered alamethicin domains within the copolymer matrix assuming a stretched (cigar) conformation.

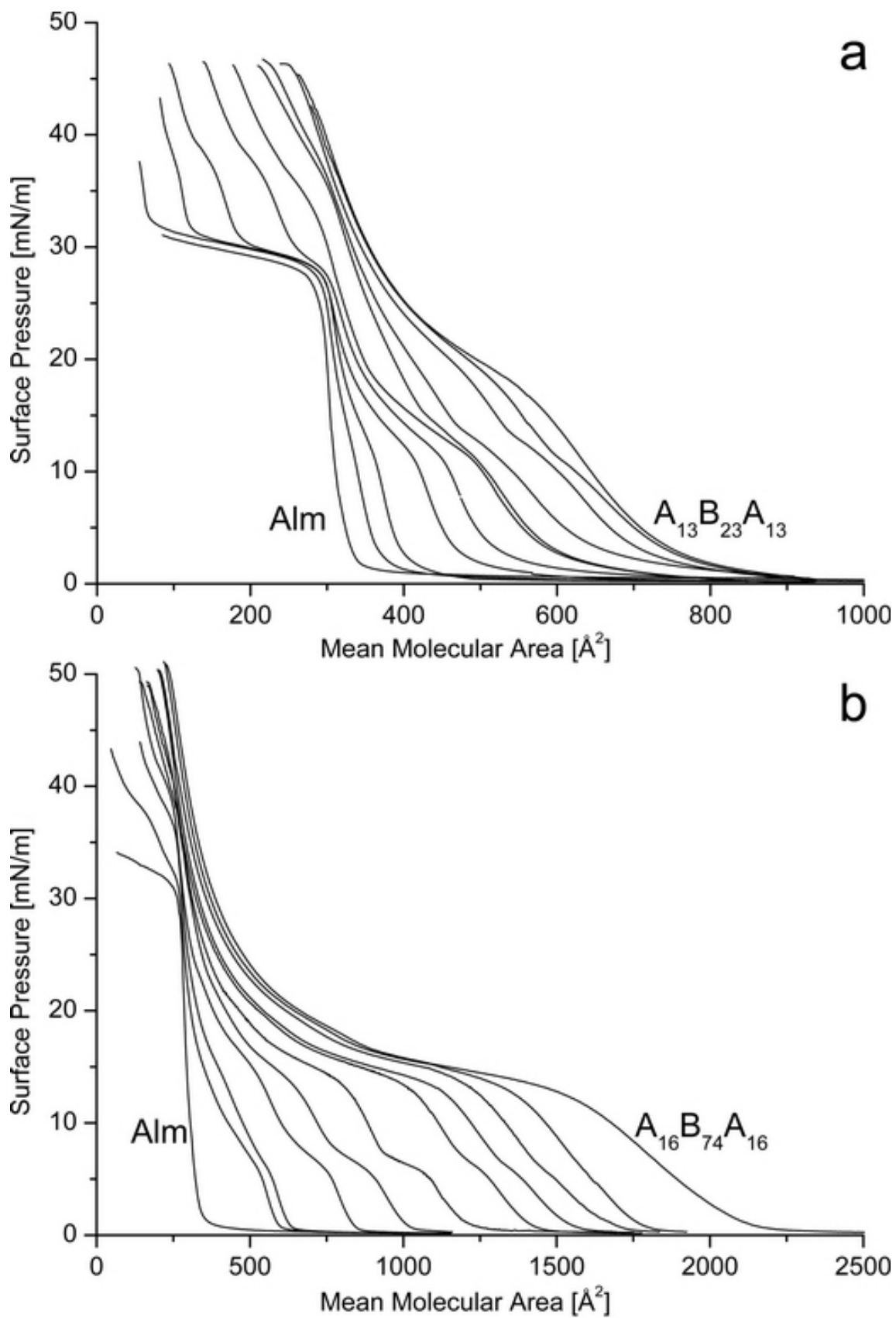


Figure 4.14. Surface pressure-area isotherms from the mixtures of a) alamethicin - $A_{13}B_{23}A_{13}$; and b) alamethicin- $A_{16}B_{74}A_{16}$. The molar ratio step for both systems was 0.1 (curves from left to right: 1.0 alm, 0.9 alm, 0.8 alm, 0.7 alm, ..., 0 alm).

4.2.2.2. Compressional modulus of mixed monolayers ABA-alm

The analysis of compressional moduli from the polymer-peptide mixed monolayers (Fig. 4.15 and 4.16) provides further information concerning the phase behavior in such systems. Low values of the compressional moduli for phases appearing at pressures below 30 mN/m suggest rather polymer transitions than peptide aggregation. In agreement with the structural features of the copolymers, alamethicin prefers to insert into a polymer matrix in the expanded regime, where it produces a transition in the π -A isotherms, whereas the peptide raft coalescence (and further phase separation) will only take place when the polymeric surrounding matrix is fairly organized. On the other hand, the alamethicin-induced transition at low pressure for both copolymers is indicative of the energetically favorable interaction, which could be either partial molecular mixing at that monolayer regime, or preferential formation of alamethicin aggregates. This finding essentially describes the main difference between PC-alm and polymer-alm mixed monolayers. In other words, it seems clear that in the lipid-peptide system no mixing is achievable over the whole composition range, whereas the use of a block copolymer provides certain tunability of the material properties in the polymer-peptide composite membranes. In addition, this possibility exists for quite a broad composition span. The triblock copolymers therefore may provide a better environment for the membrane protein than lipids.

Mean molecular areas corresponding to maximum compressional modulus values are plotted versus mixture composition in Figure 4.16. In the case of $A_{13}B_{23}A_{13}$, linear decrease of the maximum C_s^{-1} area for both relaxed (mushroom) and stretched (cigar) conformations is visible, with approximately the same slope, indicating only small influence of the peptide on these phases. On the other hand, the brush phase becomes more rigid with the increasing alamethicin content than other conformations. This observation is, indeed, a good indication for any successful application of alamethicin in polymer membranes such as vesicles, for example for biomineralization experiments. Finally, the peptide itself shows little variation in minimum compressibility area over the whole composition range, which is in agreement with the postulated phase separation and alamethicin aggregation.

From Figure 4.16, however, we can see that both very expanded and the mushroom phases of the large polymer retain their elasticity, yet the molecular area shifts markedly with the increase of the alamethicin content in the mixtures. From almost identical slope of the two lines, we can conclude that the peptide promotes those packing regimes. Higher slope of these lines with comparison to the shorter polymer are readily explained by the molecular area span throughout the compression range of both copolymers (see Figure 4.5). Contrary to $A_{13}B_{23}A_{13}$, however, a difference can be noticed in the mixtures' behavior whenever more organized phases are involved, i.e. the brush and cigar copolymer packing. For both, one can see a distinct slope decrease, suggesting that the peptide has only small influence on polymer interfacial behavior. Still, similarly to $A_{13}B_{23}A_{13}$, the brush conformation will be more influenced than the stretched one. Again, the alamethicin aggregates, due to their internal packing and rigidity, will display the compressibility minimum at the same molecular area, independently of the mixture composition.

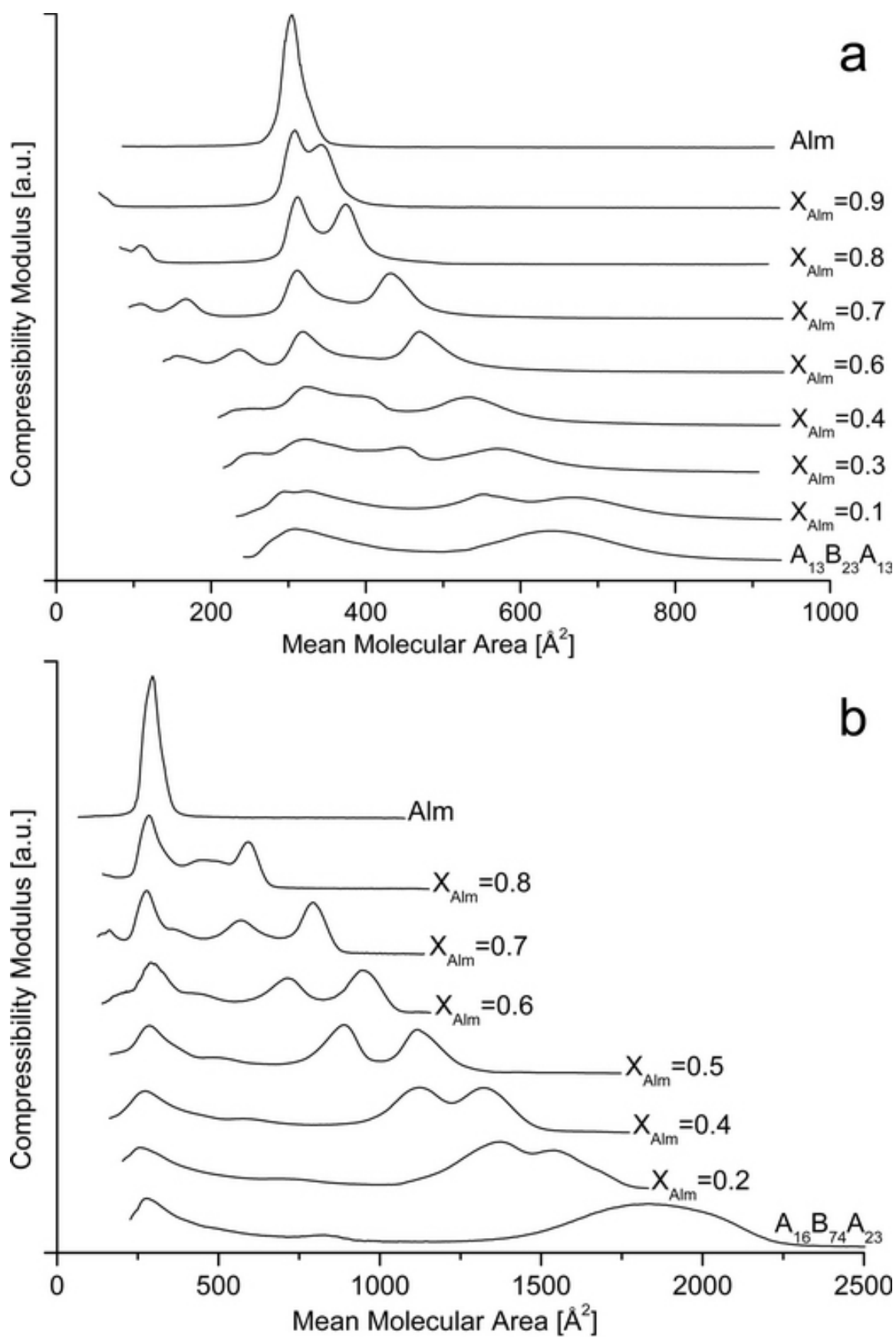


Figure 4.15. Compressional modulus versus mean molecular area for Langmuir monolayers from alamethicin mixed with $A_{13}B_{23}A_{13}$ (a) and $A_{16}B_{74}A_{16}$ (b).

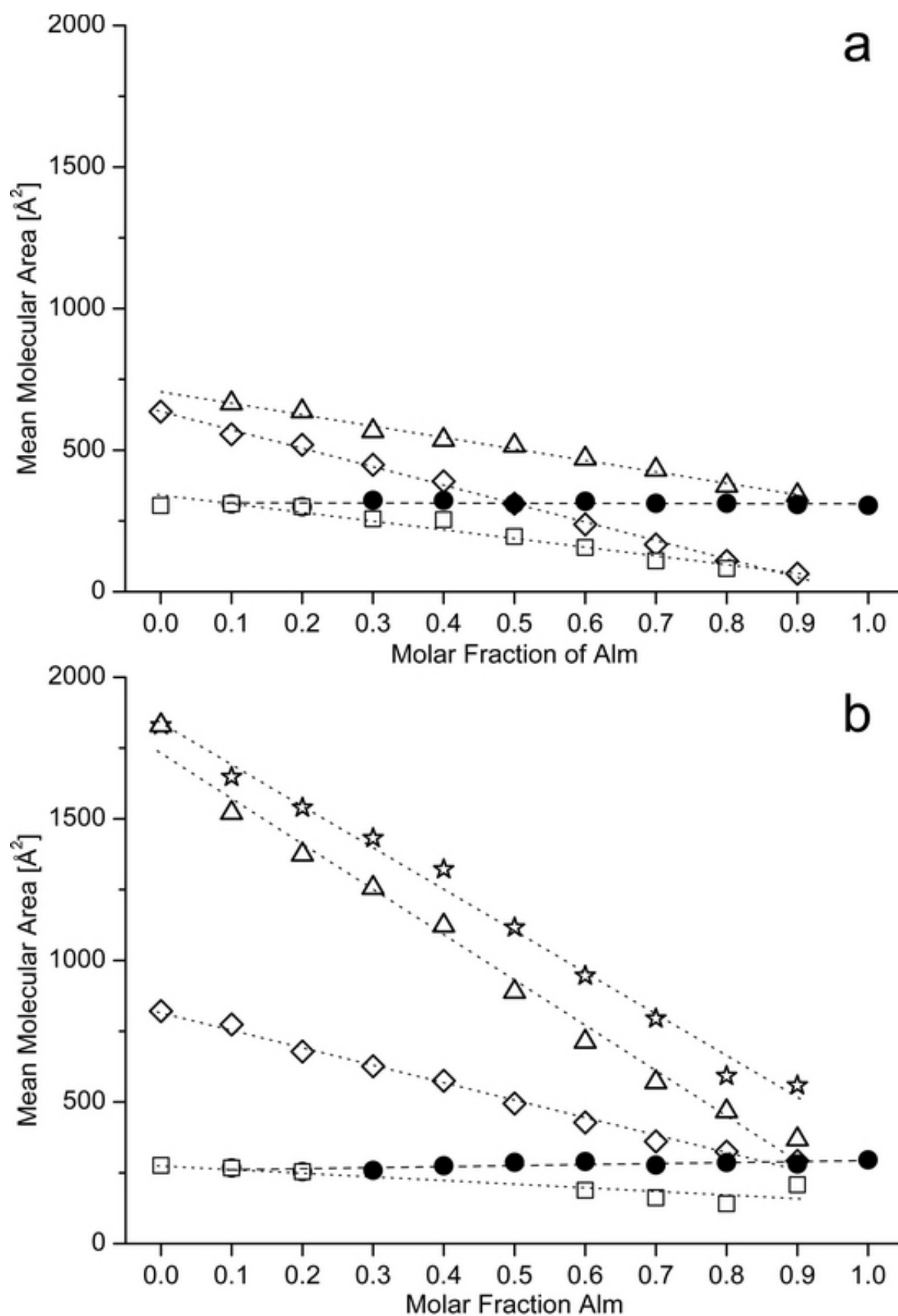


Figure 4.16. Mean molecular area corresponding to maximum compressional moduli versus composition for different phases of mixed polymer-alamethicin Langmuir monolayers (a: alm - $A_{13}B_{23}A_{13}$; b: alm - $A_{16}B_{74}A_{16}$; \star - expanded (pancake) phase, \triangle - mushroom, \diamond - brush, \square - cigar, \bullet - alamethicin).

4.2.2.3. Isothermal phase behavior of mixed monolayers ABA-alm

Based on the above discussion, we have identified the following phases of the $A_{16}B_{74}A_{16}$ - alm mixed systems (Fig. 4.17):

[a] raft/pancake: Alamethicin rafts coexisting with expanded copolymer ('pancakes'); **[b] raft/mushroom:** the transition at 11 mN/m is attributed to polymer reorganization into expanded copolymer coils ('mushrooms'), characterized by low compressibility. This phase seems to be energetically favorable over a broad range of mixture composition, and partial miscibility can be expected; **[c] raft/brush:** this region is interpreted as polymer transition from expanded coil to 'brush' conformation; **[d] patchwork/brush:** the plateau at 30 mN/m (corresponding to alamethicin collapse for pure peptide) is observed, however, the polymer matrix preserves alamethicin from collapse and plausibly alamethicin is forming multilayered patchworks; **[e] patchwork/cigar:** the high-pressure kink is indicative of further polymer stretching to yield 'cigar' conformation.

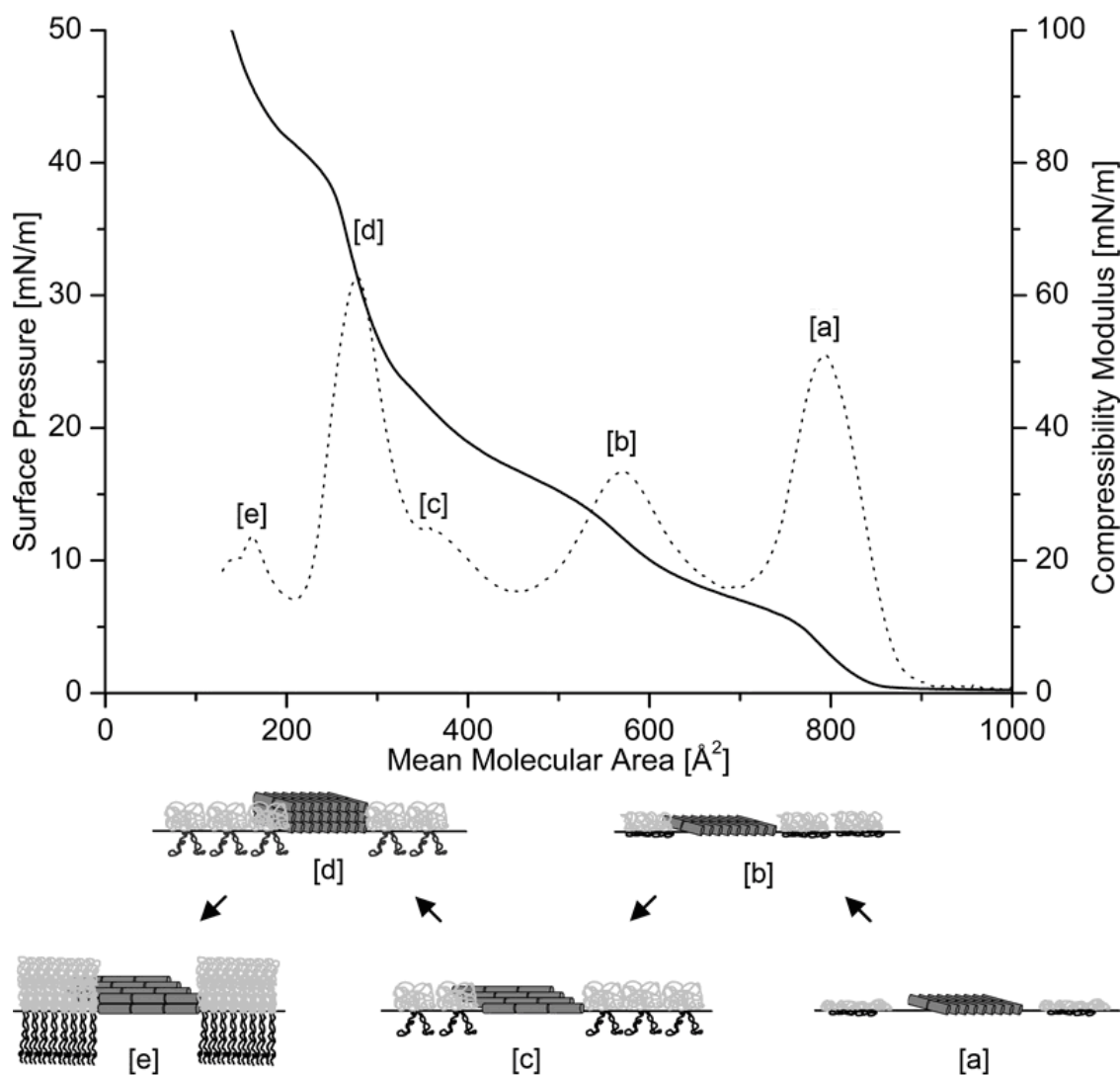


Figure 4.17. Monolayer organization from alamethicin - $A_{16}B_{74}A_{16}$ binary mixtures: surface pressure-area isotherm (solid line), compressional modulus (dotted line) of a 0.7:0.3 alm-polymer mixture and a schematic drawing of molecular packing at the air-water interface.

4.2.2.4. Brewster angle microscopy of mixed monolayers ABA-alm

The above interpretation of polymer-alamethicin composite membranes at the air-water interface has been implemented with Brewster angle images, Figure 4.18. Contrary to what was presented for the lipid-peptide system (Fig. 4.12), the alamethicin features become reduced in size in the presence of a block copolymer. After a mixed monolayer is spread, we observe a large number of small aggregates [a], similar in shape to pure alamethicin domains at that stage, however, their size is markedly different. The initial aggregate growth at the beginning of film compression ($\pi = 0$ mN/m), [b], is a trend comparable to what happens in a pure alm monolayer, yet when the surface pressure reaches the alamethicin-dependent transition at 11 mN/m, a uniform distribution of homogeneously-sized domains is observed [c]. It should be noted here, that contrary to the alm monolayers, the domains at this pressure in the mixed system are also characterized by identical thickness. This narrow size and shape distribution is interpreted in terms of favorable mixing of such domains within the polymer matrix, as discussed before. Further merging of the aggregates at higher pressure [d-f] is consistently similar to the PC-alm mixtures.

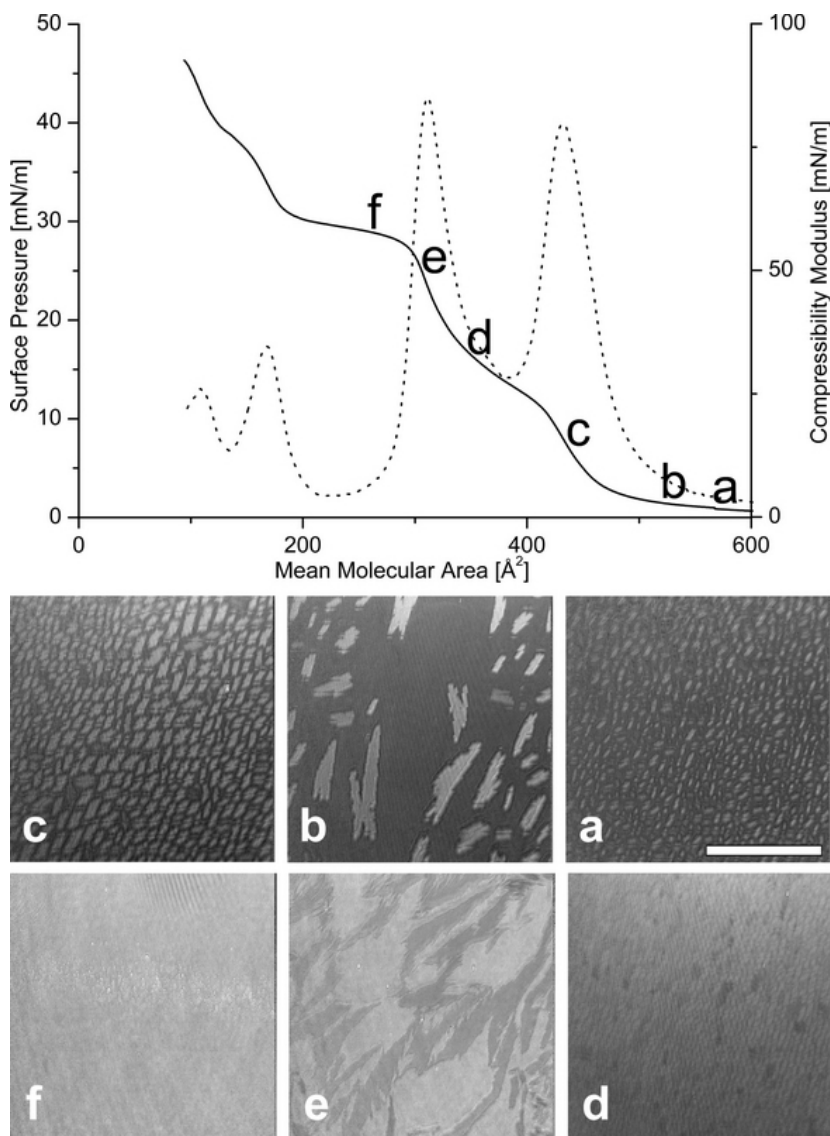


Figure 4.18. BAM images of a $A_{13}B_{23}A_{13}$ – alamethicin (molar ratio 0.3:0.7) monolayer at different surface pressures.

4.2.2.5. Excess mixing energies of mixed monolayers

Having identified the packing and individual phases in the alamethicin-triblock copolymer systems, as well as the elasticity of the membranes at the air-water interface, it was tempting to get further insight into the energetics of mixing in both PC-alm and polymer-alm systems. The excess free energies of mixing at constant surface pressure were calculated from the Langmuir monolayers data as

$$\Delta G^{exc} = \int_0^{\pi} A^{exc} d\pi, \quad (\text{Eq. 2.8})$$

where $A^{exc} = A_{12} - (A_1X_1 + A_2X_2)$. A^{exc} is the excess mean molecular area for a non-ideal system, A_1 and A_2 denote mean molecular area values for pure components, whereas X_1 and X_2 are their corresponding molar ratios. It has to be mentioned here, that due to multiple transitions present in the polymer-alm isotherms, it was not possible to compare the ΔG^{exc} values for all surface pressures, which were interesting in this study. Additionally, owing to the fact that the corresponding transitions appeared at different pressures in the two polymer-alm mixtures, quantitative comparison of the obtained energies is further impaired. Nevertheless, a qualitative trend is worth presenting here (Table 4.1).

π	PC-alm			$A_{13}B_{23}A_{13}$ -alm				$A_{16}B_{74}A_{16}$ -alm			
	0.2	0.4	0.6	0.2	0.4	0.6	0.8	0.2	0.4	0.6	0.8
5	0.4	0.3	1.3	0.9	0.2	0.4	-0.4	-2.0	0.4	-0.9	-1.5
9	0.7	0.7	2.6	1.6	0.1	0.8	-0.6	-3.5	-0.8	-6.5	-5.0
16	1.1	1.1	3.9	-0.9	-4.6	-3.4	-2.4	5.1	3.6	-2.4	-4.0
22	1.3	1.6	5.3	1.2	-1.5	-4.0	-1.9	1.1	-0.4	-2.2	-3.2
27	0.3	0.3	1.1	1.4	0.5	-2.6	-0.3	-0.3	-2.1	-2.0	-2.6

Table 4.1. Excess free energies of mixing (in kJ/mol) for mixed monolayers from alm-PC, alm- $A_{13}B_{23}A_{13}$ and alm- $A_{16}B_{74}A_{16}$ at various surface pressures (in mN/m) and molar ratios of alamethicin.

Firstly, it is noteworthy that in the PC-alm system the excess free energy of mixing is always positive throughout the whole composition range, indicating phase separation as a manifestation of positive deviations from ideal mixing. In the case of the smaller polymer investigated here, $A_{13}B_{23}A_{13}$, we observe that the ΔG_{exc} values become close to zero or slightly positive at all mixture compositions at low surface pressure. At high surface pressure (above 20 mN/m), excess free energies of mixing become more negative and for all surface pressures a minimum is present at alamethicin molar ratio of ca. 0.5. The lowest ΔG_{exc} values, however, are obtained for the surface pressure of 16 mN/m at all $A_{13}B_{23}A_{13}$ -alm compositions, this result being in excellent agreement with the postulated miscibility in this pressure range, as the decreasing ΔG_{exc} can be interpreted in terms of an energy gain due to negative mixing of the two components characterized by attractive interactions.

In the case of the larger polymer, $A_{16}B_{74}A_{16}$, the calculated excess free energies of mixing have small negative values, all comparable for 4, 23 and 27 mN/m, while the ones obtained for 9 mN/m display substantially larger negative deviations from ideal mixing. As discussed before, the alamethicin-dependent energetically favorable transition in the case of this mixed system appears at ca. 5 mN/m, which again agrees with the ΔG_{exc} calculations. The absolute energy minimum at 9 mN/m is observed at the alamethicin content of 0.6, however, for all compositions a significant energy gain is noted compared to other surface pressure values. At last I pulled open a heavy door and found myself in an old, ruined chapel, which had evidently been used as a graveyard. The ground had recently been dug over and the earth placed in great wooden boxes. There, in one of the boxes lay the count [*Stoker 1897*]!

The comparison of the excess free energies of mixing for the systems containing two different block copolymers leads to a conclusion that the larger PDMS block allows for more favorable peptide insertion in the whole surface pressure range. With membranes from both block copolymers being thicker than natural lipid bilayers, this effect could hardly be attributed to a preferential membrane thickness. Instead, in contrast to what might be intuitively anticipated, our interpretation relies on the increased $A_{16}B_{74}A_{16}$'s flexibility due to its size, which facilitates alamethicin insertion.

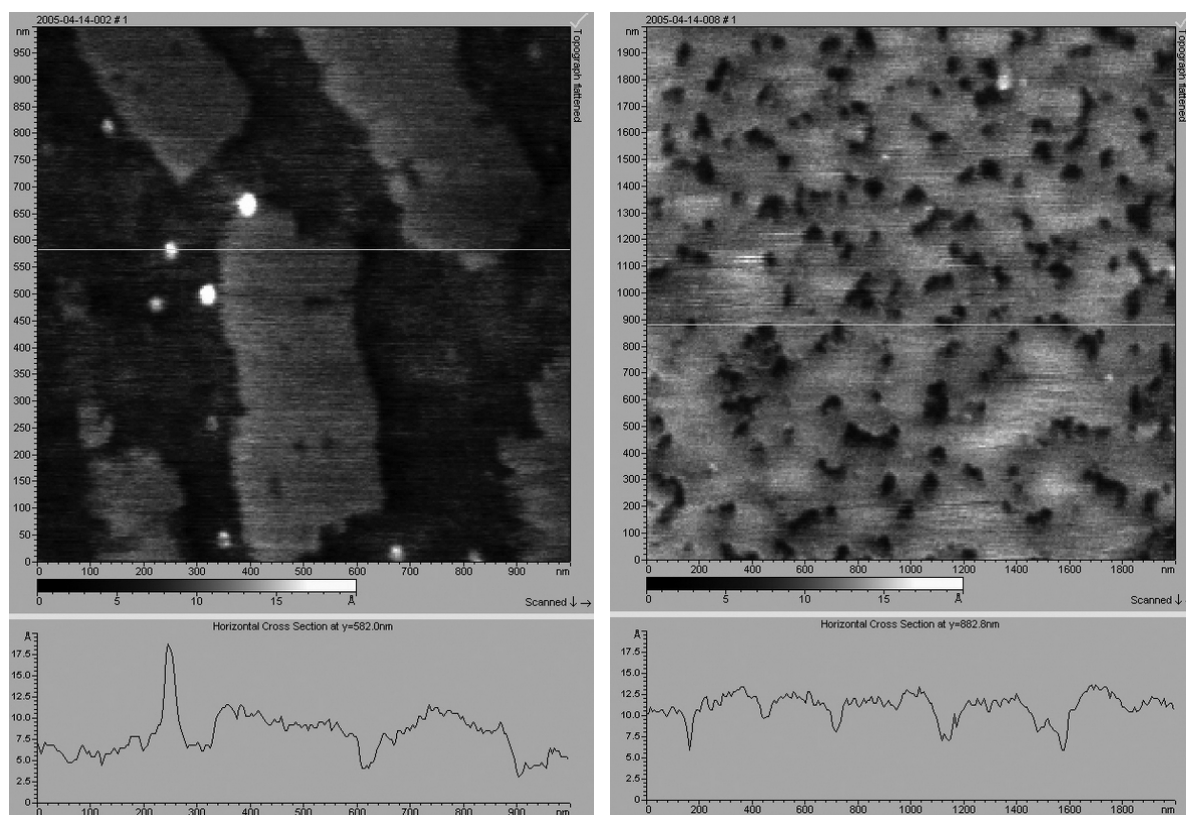
4.3. Langmuir-Blodgett films of mixed monolayers

To get further insight into the film structure of mixed monolayers and the aggregation behavior of alamethicin in block copolymer membranes, film transfers on solid substrates were performed. Due to the fact that we were interested in the monolayer properties, only single layers were deposited. As solid substrate we used mica, an ionic and highly hydrophilic material.

Amphiphile films were built from different polymer-peptide mixtures and in various phase regimes. Upon upstroke of the solid substrate from the subphase, the amphiphile film is deposited as a monomolecular layer. The quantity and the quality of the deposited monolayer are measured by the so called transfer ratio TR which is defined as the ratio between the decrease in monolayer area during a deposition stroke and the total surface area of the substrate. For ideal transfer the TR is equal to 1.

Figure 4.19 shows an atomic force micrograph (AFM) of a mixed LB film of $A_{16}B_{74}A_{16}$ and alamethicin (70:30 mol%) deposited on mica at a surface pressure of 5 mN/m with a transfer ratio of 0.439.

The visible domains might correspond to the intrinsic alamethicin aggregates, although their dimensions of $0.7\mu\text{m} \times 0.3\mu\text{m}$ are about 30 times smaller than the dimensions obtained by Brewster angle microscopy ($20\mu\text{m} \times 8\mu\text{m}$). The height of 4.5 Å of the aggregates compared to surrounding matrix is also no clear evidence of plane parallel aggregated alm α -helices (1 nm in diameter [Fox 1982]).



Figures 4.19 (left) & 4.20 (right). AFM of a LB film $A_{16}B_{74}A_{16}$:alm = 7:3 deposited on mica ($\pi = 5 \text{ mN/m}$; $TR = 0.439$).

As already indicated by the TR of 0.439, the film transfer is far from ideal. Therefore various segments of the LB film look completely different. In Figure 4.20 an AFM image of the same sample is presented. The intrinsic domains, possibly alm aggregates, are not visible. In contrast, the substrate is covered with a film strewn with numerous holes of diameters of 50-80 nm and heights of 4.5-6.5 Å. There is no evidence where these porous defects might origin from. Typical barrel-stave alamethicin oligomers are supposed to build pores of 20 Å in diameter [Woolley 1992]. Surface adsorbed plane parallel alm aggregates measured by BAM (Fig. 4.06 & 4.07) and by fluorescence microscopy [Ionov 2000] are in the size range of 50µm.

Similar results were obtained from the same amphiphile mixture at higher surface pressures. In Figure 4.21 an AFM image is presented from an LB film of $A_{16}B_{74}A_{16}$ and alamethicin (70:30 mol%) deposited on mica at a surface pressure of 12.5 mN/m with a transfer ratio of 1.333. The monolayer film is speckled with porous defects similar to the sample deposited at 5 mN/m, but the number of defects per area is far higher. This result is inconsistent with the increased transfer ratio obtained for this sample (1.333 compared to 0.439). A higher TR implies thicker or tighter packed film but in any way more defects. Due to the fact that the film thickness was not determined by scratching, it is not possible to elucidate the origin of this observation.

LB films obtained at higher surface pressures do not exhibit similar features. Due the higher compression the film surface looks far smoother and more homogenous than film surfaces attained at lower π (Fig. 4.22).

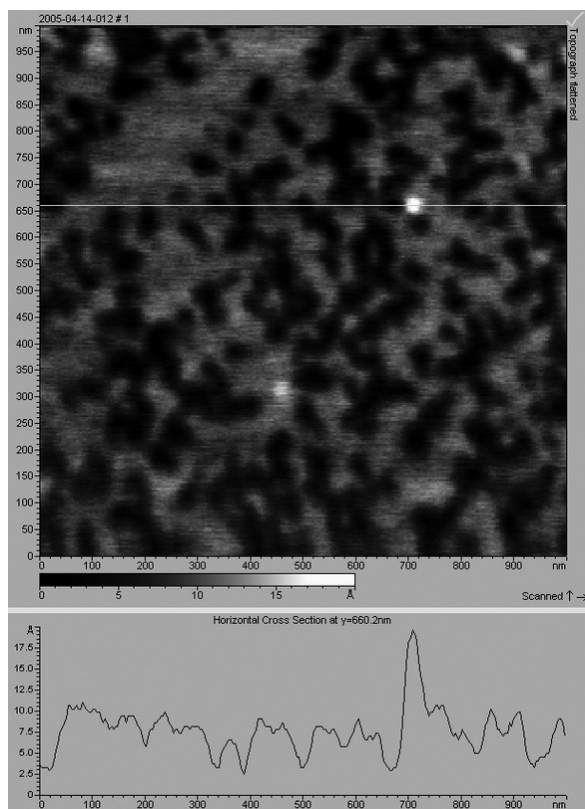


Figure 4.21. AFM of a LB film $A_{16}B_{74}A_{16}$:alm = 7:3 deposited on mica ($\pi = 12.5$ mN/m; TR = 1.333).

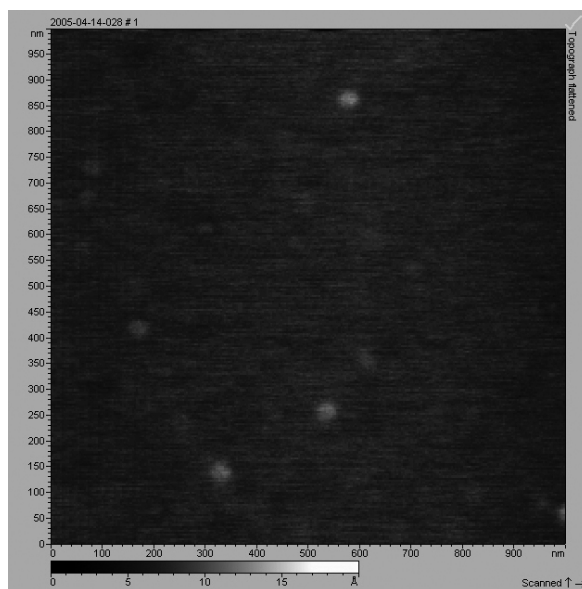


Figure 4.22. AFM of a LB film $A_{16}B_{74}A_{16}$:alm = 7:3 deposited on mica ($\pi = 25$ mN/m; TR = 1.846).

Clear evidence on the film structure from mixed monolayers could also not be obtained from different mixtures of $A_{16}B_{74}A_{16}$ and alm as well as from $A_{13}B_{23}A_{13}$ and alm. It was not possible to detect any of the features visible in BAM also by AFM. We were therefore interested if the transferred LB film retained the structure and properties of the original Langmuir film.

As mentioned already in the LB film chapter of the introduction (Chapter 2.1.5.), many difficulties were reported in finding the appropriate conditions for successful film transfers. Extensive film reorganisation and rearrangement has been observed for many systems [Kopp 1975, Rabe 1987, Rothberg 1987, Tippmann-Krayer 1991, Tippmann-Krayer 1992, Fuchs 1992, Decher 1992, Albouy 1992, Schaper 1993, Schwartz 1993, Zasadzinski 1994, Höhne 1994, Wu 1996].

In previous publications it was ascertained that PMOXA-PDMS-PMOXA triblock copolymers expose a rod-like ABA (hydrophilic–hydrophobic–hydrophilic) structure upon deposition on a variety of solid substrates (silicon wafers, glass slides, etc.) at high compression ($\pi = 45$ mN/m) [Ho 2004a, 2004b]. Therefore the monolayer structure of the triblock copolymer film is not preserved but reorganization takes place. The drastic change of milieu from air-water to air-substrate as well as film drying might lead to dewetting and desorption, molecular repacking and phase transitions.

4.3.1. Contact angle measurements

If a liquid is placed on a solid, it may either spread so as to completely wet the substrate or de-wet to form droplets with a finite contact angle. The contact angle is the angle between the substrate surface and a tangent drawn to the liquid surface at the point of contact with the solid. The equilibrium state results from a balance of the three interfacial tensions. The solid/vapour surface tensions γ_{SV} is balanced by the sum of the solid/liquid interfacial tension γ_{SL} and a component of the liquid/vapor surface tension resolved parallel to the substrate $\gamma_{SI}\cos\theta$:

$$\gamma_{SV} = \gamma_{SL} + \gamma_{SI}\cos\theta \quad (\text{Eq. 4.2})$$

This is known as the Young equation. A liquid with zero contact angle on a given solid will spread to completely wet the surface. Liquids with contact angles $0 < \theta < 90^\circ$ de-wet the solid to form droplets. Droplets of a liquid with a contact angle $\theta > 90^\circ$ will move easily about on the surface.

By measuring the contact angles of various films on solid substrates, we aimed to get insight into a hypothetical ABA reorganization upon LB deposition. The obtained contact angles of various samples are presented in Table 4.2.

As a reference, the contact angle of pure mica as a very hydrophilic substance was measured. Further references were obtained from pure PMOXA homopolymer films on mica, pure PDMS homopolymer on mica and Parafilm® (LD PE) on mica.

Sample	Contact angle
LB film A ₁₆ B ₇₄ A ₁₆ :alm = 7:3 deposited on mica ($\pi = 25$ mN/m; TR = 1.846) ($\pi = 5$ mN/m; TR = 0.439)	28° 28°
LB film NH ₂ -A ₃₀ B ₇₅ A ₃₀ -NH ₂ deposited on mica ($\pi = 26$ mN/m)	58°
LB film GluA-A ₇₅ B ₂₃ A ₇₅ -GluA deposited on mica ($\pi = 30$ mN/m)	62°
Mica (pure substrate)	13°
PMOXA spincoated on mica	20°
PDMS spincoated on mica	65°
Parafilm® (LD PE) on mica	110°

Table 4.2. Experimental contact angles of various substrates.

As expected, pure mica and PMOXA coated mica yield an extremely hydrophilic surface generating very low contact angles (13° and 20° respectively). Parafilm®, as a completely non polar olefin blend, gives a maximum contact angle of 110° . Although PDMS is a very hydrophobic polymer, PDMS coated mica yields a contact angle of only 65° . This is probably due to the fact, that it was not possible to coat the highly hydrophilic mica substrate in a homogenous way with PDMS and that therefore the measured contact angle does not refer to a pure thin PDMS film.

Two of the LB films of mixed ABA/alm composition, already investigated by AFM, were inspected by contact angle measurements. Surprisingly both deposited films exhibited the same contact angle of 28° although surface pressure of deposition and transfer ratio were considerably different.

Anyway, the contact angles of 28° suggest that the surface is hydrophilic due to the exposure of the hydrophilic A block. This would imply that a reorganization of the ABA chains from coiled loops to linear chains occurred upon transfer.

An alternative explanation for such a low contact angle would be that the hydrophobic B blocks of only one deposited layer are too thin to shield the electrostatic interactions of mica effectively. In this case, reorganization would not absolutely have to occur.

By the use of amino and glutaric acid functionalized triblock copolymers, clear evidence was found that reorganization of transferred films takes place. In comparison to alcohols, amines and glutaric acid exhibit stronger interactions with mica. Therefore amino terminated and glutaric acid terminated PMOXA-PDMS-PMOXA should exhibit a stronger tendency to adsorb on mica compared to hydroxy terminated PMOXA-PDMS-PMOXA. In fact, the contact angles of the deposited LB films of $\text{NH}_2\text{-A}_{30}\text{B}_{75}\text{A}_{30}\text{-NH}_2$ (58°) and $\text{GluA-A}_{75}\text{B}_{23}\text{A}_{75}\text{-GluA}$ (62°) proof that the hydrophobic B-blocks are exposed and that the loop monolayer structure of the ABA chains is retained.

This proof of reorganization of hydroxyl terminated triblock copolymers upon transferring them on mica explains why it was impossible to detect the intrinsic alm aggregates by AFM.

Amino and glutaric acid functionalized triblock copolymers might therefore be a well suited system to investigate monolayer films from mixed peptide/polymer blends. Although it has to be proven first that the isothermal monolayer behavior is not altered by the different end groups.

Another alternative for successful LB transfers of triblock copolymer-peptide monolayers would be the choice of a hydrophobic substrate for deposition. Although single layer transfers are more intricate with such substrates successful film transfers with PMOXA-PDMS-PMOXA were reported with silicon [Vebert 2005].

4.4. Bilayer systems of mixed membranes from block copolymers and alam

4.4.1. Biological relevance of mixed monolayers

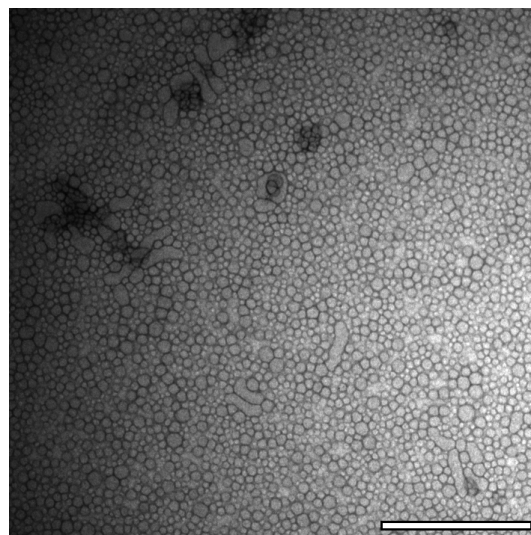
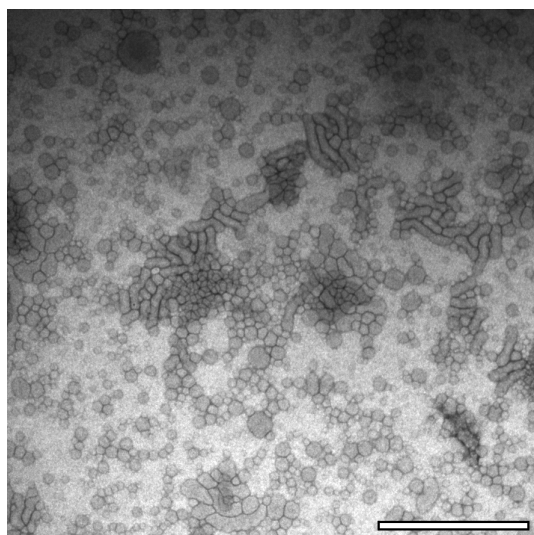
As mentioned before, this work was intended to contribute to the understanding of the physical chemistry of alamethicin incorporation into membranes from amphiphilic block copolymers, and thus the monolayer model system was applied. The concern remains to which extent a Langmuir monolayer at the air-water interface really corresponds to bilayers, as present in biological systems or block copolymer vesicles. With a strong asymmetry of dielectric constants of air and water on both sides of the film, we realize the monolayer approach may deviate slightly from fully hydrated membrane systems. On the other hand, as long as the peptide does not really span across the bilayer, and its functionality is ensured by plane-parallel organization, we believe these results can well translate to aqueous environments.

Another important fact to be mentioned is the absence of a membrane potential throughout all measurements. The voltage-gated channel forming properties of alamethicin have been described already in 1968 by Mueller & Rudin [*Mueller 1968*]. The α -helix has an excess of negative charge at the C-terminus and positive charge at the N-terminus due to alignment of the dipole moments of individual peptide bonds [*Hol 1981*]. Thus, a peptide in the α -helical conformation may be thought of as a macro-dipole with a large dipole moment. A transmembrane voltage might therefore considerably affect the conformation of alamethicin and its channel directly. Therefore not only a bilayer system could be mandatory for a perpendicular oriented barrel-stave model, but also a transmembrane potential.

4.4.2. Mixed vesicles from block copolymers and alamethicin

The preferred method to investigate polymersomes is transmission electron microscopy (TEM). TEM gives direct evidence on structure, shape and dimensions. Further, polymersomes prepared by the most convenient methods (e.g. film rehydration and solvent injection [Kita-Tokarczyk 2005a]) are generally in the size range of 10^2 nm and can therefore not be analysed by light microscopy.

Pure PMOXA-PDMS-PMOXA vesicles without alamethicin were prepared by the film rehydration method (0.4% wt/wt, 50mM PO_4^{3-} , 10mM HEPES, 10mM KCl, pH 7.4). It was found, that extended swelling times lead to a decrease of mean vesicle diameter as well as polydispersity and further to a decrease in the number of tubular and non-spherical vesicles (Fig. 4.23-4.25, Table 4.3). Not surprisingly prolonged agitation leads to the thermodynamically most favorable structures in the most convenient dimensions (assuming that polymer vesicles are thermodynamically stable superstructures [Shen 1999, Luo 2001a, 2001b]).



Figures 4.23 (left) & 4.24 (right). TEM micrographs of PMOXA_{16} - PDMS_{74} - PMOXA_{16} vesicles after 1 day and 5 days of swelling (scale bar 500nm, negative stained).

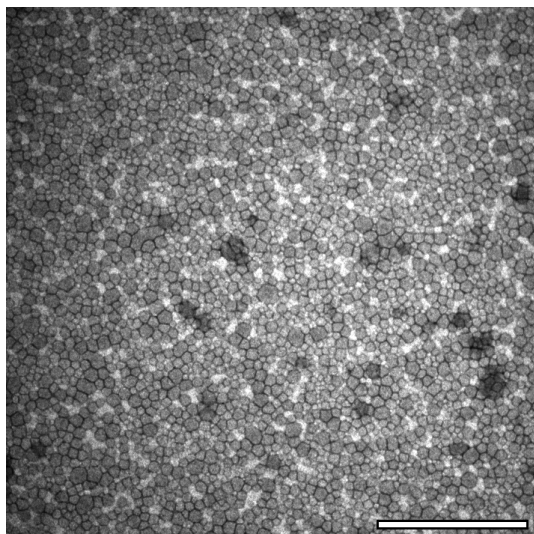


Figure 4.25. TEM micrograph of PMOXA_{16} - PDMS_{74} - PMOXA_{16} vesicles after 14 days of swelling (scale bar 500nm, negative stained).

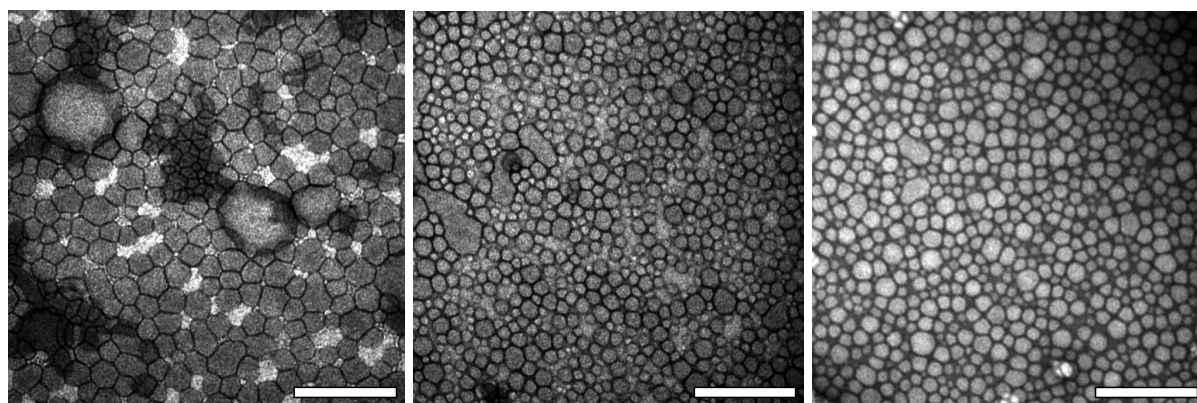
swelling time	mean \emptyset [nm]	std. dev. [nm]	# vesicles
1 day	48.52	8.31	78
5 days	31.61	7.71	184
14 days	24.90	7.25	206

Table 4.3. Decrease of mean diameter and polydispersity of $\text{PMOXA}_{16}\text{-PDMS}_{74}\text{-PMOXA}_{16}$ vesicles with increased swelling time.

To investigate the dependence of polymersomes on alamethicin content PMOXA - PDMS - PMOXA proteovesicles were prepared by the film rehydration method (one day swelling, 0.4% wt/wt, 50mM PO_4^{3-} , 10mM HEPES, 10mM KCl, pH 7.4). Six amphiphile solutions of varying alm concentration were prepared. The PMOXA_{16} - PDMS_{74} - PMOXA_{16} solutions contained molar ratios of alamethicin from 1:0 to 1:10⁻¹.

First of all it has to be mentioned that stable vesicles formed at all molar ratios investigated. Interestingly, similarly to a prolonged swelling time, an increase of alamethicin content leads to a decrease of mean vesicle diameter and further to a decrease of polydispersity and of the number of non uniform structures (Fig. 4.26-4.28, Table 4.4).

A possible explanation of this effect could be the intercalation of alm helices into the block copolymer bilayer. Alm is shorter by a factor of three (3.2nm for alm [Fox 1982]) compared to ABA (about 10nm [Nardin 2000a]) and can therefore alter the packing regime of the vesicle membrane considerably. A distorted packing shape would not only alter diameter but also the phase formed. With a decrease of critical packing parameter micellar structures might be promoted [Gennis 1989]. In fact, vesicles with a molar ratio ABA:alm of 10:1 (table 2) exhibit a very small diameter of only 25.75nm, reflecting that there is basically no inner vesicular cavity.



Figures 4.26-4.28 (left to right). TEMicrographs of proteovesicles with molar ratios $n\text{ABA} : n\text{Alamethicin}$ 1:0, 1:10⁻⁴ and 1:10⁻¹ (scale bar 200nm, negative stained).

$n_{\text{ABA}} : n_{\text{alm}}$	mean \varnothing [nm]	std. dev. [nm]	# vesicles
1:0	48.52	8.31	78
1:10 ⁻⁵	31.61	7.71	184
1:10 ⁻⁴	24.90	7.25	206
1:10 ⁻³	25.25	6.89	206
1:10 ⁻²	27.24	6.57	195
1:10 ⁻¹	25.75	6.56	212

Table 4.4. Decrease of mean vesicle diameter and polydispersity with increasing alamethicin content.

Keeping in mind that alm does not molecularly mix with triblock copolymers in Langmuir monolayers, the results obtained by TEM of mixed vesicles might indicate in contrary that a homogenous distribution of individual amphiphile molecules in a vesicular membrane is probable in fully hydrated environment.

4.4.2.1. Dynamic light scattering of mixed polymersomes

As a second tool to study the reliance of polymersome size on alm concentration dynamic light scattering was employed. Dynamic light scattering (DLS) also known as quasi-elastic light scattering (QELS) is used to study dynamics of macromolecules in solution. It involves measuring the temporal fluctuations of the intensity of scattered light. The number of photons entering a detector are recorded and analyzed by a digital correlator. The separation in time between photon countings is the correlation time. The autocorrelation function of the intensity at a certain angle can be analyzed to yield the distribution of relaxation times. The decay rates of the relaxation modes provide translational diffusion coefficients [Hamley 2000].

The used electric field autocorrelation function $g^{(1)}(\tau)$ for small monodisperse particles is described in literature [Nardin 2000a] as

$$g^{(1)}(\tau) = \exp(-Dq^2\tau), \quad (\text{Eq. 4.3})$$

where τ is the decay time and scattering vector q

$$q = \frac{4\pi n}{\lambda} \sin \frac{\theta}{2}, \quad (\text{Eq. 4.4})$$

with the solvent refractive index n , the wavelength of the incident light λ , and the scattering angle θ .

The hydrodynamic radius of the constituent particles can be obtained using the Stokes-Einstein equation for the diffusion of highly diluted and non interacting spherical particles

$$D = \frac{k_B T}{6\pi\eta R_h}, \quad (\text{Eq. 4.5})$$

where D is the translational diffusion coefficient, $k_B T$ is an estimate of the translational kinetic energy per particle, R_h is the hydrodynamic radius of the particle and η the viscosity of the surrounding medium [van Zanten 1991].

In a preliminary experiment pure PMOXA₁₆-PDMS₇₄-PMOXA₁₆ vesicles were examined. The vesicles were made by the film rehydration method in a phosphate buffer saline (0.4% wt/wt, 50mM PO₄³⁻, 10mM HEPES, 10mM KCl, pH 7.4) and stirred for one day prior to five times extrusion by 0.45 μ m membranes. A dilutions series of each of those samples (50%, 33%, 25%, 20%, 16.7%, 12.5% V/V) was prepared and each dilution was measured at six different scattering angles (30°, 45°, 60°, 90°, 120°, 150°). Angular dependent measurement was necessary due to the fact, that the vesicle size exceeded 30nm, the limit of a simple source of scattered radiation. The correlation functions were fitted using cumulant functions. ‘There’s no other place for peace,’ he said. ‘Usul, you’re crying,’ Chani murmured. ‘Usul, my strength, do you give moisture to the dead? To whose dead?’ ‘To ones not yet dead,’ he said. ‘Then let them have their time of life,’ she said. He sensed through the drug fog how right she was, pulled her against him with savage pressure. ‘Sihaya!’ he said [Herbert 1968]. Extrapolation of angular diffusion coefficients to zero scattering angle and further extrapolation of these values to zero concentration yielded the actual diffusion coefficient form which the hydrodynamic radius was calculated by the Stokes-Einstein equation. In this way it was found that polymersomes without alamethicin

have a mean hydrodynamic radius of 362.1 ± 10.8 nm ($D = 5.93 \cdot 10^{-13} \pm 1.82 \cdot 10^{-14}$ m^2s^{-1} , Fig. 4.29).

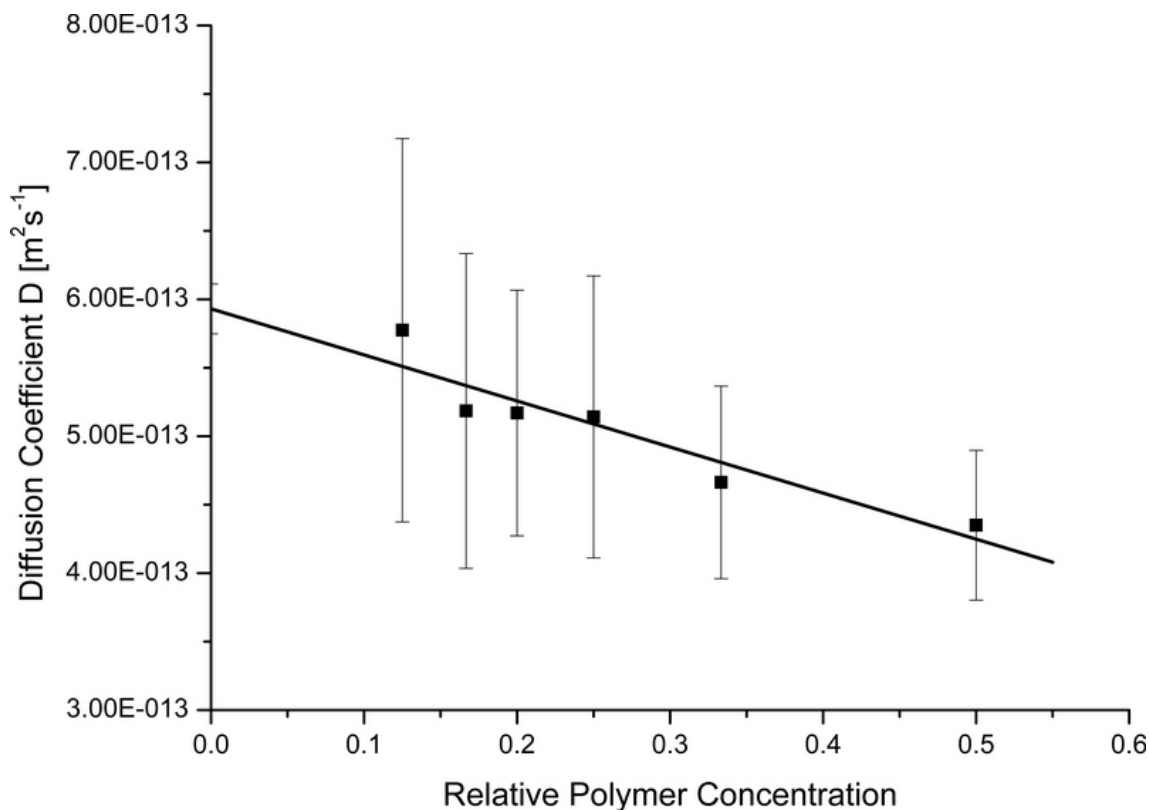


Figure 4.29. Dynamic Zimm plot and linear fit of DLS results of pure PMOXA-PDMS-PMOXA vesicles.

To measure the size of $A_{16}B_{74}A_{16}$ polymersomes depending on the amount of incorporated alamethicin, six vesicle solutions (0.4% wt/wt) were prepared with molar ratios n_{ABA} to n_{alm} of 1:0, 1:10⁻⁵, 1:10⁻⁴, 1:10⁻³, 1:10⁻² and 1:10⁻¹. The vesicles were made similar to the above pure polymersomes by the film rehydration method (1 day stirring, five times extrusion 0.45 μm). Our results suggest that upon addition of alamethicin, the hydrodynamic radius of thus formed proteovesicles decreases (Fig. 4.30). This observation can be explained by a change in packing density and therefore a decrease in packing parameter and increase in interfacial curvature. The higher the alamethicin content the higher the diffusion coefficient and therefore the smaller the proteovesicles. If that man had been an ordinary lunatic I would have taken my chance of trusting him; but he seems so mixed up with the Count in an indexy kind of way that I am afraid of doing anything wrong by helping his fads. I can't forget how he prayed with almost equal fervour for a cat, and then tried to tear my throat out with his teeth [Stoker 1897].

We interpret these results only qualitatively. Since the polymersomes exhibited, similar to TEM results after 1d, a very broad size distribution (even after several extrusions by 0.45 μm), the absolute numbers obtained by DLS are not reasonable. The quantitative output of 362nm for pure ABA vesicles by film rehydration is very contrary to the results obtained by TEM. One explanation of this observation is certainly that vesicles may shrink upon drying from hydrated state (DLS) to dry state (TEM) anyhow this effect cannot contribute to such a massive discrepancy. Experimental

observations of different systems indicated that surface active ingredients are released upon DLS sample preparation either by the syringes or the extrusion filters used [Kita-Tokarczyk 2005b]. We therefore conclude that fusion, aggregation or re-assembly is induced by extrusion and that TEM is hence yielding more reliable results.

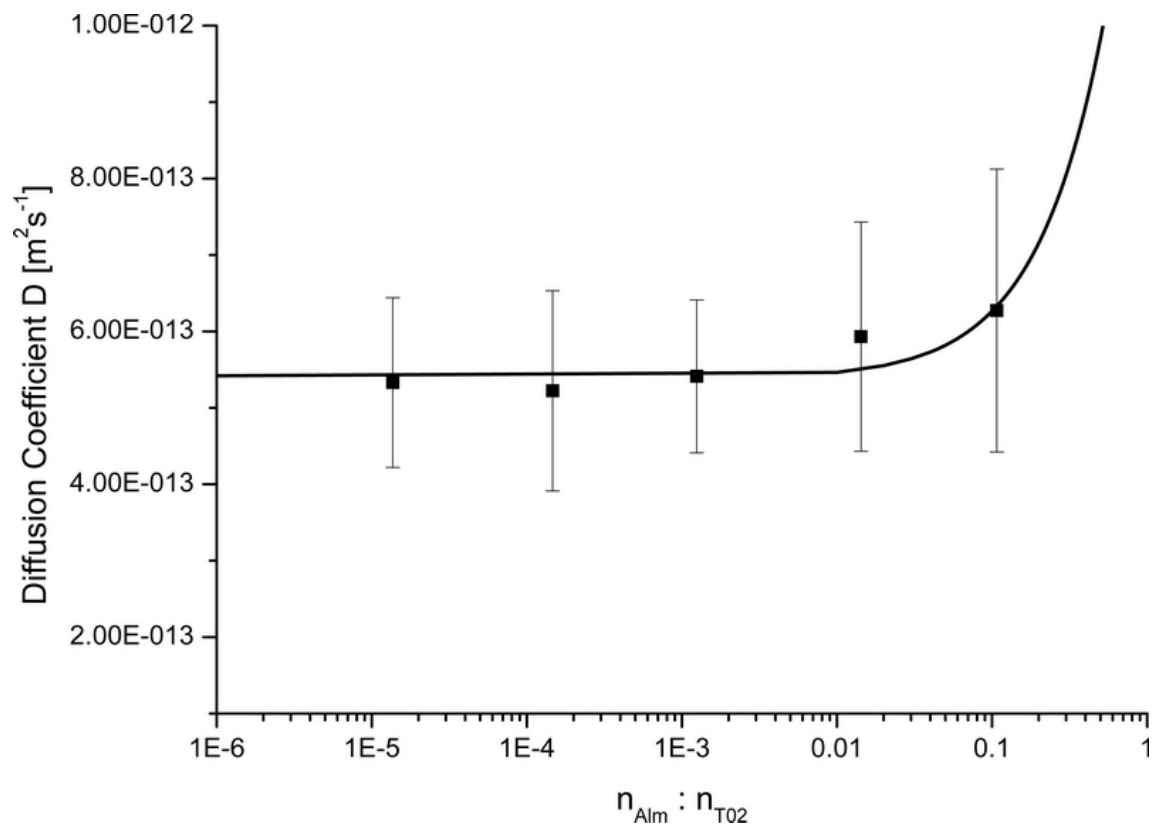


Figure 4.30. Diffusion coefficients of PMOXA-PDMS-PMOXA vesicles in function of alameithicin concentration and linear fit (logarithmic scale).

4.4.3. Ion transport activity of alamethicin in block copolymer membranes

4.4.3.1. Biomimetic mineralization in giant polymersomes

To prove the ion transport activity and therefore the functional incorporation of alm in self-assembled block copolymer membranes, a biomimetic concept of controlled mineralization in vesicles was applied.

The controlled formation of inorganic minerals within organic or polymeric matrices is successfully used by Nature to design biological composite materials such as bone or teeth [Lowenstam 1989]. Although the detailed mechanisms of biomineralization are still not clarified, various models have been suggested that increase our understanding of these biological processes [Cui 2000].

Phospholipid vesicles have been successfully used to mineralize and precipitate inorganic solids, such as e.g. calcium phosphate [Eanes 1984] or iron oxide [Mann 1986] within their interior. Similar to biological systems, also during biomimetic mineralization, specific interactions between the matrix forming material and the crystal planes of the growing nuclei are of crucial importance for the structure and morphology of the newly formed minerals [Addadi 1992]. The high diversity of block copolymer chemistry makes the self assembled superstructures of amphiphilic block copolymers ideally suited as templates for biomimetic mineralization [Coelfen 1998].

In this experiment, phosphate anions were encapsulated during vesicle formation. Since the Ca^{2+} ions from the extracellular solution are not able to permeate the triblock copolymer membranes, precipitation of calcium phosphate in the vesicle interior requires a transport system. Alamethicin, reported to be a very powerful cation transporter, was supposed to make the membrane permeable for calcium ions (see Fig. 4.31 for a schematic representation).

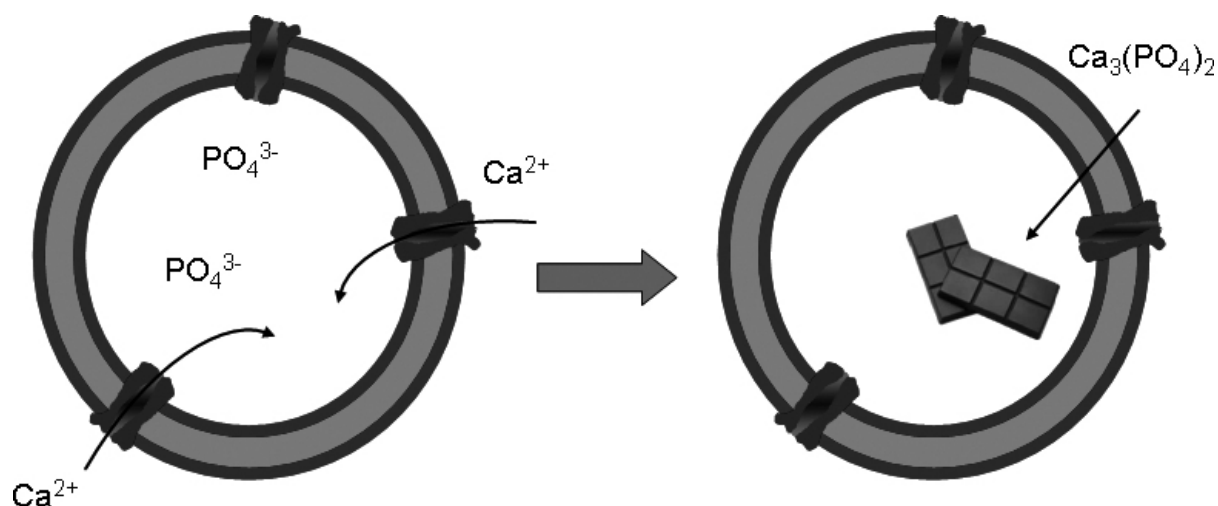


Figure 4.31. Schematic representation of a so-called biomimetic mineralization in copolymer vesicles. Phosphate is encapsulated whereas calcium ions are added to the extravesicular space. When alm (represented as a general transmembrane channel) is present in the system a formation of inorganic calcium phosphate occurs.

To facilitate observation of the precipitated calcium phosphate we used giant unilamellar PMOXA₁₆-PDMS₇₄-PMOXA₁₆ triblock copolymer vesicles (GV) prepared by electroformation [Dimitrov 1987, Bucher 1998]. The electrodes coated with PMOXA₁₆-PDMS₇₄-PMOXA₁₆ were immersed in phosphate buffer saline (50 mM PO₄³⁻, 10 mM HEPES, 10 mM KCl; pH 7.4) and an AC voltage of 5 V at a frequency of 10 Hz for 2 h followed by 30 min at 5 V and 5 Hz was applied.

Phase contrast and transmission electron microscopy investigations indicated that the resulting dispersion contained giant vesicles with diameters in the micron range in a high density (Fig. 4.32 & 4.33).

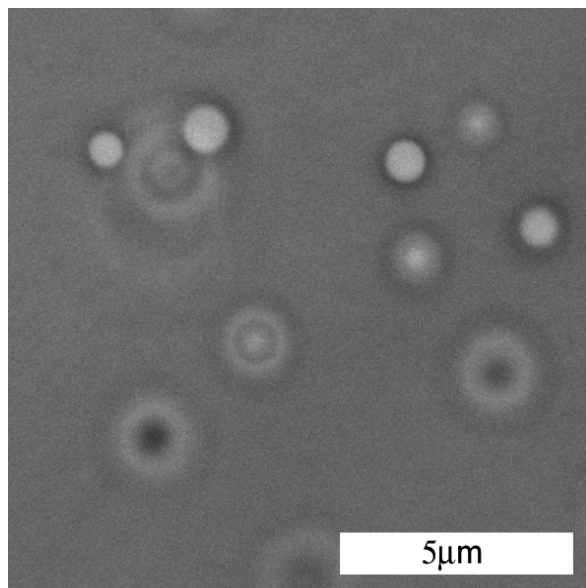


Figure 4.32. Phase contrast micrograph of giant PMOXA₁₆-PDMS₇₄-PMOXA₁₆ triblock copolymer vesicles prepared by electroformation (scale bar 5 μm).

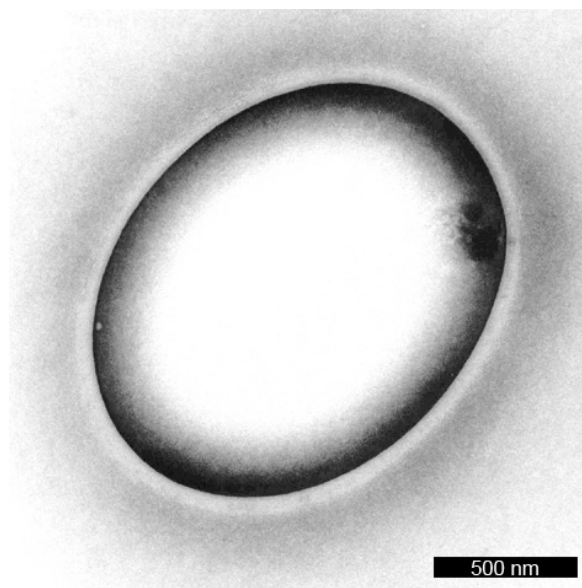


Figure 4.33. TEM image of giant PMOXA₁₆-PDMS₇₄-PMOXA₁₆ triblock copolymer vesicle prepared by electroformation (negative stained, scale bar 500 nm).

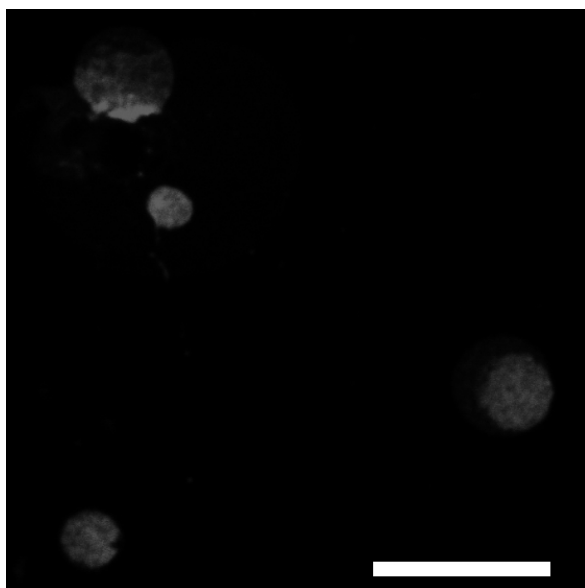


Figure 4.34. CLSM image of TAMRA functionalized giant triblock copolymer vesicles prepared by electroformation (scale bar 10 μm).

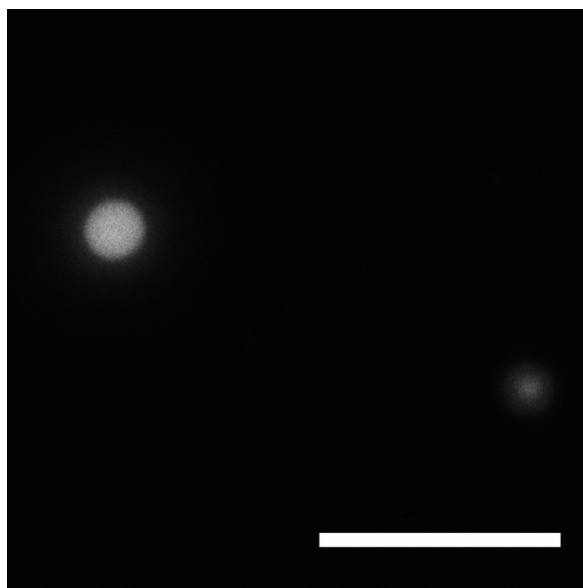


Figure 4.35. Fluorescent micrograph of DTAF functionalized triblock copolymer vesicles prepared by electroformation (scale bar 5 μm).

For better detection in light microscopy, also dye labeled triblock copolymers were employed for vesicle preparation. 5-(4,6-dichlorotriazinyl) aminofluorescein (DTAF) and tetramethyl rhodamine-5-carbonyl azide (TAMRA) end functionalized block copolymers form giant vesicular structures which are easily detectable by their intrinsic fluorescent properties (Fig. 4.34 & 4.35).

The preparation of giant vesicles was followed by subsequent removal of nonencapsulated phosphate ions by dialysis against buffer solution (10 mM HEPES, 110 mM KCl, pH 7.4). After addition of 2 ml of a calcium chloride solution (50 mM CaCl₂, 10 mM HEPES, 35 mM KCl; pH 7.4) 18 µl of an alm solution (1.28 mM, ethanol) were added. The resulting solution was investigated after 1 and 24 h by transmission electron microscopy.

In the control experiment without alm no precipitation of calcium phosphate occurred. This is in contrast to observations of the sample with alamethicin where the formation of crystals could be observed within the vesicular structures.

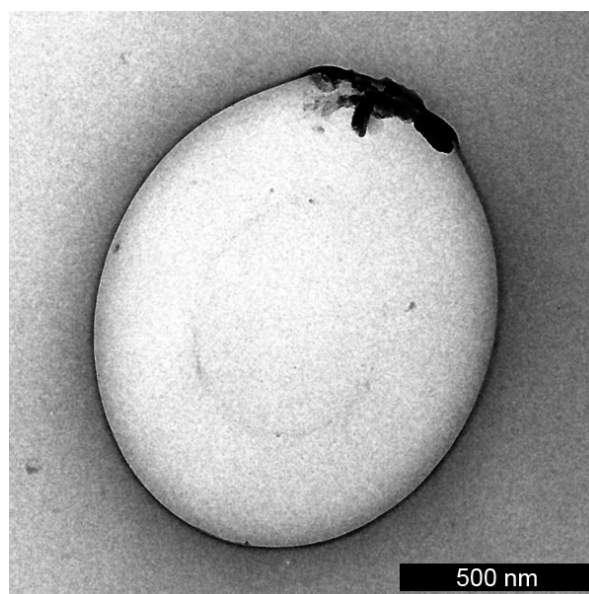
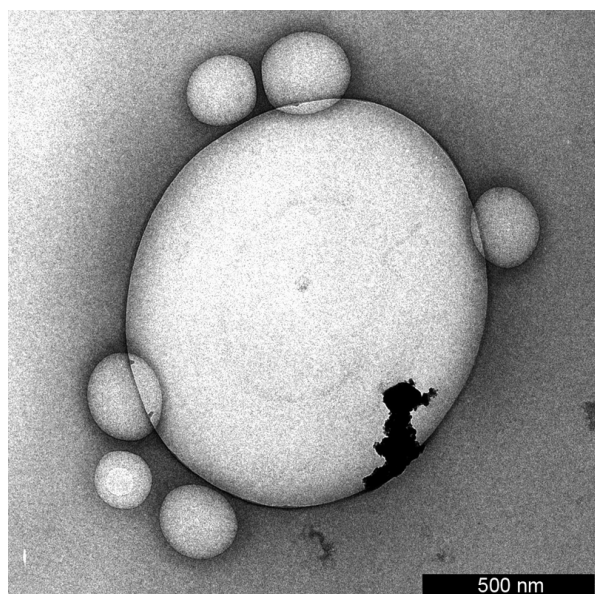
As can directly be seen in Figures 4.36 and 4.37 already after only 1 h of incubation calcium phosphate crystals start to grow at the inner surface of the polymer membrane. After 24 h a considerable fraction of the vesicle interior is filled with needle-like calcium phosphate crystals (Fig. 4.38), thus a transformation from probably amorphous to a thermodynamically more favorable crystalline calcium phosphate morphology (e.g. hydroxyapatite) might have occurred.

It has to be pointed that amorphous morphologies may be achievable by means of this biomimetic mineralization pathway and that these amorphous species are stabilized by the polymeric matrix for a certain time. In bulk, by simply adding calcium ions to phosphate (at similar concentrations like in the biomineralized experiment), fine hydroxyapatite needles are visible instantaneously (Fig. 4.39). An amorphous state is not achievable in bulk without the protecting and directing cavity of the polymer vesicle.

Longer incubation times did not lead to any detectable further growth of the crystals. Obviously after 24 h the encapsulated phosphate ions have already been consumed. This is also reflected by the fact that the volume of the minerals was always in reasonable agreement with the starting concentration of phosphate in the vesicle. Moreover, the inorganic crystals are clearly confined to the inner cavity of the vesicles thus indicating that crystal growth is limited by the shells of the block copolymer vesicles.

These results clearly prove that alm is actively increasing the permeability for divalent cations of block copolymer membranes. Mineralization of inorganic species occurs only when alamethicin is present. In the control experiment, in the absence of alm, no mineralization occurred and no crystallized species could be detected. Alamethicin is therefore fully functional in synthetic polymer membranes and retains its antimicrobial ion transport activity.

Moreover, the resulting combination of the well defined block copolymer aggregates with the specificity and efficiency of naturally occurring ion channels could be a helpful tool to get a closer insight into the principles of biomineralization.



Figures 4.36 (left) & 4.37 (right). TEM of phosphate containing triblock copolymer vesicles after 1 h of incubation with CaCl_2 -solution in the presence of alm (negative stained, scale bar 500nm).

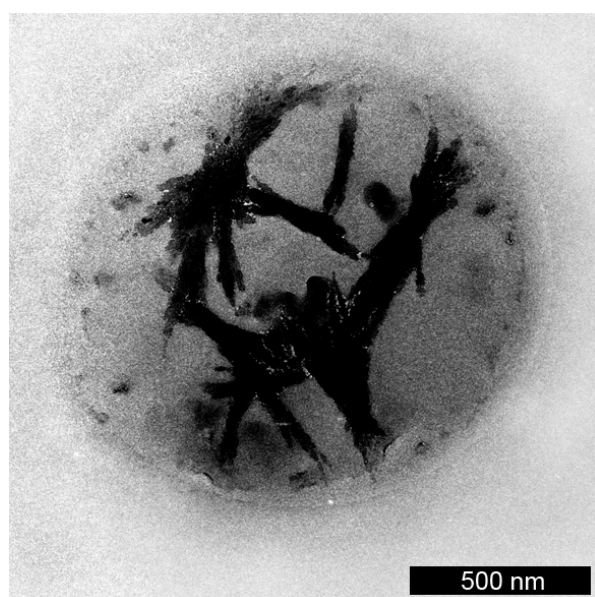


Figure 4.38. TEM of phosphate containing triblock copolymer vesicles after 24 h of incubation with CaCl_2 -solution in the presence of alm (unstained, scale bar 500nm).

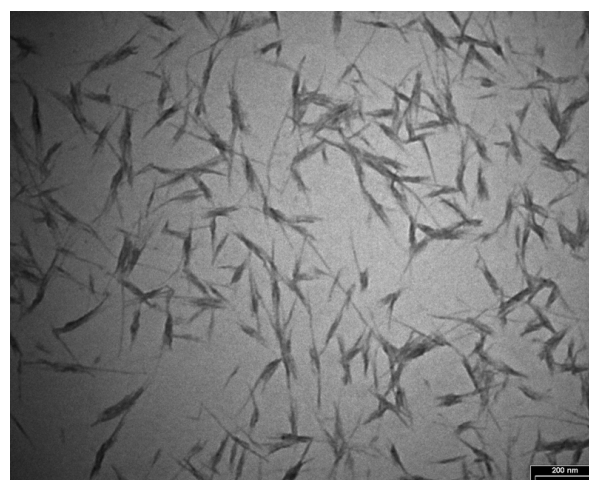


Figure 4.39. TEM of calcium phosphate needles obtained by bulk addition of calcium ions to phosphate (unstained, scale bar 200nm).

4.4.3.2. Biomimetic mineralization in small unilamellar polymersomes

After employing alamethicin successfully in giant polymersomes to transport calcium ions over the lipophilic barrier we also tried to adapt the concept to small unilamellar polymer vesicles. PMOXA₁₆-PDMS₇₄-PMOXA₁₆ polymersomes were prepared according to the film rehydration method in a phosphate buffer saline (0.4% wt/wt, 5 days swelling, 50 mM PO₄³⁻, 10 mM HEPES, 10 mM KCl; pH 7.4). In this experiment alm was added already during vesicle formation in molar ratios of n_{ABA} to n_{alm} of 1:0, 1:10⁻⁵, 1:10⁻⁴, 1:10⁻³, 1:10⁻² and 1:10⁻¹. Nonencapsulated phosphate ions were subsequently removed by dialysis against buffer solution (10 mM HEPES, 110 mM KCl, pH 7.4) followed by addition of calcium chloride solution (50 mM CaCl₂, 10 mM HEPES, 35 mM KCl; pH 7.4).

The resulting solutions were investigated after 1 day by transmission electron microscopy. Dimensions of polymersomes were in the size range of 30nm in diameter, in good agreement to the findings described above for extended swelling times. Unfortunately it was not possible to detect either amorphous or crystalline calcium phosphate in all six solutions of varying alm content. Only in the vesicle solution with the highest alm content (ratio polymer:alm = 10:1) tiny dots were detectable (Fig. 4.40). Because of their minimal size it is not possible to conclude if these dots are effectively calcium phosphate minerals or something different. Owing to the high content of alamethicin these dots might as well be aggregates of alamethicin or staining artifacts. Due to the fact that all samples were prepared, stained and investigated in the same way and only in the experiment with the highest alm content the dots were detectable, we conclude that the dots originate from alm aggregates.

This assumption is further fostered by the calculation of the possible size of a calcium phosphate mineral in a small vesicle at the deployed ion concentration. Assuming a vesicular diameter of 30nm, a Ca²⁺ concentration of 25mM and a mineral density of 3.153 gcm⁻³ (HAP, Ca₅(PO₄)₃OH [Hoffmann 2003]) a hypothetical spherical mineral particle would only be in the size range of 2-3nm in diameter and therefore hardly detectable by TEM. The cavity of small vesicles is therefore too small to host enough electrolyte (at dilute concentrations) to precipitate detectable calcium phosphate minerals.

Further reasons for the ineffective attempt to mineralize calcium phosphate in small polymersomes could be that experimental addition of alm already during vesicle preparation by film rehydration is not the proper method.

And last, if we expect the lipid covered ring model to be the valid model for pore formation, where alm helices form a pore by plane parallel aggregation, then the extreme membrane curvature of small polymersomes (in the size range of 30nm) could prevent the alm helices from plate-like aggregation.

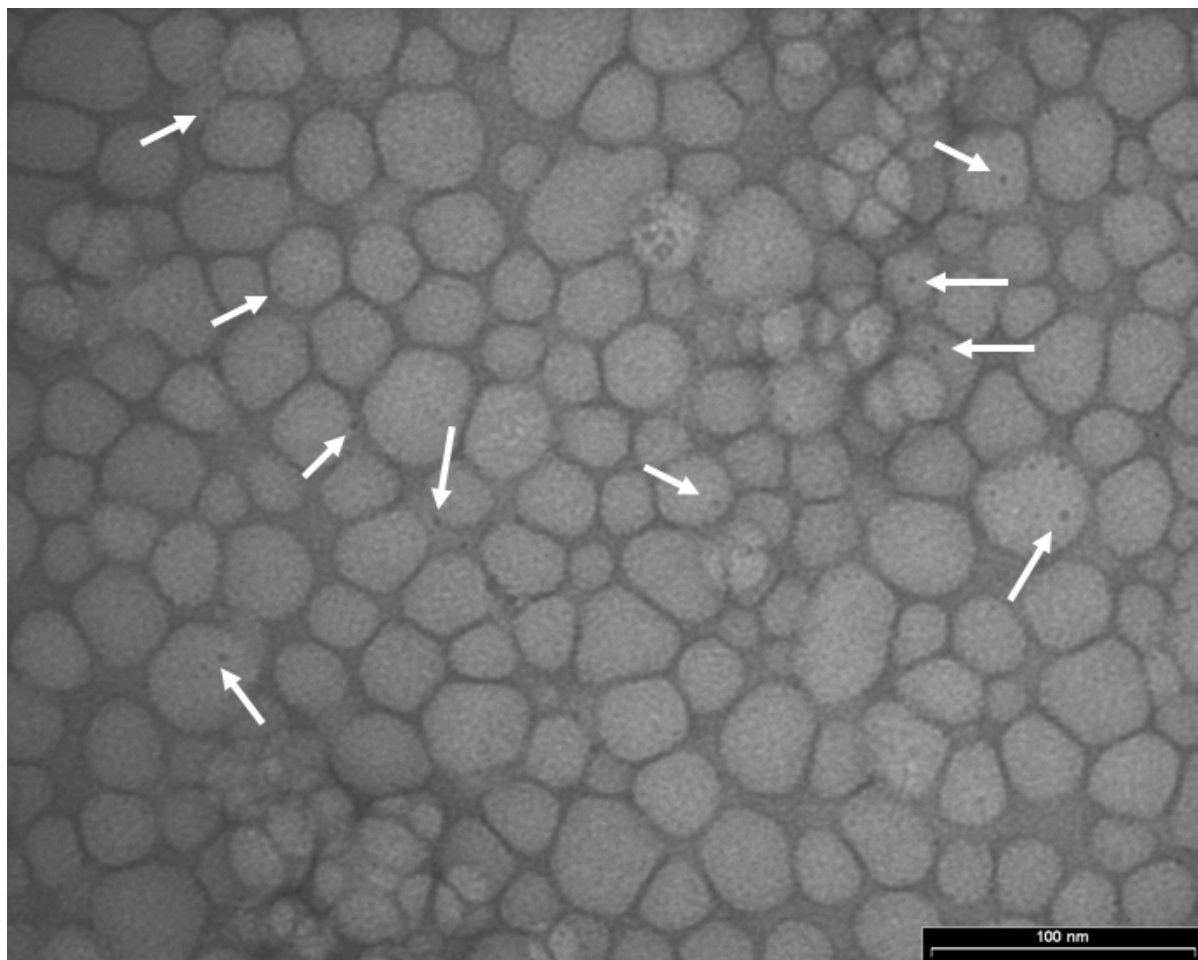


Figure 4.40. TEM of small vesicles at a molar ratio $n_{ABA} : n_{alm} = 10 : 1$ after 5 days of swelling in a phosphate buffer and 1 day incubated with calcium ions (negative stained, scale bar 100nm).

*Falls Gott die Welt geschaffen hat
war seine Hauptsorge sicherlich nicht,
sie so zu machen, dass wir sie verstehen können.*

Albert Einstein

CHAPTER 5

CONCLUSIONS AND OUTLOOK

5. Conclusions and outlook

5.1. Conclusions

Monolayers from amphiphilic block copolymers exhibit a complex behavior at the air-water interface. Our results allow for the first time the description of phase behavior in two PMOXA-PDMS-PMOXA block copolymer systems, with various sizes of the hydrophobic block. Indeed, the block length plays an important role in polymer arrangement in Langmuir films. Similarly to other self-assemblies from block copolymers, this feature is a factor which determines the material properties at different stages of the film compression. Not surprisingly, the larger polymer, with its flexibility and ability to adopt more conformations has more possibilities to host other species. Anyway it is very surprising that an artificial membrane may suit as a better environment for a biological membrane protein such as the investigated peptide, alamethicin, than natural, through evolution highly optimized, lipid membranes.

According to recent literature reports, alamethicin prefers to aggregate in the plane-parallel arrangement; therefore, its miscibility with either lipids or block copolymers at the molecular level is restricted. Analysis of the isotherm patterns favors the interpretation of immiscibility or partial miscibility, in terms of stable aggregates within a matrix. In lipid-peptide systems no mixing is achievable over the whole composition range, whereas the use of a block copolymer provides a certain tunability of the material properties in the membranes and thus yields a better compatibility between the polymer-peptide composite.

On the other hand, alamethicin promotes expanded phases of the copolymer membranes, where energetically favorable partial polymer-peptide miscibility is observed. Additionally, at high surface pressures, the peptide is preserved from collapse by the surrounding polymer matrix. A proposed barrel-stave arrangement where alm is re-oriented to a perpendicular upright state does not take place. All our monolayer experiments suggest that alamethicin prefers an aggregated state corresponding to the lipid-covered ring model.

Surface topography analysis of transferred Langmuir Blodgett films did not yield evidence for either barrel-stave or lipid-covered ring conditions. PMOXA-PDMS-PMOXA monolayer films reorganize upon transfer from the air-water interface on highly hydrophilic solid substrates.

It is reasonable to assume that a monolayer deviates slightly from fully hydrated membrane systems. We therefore investigated the channel forming properties of alamethicin also in bilayer systems, namely polymersomes. Our results indicate that alm significantly influences the bilayer properties of block copolymer membranes. In small polymersomes alm alters the packing density considerably by intercalating in the membrane and therefore strongly affects the morphology, uniformity and size distribution of the lyotropic mesophases.

In addition, biomineralization experiments in giant polymersomes in the micrometer range have shown that the peptide preserves its antimicrobial channel forming activity in artificial polymer membranes by increasing the membrane permeability for divalent cations. No conclusion could be drawn if the source of ion flux originates from pores formed according to the barrel-stave or the lipid covered ring model.

No precipitation of calcium phosphate has been found to occur in small polymer-somes. This is accounted to the minimal vesicular cavity, too small to host enough electrolyte for precipitation, or to the extreme membrane curvature of small vesicles, disabling all pore formation.

Anyhow, an increase of permeability of ions due to alamethicin has been clearly proven; although no clear-cut evidence could be obtained to which extent the antimicrobial activity is controlled by peptide concentration and how much it is influenced by a membrane potential.

We can therefore generally conclude that although alamethicin apparently possesses a very simple structure, its aggregation behavior and pore forming mechanism in membranes are complex and ambivalent. Still, after 40 years of discovery and a vast number of publications, this simple amphiphilic peptide has kept well its thrill and mysteries. Nevertheless, amphiphilic ABA triblock copolymers provide an excellent system to study ion channels yielding a vast - although sometimes controversial - information output.

5.2. Outlook

By simply investigating two polymers varying in the block length of the hydrophobic middle block a compilation of various dissimilar effects could be noted. Anyway, to deduce trends and effectively predict properties it is necessary to study a wider range of polymers, varying not only in molecular weight but also in architecture and composition (rigidity, hydrophobicity, etc.).

Even though alamethicin exhibits a rather complex behavior in membranes it generally has to be denoted as a very simple biomacromolecule. A further step into the elucidation of the nature of membrane proteins would be an extension of the system applied to more complex peptides, for instance higher molecular weight channels, oligomeric protein pores or even protein pumps. The abundance and variety of membrane channels in respect to structure as well as to function is nearly infinite in nature. Availability of such biomacromolecules is increased thanks to newly developed, more straightforward methods of engineering, production and purification. For that reason no lack of enthralling and challenging protein systems to be studied is to emerge in the near future.

The monolayer experiments performed with the system alamethicin-PMOXA-PDMS-PMOXA have produced plentiful information. However, complementary results are necessary of the structure and phase regime of the monolayer polymer matrix as well as of the peptide to achieve unequivocal conclusions. Suitable techniques to realize this task might be x-ray and neutron reflectometry [Collings 1997, Buhler 1998, Zhou 1998, Jones 1999, Hyde 2001] or surface plasmon resonance [Knoll 2003]. In addition, a variation of experimental parameters, solid substrates and functionalized block copolymers could yield LB transfers where the 'natural' monolayer structure is retained. AFM characterization could provide the requested complementarity.

By the development of more powerful computer systems new possibilities emerge to model monolayer (and bilayer) systems. Molecular dynamics simulations (e.g. coarse grain, [Srinivas 2004a, 2004b]) have already been effectively implemented to investigate the self-assembling dynamics of amphiphilic block copolymer mesophases. A further extension to systems with mixed components should be likely.

Nevertheless, investigations of fully hydrated bilayer membrane systems provide the most reliable information on the biological function of membrane proteins. A monolayer has to be accounted an approximation slightly deviating from a natural system. Therefore it is necessary to expand surveys on bilayer systems. Polymerosomes are easily achievable and might be successfully used to study single channel activity by patch clamping and conductance measurements [Tank 1982, Hanke 2000]. Another suitable method where experimental conditions can be easily tuned and direct evidence is given on channel activity as well as material properties is the black lipid membrane technique successfully employed for lipidic and polymeric systems [Mueller 1963, Nardin 2000a].

*Wissenschaft: Es ist nicht ihr Ziel,
der unendlichen Weisheit eine Tür zu öffnen,
sondern eine Grenze zu setzen dem unendlichen Irrtum.*

Bertolt Brecht

CHAPTER 6

REFERENCES

6. References

- Abu-Arish A., Frenkiel-Krispin D., Fricke T., Tzfira T., Citovsky V., Wolf S.G., Elbaum M., *J. Biol. Chem.*, 2004, 279, 25359.
- Adamson A.W., *Physical Chemistry Of Surfaces*, Wiley, New York, 1976.
- Addadi L., Weiner S., *Angew. Chem. Int. Ed. Engl.*, 1992, 31, 153.
- Aguilella V., Bezrukov S., *Eur. Biophys. J.*, 2001, 30, 233.
- Ahmed F., Alexandris P., Neelamegham S., *Langmuir*, 2001, 17, 537-546.
- AIP Emilio Segrè Visual Archives, *Physics Today Collection*, <http://photos.aip.org/>.
- Albertowa Z., *O sztuce Japonii*, Wiedza Powszechna, Warsaw, 1987.
- Alberts B., *Molecular Biology Of The Cell*, Garland Publishing, New York, 1994.
- Alberts B., Johnson A., Lewis J., Raff M., Roberts K., Walter P., *Functions Of Plasma Membrane Proteins*, Garland Publishing, New York, 1998.
- Albouy P.A., Vandevyver M., Perez X., Escoffet C., Markovitsi D., Veber M., Jallabert C., Strzelecka H., *Langmuir*, 1992, 8, 2262.
- Alexander S., *J. Phys. (France)*, 1977, 38, 977.
- Angelova M.I., Dimitrov D.S., *Faraday Discuss. Chem. Soc.*, 1986, 81, 303.
- Angelova M.I., Dimitrov D.S., *Mol. Cryst. Liq. Cryst.*, 1987, 1523, 89.
- Ariga K., Okahata Y., *Langmuir*, 1994, 10, 3255.
- Azzam R.M.A., Bashara N.M., *Ellipsometry And Polarized Light*, North-Holland, Amsterdam, 1992.
- Bacon K.J., Barnes G.T., *J. Colloid Interface Sci.*, 1978, 67, 70.
- Baekmark T.R., Elender G., Lasic D.L., Sackmann E., *Langmuir*, 1995, 11, 3975-3987.
- Baekmark T.R., Wiesenthal T., Juhn P., Albersdörfer A., Nuyken O., Merkel R., *Langmuir*, 1999, 15, 3616-3626.
- Bagatolli L.A., Gratton E., *Biophysical Journal*, 1999, 77, 2090.
- Balestrieri C., Camussi G., Giovane A., Iorio E.L., Quagliuolo L., Servillo L., *Anal. Biochem.*, 1996, 233, 145-150.
- Barranger-Mathys M., Cafiso D.S., *Biochemistry*, 1996, 35, 498-505.
- Bates F.S., Schulz M.F., *Faraday Discussions*, 1994, 98, 7.
- Baumann G., Mueller P., *J. Supramol. Struct.*, 1974, 2, 538-557.
- Bechinger B., *Crit. Rev. Plant Sci.*, 2004, 23, 271.
- Beisswanger G., *Chemie in unserer Zeit*, 1991, 2, 97-101.
- Bigelow J., (Ed.), *The Complete Works Of Benjamin Franklin Vol. 5*, G.P. Putnam's Sons, New York, 1966.
- Bijsterbosch H.D., de Haan V.O., de Graaf A.W., Mellema M., Leermakers F.A.M., Cohen S.M.A., van Well A.A., *Langmuir*, 1995, 11, 4467.
- Binks B.P., *Adv. Colloid Interface Sci.*, 1991, 34, 343.
- Birdi K.S., *Lipid And Biopolymer Monolayers At Liquid Interfaces*, Plenum Press, New York, 1989.
- Blodgett K.B., *J. Amer. Chem. Soc.*, 1934, 56, 495.
- Blodgett K.B., *J. Amer. Chem. Soc.*, 1935, 57, 1007.
- Blodgett K.B., *Langmuir I., Phys. Rev.*, 1937, 51, 964.

- Blodgett K.B., *Phys. Rev.*, 1939, 55, 391.
- Boheim G., Hanke W., Jung G., *Biophys. Struct. Mechan.*, 1983, 9, 181-191.
- Boman H.G., Marsh J., Goode J.A., (Eds.), *Antimicrobial Peptides*, Ciba Foundation Symposium 186, John Wiley & Sons, Chichester, 1994.
- Bouchaud E., Daoud M., *J. Phys. (France)*, 1987, 48, 1991.
- Brancato S., Serfis A., *J. Colloid Interface Sci.*, 2001, 239, 139.
- Brandani P., Stroeve P., *Macromolecules* 2003, 36, 9502.
- Braun M., Killmann H., Maier E., Benz R., Braun V., *Eur. J. Biochem.*, 2002, 269, 4948.
- Breed J., Biggin P.C., Kerr I.D., Smart O.S., Sansom M.S.P., *Biochim. Biophys. Acta*, 1997, 1325, 235-249.
- Bremer A., Häner M., Aebi U., *Cell Biology: A Laboratory Handbook*, Academic Press, San Diego, 1998, 277-284.
- British Plastics Federation, <http://www.bpf.co.uk/>.
- Brockman H., *Chem. Phys. Lipids*, 1994, 73, 57.
- Brockman H., *Curr. Op. in Struct. Biol.*, 1999, 9, 438.
- Broekaert W.F., Cammue B.P.A., De Bolle M.F.C., Thevissen K., De Samblanx G.W., Osborn R.W., *Crit. Rev. Plant Sci.*, 1997, 16, 297-323.
- Brown G. H., Wolker J. J., *Liquid Crystals And Biological Structures*, Academic Press, London, 1979.
- Bucher P., Fischer A., Luisi P.L., Oberholzer T., Walde P., *Langmuir*, 1998, 14, 2712.
- Buhler E., Dobrynin A.V., DeSimone J.M., Rubinstein M., *Macromolecules*, 1998, 31, 7347.
- Cadenhead D.A., Philips M.C., *Adv. Chem. Ser.*, 1968, 84, 131.
- Cadenhead D.A., Müller-Landau F., *J. Colloid Interface Sci*, 1980, 78, 269.
- Cantor R.S., *Biophys. J.*, 2002, 82, 2520-2525.
- Castano S., Desbat B., Laguerre M., Dufourcq J., *Biochim. Biophys. Acta*, 1999, 1416, 176.
- Castillo R.C., National University of Mexico, <http://www.fisica.unam.mx/liquids/>.
- Cevc G., Marsh D., (Eds.), *Phospholipid Bilayers - Physical Principles And Models*, Vol. 5, John Wiley&Sons, New York, 1987.
- Chattoraj D.K., Birdi K.S., *Adsorption And The Gibbs Surface Excess*, Plenum Press, New York, 1984.
- Chugh J.K., Brückner H., Wallace B.A., *Biochemistry*, 2002, 41, 12934-12941.
- Coelfen H., Antonietti M., *Langmuir*, 1998, 14, 582.
- Collings P. J., Hird M., *Introduction To Liquid Crystals*, Taylor and Francis, London, 1997.
- Costin I.S., Barnes G.T., *J. Colloid Interface Sci*, 1975, 51, 106.
- Crisp D.J., *Surface Chemistry*, Butterworth, London, 1949.
- Cui F. Z., Zhang Y., Cai Q., *Mater. Res. Soc. Symp. Proc.*, 2000, 599,317.
- Curtius T., *J. Prakt. Chem.*, 1915, 91, 1.
- Daghastanli K.R.P., Ferreira R.B., Theidei Jr. G., Maggio B., Ciancaglini P., *J. Coll. Surf. B: Biointerfaces*, 2004, 36, 127.
- Decher G., Maclennan J., Sohling U., Reibel J., *Thin Solid Films*, 1992, 210/211, 504.
- Defay R., Prigogine I., Belemans A., Everett D.H., *Surface Tension And*

- Adsorption, Longmans, London, 1966.
- Denisov G., Wanaski S., Luan P., Glaser M., McLaughlin S., *Biophys. J.*, 1998, 74, 731.
- Dettre R.H., Johnson R.E., *Colloid Interface Sci.*, 1966, 21, 367.
- Devaux P.F., Papers 1903-13 reviewed in *Ann. Report Smithsonian Inst.* 1913, 261 & *Soc. Franc. Phys.* 1914, 55, 3.
- Di Marzio E.A., *Prog. Polym. Sci.*, 1999, 24, 329-77.
- DiDonna B., University of Pennsylvania, Philadelphia/PA,
<http://www.physics.upenn.edu/~bdidonna/>.
- Dimitrov D.S., Angelova M.I., *Progr. Colloid & Polymer Sci.*, 1987, 73, 48.
- Dimova R., Seifer U., Pouligny B., Förster S., Döbereiner H.G., *Eur. Phys. J. E.*, 2002, 7, 241.
- Discher B.M., Won Y.Y., Ege D.S., Lee J.C.M., Bates F.S., Discher D.E., Hammer D.A., *Science*, 1999, 284, 1143.
- Discher B.M., Hammer D.A., Bates F.S., Discher D.E., *Curr. Opin. Colloid Int. Sci.*, 2000, 5, 125.
- Discher D.E., Eisenberg A., *Science*, 2002, 297, 967-973.
- Duckely M., Hohn B., *FEMS Microbiology Lett.*, 2003, 223, 1.
- Duclohier H., Wroblewski H., *J. Membr. Biol.*, 2001, 184, 1.
- Dynarowicz-Łatka P., Kita K., *Adv. Coll. Interf. Sci.*, 1999, 79, 1.
- Eanes E.D., Hailer A.W., Costa J.L., *Calcif. Tissue Int.*, 1984, 36, 421.
- Eicke H.F., Meier W., Hammerich H., *Colloids and Surfaces A*, 1999, 156, 249.
- Eisenberg B., *Acc. Chem. Res.*, 1998, 31, 117.
- Eisenberg M., Hall J.E., Mead C.A., *J. Membrane Biol.*, 1973, 14, 143-176.
- Evans E., Needham D., *J. Phys. Chem.*, 1987, 91, 4219.
- Fauré M.C., Bassereau P., Carignano M.A., Szleifer I., Gallot Y., Andelman D., *Eur. Phys. J. B*, 1998, 3, 365-375.
- Feng S., *Langmuir*, 1999, 15, 998.
- Föster S., Plantenberg T., *Angew. Chem.*, 2002, 114, 712-739.
- Förster S., Antonietti M., *Adv. Mat.*, 2003, 15, 1323.
- Fox R.O., Richards F.M., *Nature*, 1982, 300, 325-330.
- Franklin B., *Philos. Trans. Royal Chem. Soc.*, 1774, 64, 445.
- Franklin J.C., Ellena J.F., Jayasinghe S., Kelsh L.P., Cafiso D.S., *Biochemistry*, 1994, 33, 1043-1050.
- Friedrich T., *Biochim. Biophys. Acta*, 1998, 1364, 134.
- Fuchs H., Chi L.F., Eng L.M., Graf K., *Thin Solid Films*, 1992, 210/211, 655.
- Fulford G.D., *Isis*, 1968, 59, 198.
- Furukawa J., Saegusa T., Mise N., *Makromol. Chem.*, 1960, 38, 244.
- Gabrielli G., Pugelli M., *J. Coll. Interf. Sci.*, 1982, 86, 485.
- Gaines, G.L., *Insoluble Monolayers At The Liquid-Gas Interface*, Wiley-Interscience, New York, 1966.
- Gaines G.L., *Thin Solid Films*, 1983, 99, ix.
- Galvez Ruiz M.J., Cabrerizo Vilchez M.A., *Coll. Polym. Sci.*, 1991, 269, 77.
- GE The General Electric Story - A Photohistory, *Hall Of History News*, 1992, 10, 53.
- Gemma N., Egusa S., Azuna M., *Phys. Rev. B*, 1992, 46, 1655.
- Gennis R.B., *Biomembranes: Molecular Structure And Function*, Springer Verlag, Heidelberg, 1989.

- Giles C.H., Forrester S.D., *Chem. Ind. London*, 1971, 42.
- Gingell D., Owens N., Hodge P., Nicholas C.V., O'Dell R., *J. Biomed. Mat. Res.*, 1994, 28, 505.
- Goodrich F.C., *Proceedings Of The 2nd International Congress On Surface Activity*, Butterworth, London, 1957, 85.
- Goodwin J., *Colloids And Interfaces With Surfactants And Polymers*, John Wiley & Sons, Chichester, 2004.
- Gordon L.G.M., Haydon D.A., *Phil. Trans. R. Soc. London B*, 1975, 270, 433-447.
- Gordon L.G.M., Haydon D.A., *Biochimica et Biophysica Acta*, 1976, 436, 541-556.
- Graff A., Sauer M., van Gelder P., Meier W., *Proc. Natl. Acad. Sci. USA*, 2002, 99, 5064.
- Gutberlet T., Wurlitzer A., Dietrich U., Politsch E., Cevc G., Steitz R., Lösche M., *Physica B*, 2000, 283, 37-39.
- Hadjichristidis N., Pispas S., Floudas G.A., *Block Copolymers*, John Wiley & Sons, Hoboken, 2004.
- Hal J.E., Vodyanoy I., Balasubramanian T.M., Marshall G.R., *Biophys. J.*, 1983, 45, 233-247.
- Halperin A., *Macromolecular Reports*, 1992, A29, 107.
- Hamley I.W., *Introduction To Soft Matter*, John Wiley & Sons, Chichester, 2000.
- Hamley I. W., *Angew. Chem. Int. Ed. Engl.*, 2003a, 42, 1692.
- Hamley I.W., *Nanotechnology*, 2003b, 14, R39.
- Hanke W., *CRC Critical Reviews in Biochemistry*, 2000, 19, 1-44.
- Hardy W.B., *Proc. Roy. Soc. (London)*, 1911, A86, 634 & 1913, A88, 303.
- Harkins W.D., *J. Amer. Chem. Soc.*, 1917, 39, 354 & 541.
- Harkins W.D., Jordan H.F., *J. Amer. Chem. Soc.*, 1930, 52, 1751.
- Harkins W.D., *The Physical Chemistry Of Surface Films*, Reinhold Publishing Corporation, New York, 1952.
- Henderson J.A., Richards R.W., *Macromolecules*, 1993, 26, 65.
- Hénon S., Meunier J., *Rev. Sci. Instrum.*, 1991, 62, 936.
- Herbert F., *Dune, Hodder and Stoughton*, London, 1968.
- Hett W.S., *Aristotle, Problemata, Book 23, No 38*, Heinemann, New York, 1937.
- Heyse S., Ernst O.P., Dienes Z., Hofmann K.P., Vogel H., *Biochemistry*, 1998, 37, 507.
- Hille B., *Ion Channels Of Excitable Membranes*, Sinauer Associates, Sunderland, 2001.
- Ho D., Chu B., Schmidt J.J., Brooks E.K., Montemagno C.D., *IEE Trans. Nanotechn.*, 2004a, 3, 256-263.
- Ho D., Chu B., Lee H., Montemagno C.D., *Nanotechnology*, 2004b, 15, 1084-1094.
- Hoffmann I., 1973, <http://www.daserste.de/checkeins/samstrasse/>.
- Hoffmann U., Kwait D.C., Handwerker J., Chan R., Lamuraglia G., Brady T.J., *Radiology*, 2003, 229, 375-381.
- Höhne U., Möhwald H., *Thin Solid Films*, 1994, 243, 425.
- Hol W.G.J., Halie L.M., Sander C., *Nature*, 1981, 294, 532-536.
- Holland P.M., Rubingh D.N., *Surfactant Sci. Ser.*, 1991, 37, 141.
- Hönig D., Möbius D., *J. Phys. Chem.*, 1991, 95, 4590.
- Hottle J.R., Kim H.J., Deng J., Farmer-Creely C.E., Viers B.D., Esker A.R., *Macromolecules*, 2004, 37, 4900-4908.

- Huang H.W., *Biochemistry*, 2000, 39, 8347-8352.
- Huang L., Yuan H., Zhang D., Zhang Z., Guo J., Ma J., *Appl. Surf. Sci.*, 2004, 225, 39-46.
- Huh C., Mason S.G., *Colloid & Polymer Sci.*, 1975, 253, 266.
- Hyde S.T., *J. Phys.*, 1990, 51, C7, 209-228.
- Hyde S. T., *Identification Of Lyotropic Liquid Crystalline Mesophases*, John Wiley & Sons Ltd., Hoboken, 2001.
- Ikada Y., Iwata H., Nagaoka S., Horii F., *J. Macromol. Sci.-Phys.*, 1980, B17, 191.
- Intaglio Fine Art, Cheltenham/UK, <http://www.intaglio-fine-art.com/>.
- Ionov R., El-Abed A., Angelova A., Goldmann M., Peretti P., *Biophys. J.*, 2000, 78, 3026.
- Ionov R., El-Abed A., Goldmann M., Peretti P., *J. Phys. Chem. B*, 2004, 108, 8485.
- Israelachvili J.N., *Intermolecular And Surface Forces*, Academic Press, London, 1992.
- IUPAC Glossary
<http://www.chem.qmul.ac.uk/iupac/>.
- Jen W.C., Jones G.A., Brewer D., Parkinson V.O., Taylor A., *J. Appl. Bacteriol.*, 1987, 63, 293-298.
- Jenekhe S.A., Chen X.L., *Abstr. Pap. Am. Chem. Soc.*, 2000, 220, PMSE-268.
- Jones R.A.L., Richards R.W., *Polymers At Surfaces And Interfaces*, Cambridge University Press, Cambridge, 1999.
- Jung G., Hummel R.P., Voges K.P., Albert K., Toniolo C., *Peptides: Chemistry and Biology. Proceedings of the 10th American Peptide Symposium*, Marshall G.R. (Ed.), ESCOM, Leiden, 1988, 37-38.
- Kaufmann T., Biocentre, University of Basel,
<http://www.mih.unibas.ch/Homepages/ENGEL/Kaufmann/>.
- Kawakatsu T., Kawasaki K., Andelman D., *KEK Proc.*, 1993, 93, 3-5.
- Kent M.S., Lee L.T., *Macromolecules*, 1992, 25, 6240.
- Kessel A., Schulten K., Ben-Tal N., *Biophys. J.*, 2000, 79, 2322-2330.
- Kikukawa T., Araiso T., *Arch. Biochem. Biophys.*, 2002, 405, 214-222.
- Kita K., *Charakterystyka Filmow Langmuira I Langmuira-Blodgett Utworzonych Przez Kwasy Polifenylokarboksylowe I Ich Pochodne*, PhD thesis, Jagiellonian University, Krakow/Pol, 2002.
- Kita-Tokarczyk K., Grumelard J., Haeffele T., Meier W., *Polymer*, 2005a, 46, 3540-3563.
- Kita-Tokarczyk K., oral communication, Department of Chemistry, University of Basel, 2005b.
- Klebba P.E., *Res. Microbiology*, 2002, 153, 417.
- Kleinkauf H., von Doehren H., *Annu. Rev. Microbiol.*, 1987, 41, 259-289.
- Klok H.A., Lecommandoux S., *Adv. Mater.*, 2001, 13, 1217-29.
- Knoll W., *Annu. Rev. Phys. Chem.*, 1998, 49, 568.
- Kobayashi S., Saegusa T., *Ring Opening Polymerization*, Vol. 2, Chapter 11, Elsevier, Essex, 1984.
- Kobayashi S., *Prog. Polym. Sci.*, 1990, 15, 751.
- Kopp F., Fringeli U.P., Mühlethaler K., Günthard H.H., *Biophys. Struct. Mech.*, 1975, 1, 75.
- KSV Instruments Ltd, Helsinki, Finland,
<http://www.ksvltd.com/>.
- Kuhn H., *Naturwiss.* 1967, 54, 429.
- Kuhn H., Möbius D., *Angewandte Chemie Int'l Ed*, 1971, 10, 629.
- Kuhn H., Möbius D., Bücher H., *Physical Methods Of Chemistry*, Vol. 1,

- Part 3B, Chapter 7, Weissberger A. & Rossiter B. (Eds.), Wiley, New York, 1972.
- Kuksis A., Animal Lecithins, Lecithins, Szuhaj & List (Eds.), AOCS, Champaign, 1985, 105-162.
- Kunststoff-Schweiz, <http://www.kunststoffschweiz.ch/>.
- Langmuir I., Met. Chem. Eng., 1916, 15, 469.
- Langmuir I., J. Amer. Chem. Soc., 1917a, 39, 1848.
- Langmuir I., Proc. Natl. Acad. Sci. USA, 1917b, 3, 251.
- Lasic D.D., Joannic R., Keller B.C., Frederik P.M., Auvray L., Adv. Colloid Interf. Sci., 2001, 89-90, 337-49.
- Lechner M.D., Gehrke K., Nordmeier E.H., Makromolekulare Chemie, Birkhäuser, Basel, 2003.
- Lee A.G., Biochimica et Biophysica Acta, 1977, 472, 237-281.
- Lee J.C.M., Bermudez H., Discher B.M., Sheehan M.A., Won Y.Y., Bates F.S., Discher D.E., Biotechnology and Bioengineering, 2001, 73, 135.
- Lee J.C.M., Santore M., Bates F.S., Discher D.E., Macromolecules, 2002, 35, 323-326.
- Ligoure C., J. Phys. II (France), 1993, 3, 1607.
- Lohner K., Latal A., Lehrer R.I., Ganz T., Biochemistry, 1997, 26, 1525-1531.
- Lowenstam H.A., Weiner S., On Biomineralization, Oxford University Press, Oxford, 1989.
- Luo L., Eisenberg A., J. Amer. Chem. Soc., 2001a, 123, 1012-1013.
- Luo L., Eisenberg A., Langmuir, 2001b, 17, 6804-6811.
- Majewski J., Kuhl T.L., Gerstenberg M.C., Israelachvili J.N., Smith G.S., J. Phys. Chem. B, 1997, 101, 3122-3129.
- Mann S., Hannington J.P., Williams R.J.P., Nature, 1986, 324, 565.
- Marsh D., Handbook Of Lipid Bilayers, CRC Press, London, 1990.
- Marsh D., Biochem. J., 1996, 315, 345-361.
- Martin D.R., Williams R.J.P., Biochemical Society Transactions, 1975, 3, 166-167.
- Martin D.R., Williams, R.J.P., Biochem. J., 1976, 153, 181-190.
- Martin E., Ganz T., Lehrer R.I., J. Leukocyte Biol., 1995, 58, 128-136.
- Martin P., Szablewski M., Tensiometers And Langmuir-Blodgett Troughs, Nima Technology, Coventry, 1999.
- Maskos M., Harris J. R., Macromol. Rapid Comm., 2001, 22, 271.
- Mathew M.K., Nagaraj R., Balaram P., J. Membrane Biol., 1982, 65, 13-17.
- Matuo H., Motomura K., Matuura R., Chem. Phys. Lipids, 1981, 28, 385.
- Meier W., Chem Soc Rev, 2000, 29, 295-303.
- Mendelsohn R., Moore D.J., Chem. Phys. Lipids, 1998, 96, 141.
- Meng F., Hiemstra C., Engbers G.H.M., Feijen J., Macromolecules, 2003, 36, 3004.
- Mestres C., Alsina M.A., Espina M., Rodriguez L., Reig F., Langmuir, 1992, 8, 1388.
- Meyer P., Reusser F., Experientia, 1967, 23, 85-86.
- Micol V., Sanchez-Pinera P., Villalain J., de Godos A., Gomez-Fernandez J.C., Biophys. J., 1999, 76, 916.
- Mueller P., Rudin D.P., Tien H.T., Wescott W.C., J. Phys. Chem., 1963, 67, 534.
- Mueller P., Rudin D.O., Nature, 1968, 217, 713-719.

- Muñoz M.G., Monroy G., Ortega F., Rubio R.G., Langevin D., *Langmuir*, 2000, 16, 1083-1093.
- Myrvold R., Hansen F.K., Balinour B., *Coll. Surf. A: Phys. Eng. Asp.*, 1996, 117, 27-36.
- Nagaraj R., Balaram P., *Acc. Chem. Res.*, 1981, 14, 356-362.
- Nanofilm, BAM2plus Hypertext User Manual, Rev. 4, Nanofilm Technologie GmbH, Göttingen, 2002.
- Napoli A., Boerakker M.J., Tirelli N., Nolte R.J.M., Sommerdijk N.A.J.M., Hubbell J.A., *Langmuir*, 2004, 20, 3487.
- Nardin C., Hirt T., Leukel J., Meier W., *Langmuir*, 2000a, 16, 1035-1041.
- Nardin C., Thoeni S., Widmer J., Winterhalter M., Meier W., *Chem. Comm.*, 2000b, 15, 1433.
- Nardin C., Meier W., *Chimia*, 2001a, 55, 142-146.
- Nardin C., Widmer J., Winterhalter M., Meier W., *Eur. Phys. J. E: Soft Matter*, 2001b, 4, 403.
- New R.R.C., *New Liposomes - A Practical Approach*, IRL Press, Washington, 1990.
- Nikaido H., *Mol. Microbiology*, 1992, 6, 435.
- O'Connor S.M., Gehrke S.H., Retzinger G.S., *Langmuir*, 1999, 15, 2580-2585.
- Ober R., Vilanove R., *Coll. Polymer Sci.*, 1977, 255, 1067.
- Ohya-Nishiguchi H., *Bull. Chem. Soc. Jpn.*, 1979, 52, 2064.
- Ovchinnikov Y.A., Kryushkin A.A., Kozhevnikova I.V., *Zh. Obshch. Khim.*, 1971, 41, 2085.
- Ovchinnikov Y.A., Ivanov V.T., Shkrob A.M., *Membrane-Active Complexons*, B.B.A. Library Vol. 12, Elsevier, Amsterdam, 1974.
- Pallas N.R., *Colloids & Surfaces*, 1983, 6, 221.
- Pandey R.C., Cook J.C., Rinehart K.L., *J. Amer. Chem. Soc.*, 1977, 99, 8469-8483.
- Pata V., Dan N., *Biophys. J.*, 2003, 85, 2111.
- Payne J.W., Jakes R., Hartley B.S., *Biochem J.*, 1970, 117, 757-766.
- Peterson I.R., Russel G.J., Roberts G.G., *Thin Solid films*, 1983, 109, 371.
- Peterson I.R., Brzezinski V., Kenn R.M., Steitz R., *Langmuir*, 1992, 8, 2995-3002.
- Peterson I.R., Kenn R.M., *Langmuir*, 1994, 10, 4645-4650.
- Plastics Historical Society: <http://www.plastiquarian.com/>.
- Pockles A., *Nature*, 1891, 43, 437.
- Prosize W. E., *Commercial Lecithin Products*, Lecithins, Szuhaj & List (Eds.), AOCS, Champaign, 1985.
- Rabe J.P., Swalen J.D., Rabolt J.F., *J. Chem. Phys.*, 1987, 86, 1601.
- Rackham H., *Gaius Plinius Secundus Maior, Naturalis Historia, Vol. 1*, Heinemann, London, 1964.
- Rayleigh Lord, *Proc. R. Soc. Ser. A*, 1890, 47, 364.
- Rayleigh Lord, *Philos. Mag.* 1899, 48, 321.
- Reeves J.P., Dowben R.M., *J. Cell. Physiol.*, 1969, 73, 49.
- Regenbrecht M., Akari S., Förster S., Möhwald H., *J. Phys. Chem. B*, 1999, 103, 6669.
- Ringhof T., 2004, www.le-solutions.de/berichte/fruchtfliegen/.
- Rizzo V., Stankowski S., Schwarz G., *Biochemistry*, 1987, 26, 2751-2759.

- Roberts G.G., Langmuir-Blodgett Films, Plenum Press, New York, 1990.
- Rochford B.R., Ph.D. thesis, University of Durham, 1995.
- Rodriguez Patino J.M., Sanchez C.C., Rodriguez Nino M.R., Langmuir, 1999, 15, 2484.
- Rothberg L., Higashi G.S., Allara D.L., Garoff S., Chem. Phys. Lett., 1987, 133, 67.
- Saegusa T., Kobayashi S., Encyclopedia Of Polymer Science And Technology, Suppl. Vol. 1, Wiley, New York, 1976, 220.
- Sandretto Museum Collegno, Italy, <http://www.sandretto.it/>.
- Sansom M.S., Q. Rev. Biophys., 1993a, 26, 365-421.
- Sansom, M. S. P., Eur. Biophys. J., 1993b, 22, 105-124.
- Sansom, M.S.P., Curr. Biology, 1999, 9, R254.
- Sauer M., Haefele T., Graff A., Nardin C., Meier W., Chem. Commun., 2001, 2452.
- Schaper A., Wolthaus L., Möbius D., Jovin T.M., Langmuir, 1993, 9, 2178.
- Schillén K., Bryskhe K., Mel'nikova Y.S., Macromolecules, 1999, 32, 6885.
- Schwartz D.K., Viswanathan R., Zasadzinski J.A.N., Langmuir, 1993, 9, 1384.
- Scotto A.W., Gompper M.E., Biochemistry, 1990, 29, 7244.
- Shen H., Eisenberg A., J. Phys. Chem. B, 1999, 103, 9473-9487.
- Shiku H., Dunn R.C., J. Microsc. 1999, 194, 455-466.
- Smith G.R., Sansom M.S.P. Biophys. Chem. 1999, 79, 129-151.
- Srinivas G., Shelley J.C., Nielsen S.O., Discher D.E., Klein M.L., J. Phys. Chem. B, 2004a, 108, 8153-8160.
- Srinivas G., Discher D.E., Klein M.L., Nature Materials, 2004b, 3, 638-644.
- Starostin A.V., Butan R., Borisenko V., James D.A., Wnschuh H., Sansom M.S.P., Woolley G.A., Biochemistry, 1999, 38, 6144-6150.
- Stoenescu R., Asymmetric Amphiphilic Triblock Copolymers, PhD thesis, University of Basel, 2004.
- Stoker B., Dracula, Constable, London, 1897.
- Streich D., Haefele T., Meier W., Nachrichten aus der Chemie, 2004, 52, 126-130.
- Tabor D., J. Colloid Interface Sci., 1980, 75, 240.
- Takahashi A., Yoshida A., Macromolecules, 1982, 15, 1196.
- Tan J.S., Butterfield D.E., Voyecheck C.L., Caldwell K.D., Li J.T., Biomaterials, 1993, 14, 823.
- Tandford C., Science, 1978, 200, 1012-1018.
- Tank D., Miller C., Webb W.W., Proc. Natl. Acad. Sci. U.S.A., 1982, 79, 7749.
- Taylor R., de Levie R., Biophys. J., 1991, 59, 873.
- Tieleman D.P., Berendsen H.J.C., Sansom M.S.P., Biophys. J., 1999, 76, 1757-1769.
- Tieleman D.P., Sansom M.S.P., Int. J. Quantum Chem., 2001a, 83, 166-179.
- Tieleman D.P., Berendsen H.J.C., Sansom M.S.P., Biophys. J., 2001b, 80, 331-346.
- Tippmann-Krayer P., Möhwald H., Langmuir, 1991, 7, 2298.
- Tippmann-Krayer P., Kenn R.M., Möhwald H., Thin Solid Films, 1992, 210/211, 577.

- Tolkien J.R.R., *The Hobbit*, 1937, George Allen & Unwin, London.
- Traube I., *Liebigs Annalen der Chemie*, 1891, 265, 27.
- Tredgold R.H., *Rep. Prog. Phys.*, 1987, 50, 1609.
- van Gelder P., Dumas F., Winterhalter M., *Biophysical Chemistry*, 2000, 85, 153.
- van Zanten J.H., Monbouquet H.G., *J. Colloid Interface Sci.*, 1991, 146, 330.
- Vance D., Vance J., *Biochemistry Of Lipids, Lipoproteins And Membranes*, Elsevier, Amsterdam, 1991.
- Vebert C., oral communication, Department of Chemistry, University of Basel, 2005.
- Vijayan K., Discher D.E., Lal J., Janmey P., Goulian M., *J. Phys. Chem. B*, 2005, 109, 14356.
- Vilanove R., Rondelez F., *Phys. Rev. Letters*, 1980, 45, 1502.
- Vodyanoy I., *Langmuir*, 1991, 7, 207-208.
- Volinsky R., Kolusheva S., Berman A., Jelinek R., *Langmuir*, 2004, 20, 11084.
- Wabel C., *Influence Of Lecithin On Structure And Stability Of Parenteral Fat Emulsions*, PhD thesis, Friedrich-Alexander-Universität Erlangen-Nürnberg, July 1998.
- Wesemann A., Ahrens H., Steitz R., Förster S., Helm C.A., *Langmuir*, 2003, 19, 709-716.
- White S., Wimley W., *Biochim. Biophys. Acta*, 1998, 1376, 339-352.
- Widmer J., *Nanoreaktoren Aus Amphiphilen ABA-Triblock-Copolymeren*, Diploma thesis, Universität Basel, Juni 2000.
- Wilhelmy L., *Ann. Physik*, 1863, 119, 177.
- Wolfe S.L., *Molecular And Cellular Biology*, Wadsworth Publishing Company, London, 1993, 155.
- Won Y.Y., Ege D.S., Lee J.C.M., Bates F.S., Discher D.E., Hammer D.A., *Science*, 284, 1143, 1999.
- Woolley G.A., Wallace B.A., *J. Membrane Biol.*, 1992, 129, 109-136.
- Wu F., Gericke A., Flach C.R., Mealy T.R., Seaton B.A., Mendelsohn R., *Biophys. J.*, 1998, 74, 3273.
- Wu H., Foster M.D., Ross S.A., Mattice W.L., Matties M.A., *Langmuir*, 1996, 12, 3015.
- Wu S., *Polymer Interace & Adhesion*, Marcel Dekker, New York, 1982.
- Yu Z., Jin J., Cao Y., *Langmuir*, 2002, 18, 4530-4531.
- Yun H., Choi Y.W., Kim N.J., Sohn D., *Bull. Korean Chem. Soc.*, 2003, 24, 377.
- Zasadzinski J.A., Viswanathan R., Madsen L., Garnaes J., Schwartz D.K., *Science*, 1994, 263, 1726.
- Zhang L., Eisenberg A., *Science*, 1995, 268, 1728.
- Zheng S., Strzalka J., Jones D.H., Opella S.J., Blasie J.K., *Biophys. J.*, 2003, 84, 2393.
- Zhou S., Chu B., *Macromolecules*, 1998, 31, 7746.
- Zhulina E.B., Borisov O.V., Pryamitsyn V.A., Birshtein T.M., *Macromolecules*, 1991, 24, 140.

*Bedenkt, wozu dies Dasein euch gegeben;
Nicht um dem Viehe gleich zu brüten, nein,
Um Wissenschaft und Jugend zu erstreben.*

Dante Alighieri

CHAPTER 7

APPENDIX

Appendix A - Abbreviations

α	disordered lyotropic mesophase	Cs^{-1}	Compressional modulus
A	mean molecular area	δ	partly ordered, helical lyotropic mesophase
AA	amino acid	d	doublet; film thickness
AB	diblock copolymer	D	Dalton = $gmol^{-1}$; translational diffusion coefficient
ABA	symmetric triblock copolymer	DC	direct current
Ac	acetyl	DC ₁₈ Gly	dioctadecanoyl glycerol
AC	alternating current	DIC	differential interference contrast
AD	anno domini	DIS	disordered state
AFM	atomic force microscopy	DLS	dynamic light scattering
Aib	1-amino isobutyric acid	DMPC	dimyristoyl phosphatidylcholine
Ala	alanine	DOPC	dioleoyl phosphatidylcholine
alm	alamethicin	DOPE	dioleoyl phosphatidylethanolamine
ATP	adenosine triphosphate	DPPC	dipalmitoyl phosphatidylcholine
β	partly ordered, untilted lyotropic mesophase	DSPE	distearoyl phosphatidylethanolamine
β'	partly ordered, tilted lyotropic mesophase	DTAF	5-(4,6-dichlorotriazinyl) aminofluorescein
b	block	η	viscosity
BAM	Brewster angle microscopy	f	block length fraction
BC	before Christ's birth	FITC	fluorescein isothiocyanate
BCC	body-centred cubic	FTIR	Fourier-transformation infrared spectroscopy
BP	band pass filter	γ	surface tension
BS	barrel-stave model	g	graft
χ	Flory-Huggins interaction parameter	G	gaseous monolayer state; gyroid morphology; Gibbs free energy
C	crystalline lyotropic mesophase; hexagonal packed cylinder morphology; instrument constant	Gln	glutamine
CCD	charge-coupled device	Glu	glutamic acid
CD	circular dichroism	Gly	glycine
CLSM	confocal laser scanning microscopy		
CPP	critical packing parameter		
CPS	Close packed spheres		
Cs	Compressibility		

GV	giant vesicle	ODT	order-disorder transition
H	hexagonal lyotropic mesophase; mean curvature	π	surface pressure
HAP	hydroxyapatite	π_c	collapse pressure
HEPES	4-(2-hydroxyethyl)piperazine-1- ethanesulfonic acid	P	oblique or centred lyotropic mesophase
HLB	hydrophilic-to-hydrophobic bal- ance	PA	phosphatidic acid
HOPG	highly oriented pyrolyzed graphite	PBT	poly(butylene glycol terephtha- late)
I	oil-in-water type lyotropic mesophase; intensity of light	PC	phosphatidylcholine
II	water-in-oil type lyotropic mesophase	PDMS	poly(dimethylsiloxane)
IR	infrared	PE	phosphatidylethanolamine
ITO	indium-tin-oxide	PEE	poly(ethyl ethylene)
IUPAC	International Union of Pure and Applied Chemistry	PEMA	poly(ethyl methacrylate)
κ_i	principal curvature	PEO	poly(ethylene oxide)
K_G	Gaussian curvature	PET	poly(ethylene terephthalate)
L	lamellar lyotropic mesophase; chain length	PH	phase contrast
L_1	liquid-expanded monolayer state	PhI	phenylalaninol
L_2	liquid-condensed monolayer state	PI	phosphatidylinositol
LB	Langmuir-Blodgett	PLPC	palmitoyl-linoleoyl phosphati- dylcholine
LCR	lipid-covered ring model	PMAA	poly(methacrylate)
LD PE	low density polyethylene	PMMA	poly(methyl methacrylate)
Leu	leucine	PMOXA	poly(2-methyloxazoline)
LPC	lyso-phosphatidylcholine	POPC	palmitoyl-oleoyl phosphatidyl- choline
LPE	lyso-phosphatidylethanolamine	POSS	polyhedral oligomeric silses- quioxane
m	multiplet	PPO	poly(propylene oxide)
M	micellar lyotropic mesophase	ppm	parts per million
MW	molecular weight	Pro	proline
N	degree of polymerization	PS	phosphatidylserine; poly(styrene)
N.A.	numerical aperture	PTFE	poly(tetrafluor ethylene)
n_i	refractive index of medium i	PVAC	poly(vinyl acetate)
NMR	nuclear magnetic resonance spectroscopy	PVC	poly(vinyl chloride)
ODA	octadecylamine	Q	cubic or viscous isotropic lyo- tropic mesophase

QELS	quasi-elastic light scattering	T	temperature
R	rhombohedral lyotropic mesophase	TAMRA	tetramethyl rhodamine-5-carbonyl azide
R_h	hydrodynamic radius	TEM	transmission electron microscopy
R_i	radius of curvature	TMS	tetramethylsilane
s	singlet	TR	transfer ratio
S	quasi-solid or superliquid monolayer state; body-centred cubic morphology	U22324	alamethicin
SAPC	stearoyl-arachidoyl phosphatidylcholine	UCOT	upper critical ordering temperature
SLPC	stearoyl-linoleoyl phosphatidylcholine	UP	unsaturated polyester
SOPC	stearoyl-oleoyl phosphatidylcholine	V	hydrophobic volume
SPM	sphingomyelin	V/V	volume percent
θ	contact angle; scattering angle; Brewster angle	Val	valine
t	triplet	wt/wt	weight percent
		X_i	molar fraction of component i
		XRD	x-ray diffraction

Appendix B - Historical timeline of natural and synthetic macromolecules

Overview adapted from [*Plastics Historical Society, Sandretto Museum, Kunststoff-Schweiz, British Plastics Federation*].

- 1000BC A resin from a lacquer tree *Rhus verniciflua* is used by the Chinese to form waterproof and durable coatings.
- 0 Horn behaves like a typical thermoplastic sheet and can be split and moulded into shape after heating in hot water.
- 77 Amber is described by Pliny the Elder (23 - 79) in the work *Natural History*. It is a thermoplastic resin from fossilized trees and is found mainly on the Baltic Coast.
- 400 Tortoiseshell can be cut and shaped, similar to horn, to keep an attractive pattern for a variety of articles.
- 800 Gutta percha - a natural resin from the bark of Malayan trees.
- 1550 Valdes describes first reference to natural rubber in reports of expeditions to Central America. The native Indians used the material for sports and waterproofing.
- 1531 Either the alchemist Bartholomäus Schobinger [*Sandretto Museum*] or the Benedictine monk Wolfgang Seidel [*Kunststoff-Schweiz*] invents a firm transparent material on the base of casein from cheese.
- 1596 John Huyglen von Linschoeten, after visiting India, describes the use of shellac, a natural resin produced by scale insects.
- 1650 John Tradescant introduces gutta percha to the West after his travels in the East collecting plants.
- 1725 London is established as an important horn moulding centre with metal dies being manufactured for snuff boxes.
- 1731 Charles Marie de la Condamine reports natives in Amazon basin using rubber for waterproofing and flexible bottles. Rubber imported into Europe in 1736 but evidence suggests that it was in use by the natives for several thousand years.
- 1820 Thomas Hancock discovers that if strongly processed (masticated) then rubber became plastic and could be made to flow and develops the method of milling rubber.
- 1823 Scottish chemist Charles Macintosh begins using rubber to waterproof fabrics.
- 1835 Regnault reports first production of vinyl chloride monomer.
- 1831 First description of styrene.
- 1839 Charles Goodyear discovers the process of mixing natural rubber with sulphur to make a stronger and more resilient product; the process was later termed 'vulcanisation'.

-
- Payen isolates cellulose as the principal constituent of wood.
- 1844 F. Walton produces linoleum
- 1851 'Ebonite' is patented and commercialised by Nelson Goodyear. It is a milestone because it is the first thermosetting material and because it involves modification of the natural material.
- 1854 Shellac (mixed with woodflour) patented as a moulding material by Samuel Peck.
- 1855 François Lepage patents 'Bois Durci', an animal polymer composite based on albumen (from blood or egg white) with wood powder as filler
- 1859 Butlerov describes formaldehyde polymers.
- 1862 The first man-made plastic 'Parkesine', made from cellulose nitrate, is unveiled by Alexander Parkes at the 1862 Great International Exhibition in London.
- 1868 From a starting point of cellulose nitrate and camphor, John Wesley Hyatt and his brother Isaiah obtain 'Celluloid', very similar to Parkesine but less brittle.
- 1872 Adolph Bayer reports reactions of phenols and aldehydes to give resinous substances.
- 1876-77 Seeds of Brazilian rubber trees smuggled out of Brazil by Sir Henry Wickham and later sent to Asia where they form the basis of the world's rubber industry.
- 1880 Shellac used by the Berliner label to produce phonograph records because of the ability to reproduce fine detail - shellac was used until 1952 when PVC was first introduced for this purpose.
- 1884 Louis Bernigaud (Count of Chardonnet) produces 'artificial silk' fibres from cellulose (later to be termed 'Rayon').
- 1899 W. Kritsche and A. Spitteler discover and patent casein plastics known as 'Galalith'. Casein is made from skimmed milk curdled with rennet which is cured by immersion in formaldehyde.
- 1903 Stern and Charles Topham develop method for producing artificial silk ('Viscose').
- 1905 J. Edwin Brandenberger [*Sandretto Museum*] or Charles Frederick Cross (1908) [*Plastics Historical Society*] invents 'Cellophane' made from cellulose acetate and viscose rayon.
- 1909 Leo Baekeland patents 'Bakelite', the first true plastic Phenol-Formaldehyde thermoset to replace traditional materials such as wood, ivory and ebonite.
- 'Formica', layers of paper impregnated with phenolic and melamine resins and pressed into sheets, first produced by Herbert Faber and Daniel O'Connor.
- 1912 I. Ostromislensky patents polymerisation of vinyl chloride to give PVC but decomposition during processing prevents commercial development.
-

-
- 1915 Production of the first synthetic elastomer in Leverkusen.
- 1918 The Czech Hans John prepares resins by reacting urea with formaldehyde and patents the urea-formaldehyde resin systems.
- 1922 Hermann Staudinger synthesises rubber.
- 1924 Edmund Rossiter develops urea thiourea formaldehyde to give the first water-white transparent thermosetting moulding powder, marketed as 'Beetle'.
- 1926 Hermann Staudinger starts work on 'macromolecules' that will eventually show that polymers are long chains of monomers joined together (polymerised).
- 1927 Otto Rohm develops poly(methyl methacrylate)
- 1928 Ziegler becomes interested in organo-metallic chemistry and starts to lay the foundations for polyethylenes and polypropylenes.
- 1930 BASF / I.G.Farben develops polystyrene.
- 1931 Carothers develops 'Neoprene'.
E.W. Fawcett and R.O. Gibson from Imperial Chemical Industries develop polyethylene by accident.
- 1933 Polyethylene is discovered in 1933 by scientists working for ICI.
- 1934 Wallace Hume Carothers at Du Pont develops 'Nylon'.
- 1935 Henkel patents the production of resins based on melamine.
- 1937 Otto Bayer starts development of polyurethanes at I.G.Farben.
- 1938 Roy Plunkett (Du Pont) accidentally discovers poly(tetrafluoroethylene) (PTFE)
P. Schlack develops 'Perlon'.
- 1941 J.R. Whinfield and J.T. Dickson develop poly(ethylene terephthalate) (PET) initially used as a fibre (Terylene and Dacron).
- 1942 'Super Glue' (methyl cyanoacrylate) first discovered by Harry Coover (Eastman Kodak).
- 1943 First silicone resins
- 1949 'Silly Putty' invented by James Wright (GE) after mixing silicone oil with boric acid.
- 1951 Polypropylene (PP) developed by Paul Hogan and Robert Banks.
- 1953 Karl Ziegler develops metal ion catalysts for regular polymerisation of polyethylene. Giulio Natta develops metal ion catalysts for production of isotactic polymers.
Hermann Staudinger wins Nobel Prize for Chemistry for the study of polymers.
Herman Schnell at Bayer first synthesises polycarbonate at Bayer.
- 1959 Acetals (POM) introduced by Du Pont under the trade name 'Delrin'.
- 1960 Copolymers from ethylene and vinyl acetate are developed
-

-
- 1963 Polybutylene glycol terephthalate PBT
Ziegler and Natta share Nobel Prize for Chemistry for the synthesis of polymers.
- 1964 General Electric Co. develops PPO
- 1965 Union Carbide introduces the UDEL polysulfone resins, aromatic thermoplastics that resist high working temperatures
Du Pont develops ionomeric thermoplastic polymers
First patent for the production of vinyl-propylene chloride copolymers
- 1968 BASF starts selling photopolymeric plates for Nyloprint printing
Phillips Petroleum starts industrial production of low linear density polyethylene
- 1970 James Economy develops 'Ekonol', a moldable high temperature polymer which leads in 1971 to the development of liquid crystal polymers.
- 1971 Phillips Petroleum starts industrial production of 'Ryton' polyphenylene sulphide, the most resistant of all thermoplastics to flames
- 1972 Production of Aramidic fibers (Du Pont's Kevlar)
- 1974 Oil crisis strikes! Petrochemical based polymer prices increase by 50-100%.
- 1975 Mitsui Petrochemicals produces polymethylpentene, developed in 1965 by ICI and obtained in a laboratory by Giulio Natta
- 1980 BASF designs polypyrrole-based conducting polymers
- 1983 Introduction of the polyaryl sulfone technopolymer
- 1986 ICI develops 'Biopol', a thermoplastic of biodegradable vegetable origin, which will be followed a few years later by Mater-B of Montedison, a starch-based polymer
- 1986 Rohm and Haas develops polyacryl-imidic copolymers, with high gas barrier properties
- 1990 Warner Lambert develops 'Novon' - a bio-degradable plastic.
- 2000 A.J. Heeger, A.G. MacDiarmid and H. Shirakawa are awarded the Nobel Prize in Chemistry for the discovery and development of conductive polymers.

Appendix C - Resume

Thomas F. Haefele

Personal Details

Date of Birth December 28, 1976

Nationality Swiss

Education

University of Basel, CH	Ph.D. under the supervision of Prof. Dr. W. Meier, Focus: Polymerphysics, Polymer-peptide hybrid materials	01/2002 - 12/2005
----------------------------	---	----------------------

University of Basel, CH	Degree in Chemistry, minor subject Molecular Biology Thesis: Biomineralization in copolymer vesicles	10/1996 - 10/2001
----------------------------	---	----------------------

Upper-track Secondary School, CH	'De Wette-Gymnasium' Advanced level certificate in Science & Mathematics	04/1987 - 06/1995
--	---	----------------------

Lectures were attended of:

E. Constable, M. Dürrenberger, H. Gampp, W. Gehring, G. Gescheidt, B. Giese, H.P. Hauri, P.C. Hauser, J. Heeb, A. Hermann, C. Housecroft, H. Huber, H.C. Im Hof, U. Jenal, B. Jung, M. Jungen, T. Kaden, W. Keller, J.P. Maier, W.P. Meier, K. Naumann-Magnusson, M. Neuburger-Zehnder, M. Oehme, M.A. Rüegg, C. Schönenberger, G. Schwarz, J. Seelig, U. Séquin, J. Sick, H. Sigel, P. Strazewski, L. Tauscher, C. Ullrich, A. Vedani, A. Wiemken, H.J. Wirz, W.D. Woggon, S. Zschokke, A. Zuberbühler

Appendix D - Publications and presentations

Publications

Phase behavior of mixed Langmuir monolayers from amphiphilic block copolymers and an antimicrobial peptide

T. Haefele, K. Kita-Tokarczyk, W. Meier, Langmuir, 2006, 22(3), 1164-1172.

Hybrid nanocapsules: Interactions of ABA block copolymers with liposomes

T. Ruyschaert, A. Sonnen, T. Haefele, W. Meier, M. Winterhalter, D. Fournier, JACS, 2005, 127(17), 6242-6247.

Block copolymer vesicles – Using concepts from polymer chemistry to mimic biomembranes

K. Kita-Tokarczyk, J. Grumelard, T. Haefele, W. Meier, Polymer, 2005, 46, 3540-3563.

The 'Hottest Article' within 'Polymer' on ScienceDirect.com, April - June 2005!

Plastikfolien mit biologischer Funktion

D. Streich, T.F. Haefele, W.P. Meier, Nachrichten aus der Chemie, 2004, 52(2), 126-130.

Ion-carrier controlled precipitation of calcium phosphate in giant ABA triblock copolymer vesicles

M. Sauer, T. Haefele, A. Graff, C. Nardin, W. Meier, Chem. Commun., 2001, 2452-2453.

Oral Presentations

Bioinspired mineralization in triblock copolymer vesicles

30.06.03, PHOPOC '03, Vienna/A.

Giant vesicles made out of amphiphilic triblock copolymers

15.03.03, SYCA 1st Swiss Snow Symposium, Saas Balen/CH.

Biomimetic mineralization in triblock copolymer vesicles

25.04.02, Basler Jungchemikerforum, Basel/CH.

Poster Presentations

Isothermal phase behavior of mixed films of block copolymer and pore-forming peptides

20.09.05, Bayreuth Polymer Symposium, Bayreuth/D.

Isothermal behavior of polymer/peptide composites

16.08.05, Polymer Vesicles, Beuggen/D.

Isothermal phase behavior of peptide containing block copolymer membranes

20.06.05, EuCheMS Nanoscale Surface Self-Assembly, Stockholm/S.

Incorporation of pore forming peptides into self-assembled polymer membranes

07.04.05, 7th young scientists' conference on chemistry, Berlin/D.

Functionalisation of polymer films with natural pore peptides

22.03.05, PGS Polymers in Life Sciences, Basel/CH.

Ion channel incorporation into amphiphilic block copolymer membranes

15.09.04, PHOPOC `02, Vienna/A.

Posterprize for best poster!

Ion channel incorporation in polymer membranes

31.03.04, PGS Polymers in Life Sciences, Basel/CH.

